Theory of hyperfine and superfine levels in symmetric polyatomic molecules. II. Elementary cases in octahedral hexafluoride molecules

William G. Harter
School of Physics, Georgia Institute of Technology, Atlanta, Georgia 30332
(Received 9 October 1980)

A simple approximate theory is developed for high-J spin-rotational levels and very-high-resolution spectra of octahedral XY_6 (X spin-zero, Y spin-1/2) molecules. The structure and theory of SF_6 spectra is reintroduced and the properties of rotational energy level and spectral clusters are explained in terms of angular-momentum uncertainty relations and axis tunneling. An analogy between axis tunneling and nuclear-spin tunneling is used to provide a simple quasiparticle picture of hyperfine effects in strong (case-2) rotational clusters. Analogous types of clusters within clusters are discussed using this theoretical model. The possibility emerges for new and very sensitive type of spectra which we label superhyperfine structure. This structure has some remarkable similarities with nuclear magnetic resonance (NMR) spectra, and it might be an even more revealing indicator of internal molecular dynamics than NMR. Model Hamiltonians are represented in all the elementary types of cluster bases and some examples are solved using tableau techniques. Level correlations between case-1 and case-2 clusters are sketched. Nomograms for visualizing laser-saturation-absorption spectra are introduced, and examples of case-1 to case-1 and case-2 to case-1 transitions are given.

I. INTRODUCTION

Octahedral XY_6 molecules have been getting considerable attention recently partly because of UF_6 laser isotope-enrichment programs. The prognosis for uranium enrichment by laser is still secret, but there have been some unexpected benefits of these programs. These include a number of surprising and subtle quantum effects shown by the laser spectroscopy of the molecule UF_6 and its prototype SF_6. Certain of these effects are leading to a better understanding of high quantum states of complex systems than was provided by conventional classical or quantum theories.

This article and a previous one[1] (the previous article will be labeled I) treat a new approach to the theory of high-resolution molecular spectra. Article I introduced the theory of spectral clusters and nuclear spin or hyperfine structure in trigonal XY_3 and tetragonal XY_4 molecules. This article does the same for octahedral XY_6 molecules such as SF_6 and UF_6. The present article is mostly self-contained, and it has a more extensive introduction in Sec. II to the theories of high-resolution spectra than was given in article I. However, the introduction of tableau notation and calculus has been given by way of simpler XY_3 and XY_4 molecules in article I. It is much easier to compare the tableau analysis to conventional Racah algebra and point group theory using simple examples.

Indeed, it might have been easier to understand high-resolution spectra of octahedral XY_6 molecules if one could first study analogous but simpler hyperfine structure for heavy tetrahedral XY_4 molecules. However, the most high-resolution spectra are being taken for the octahedral molecules SF_6 and UF_6.[2,3] Very-high-resolution hyperfine spectra have recently been taken by Borde *et al.*, in the 10-μm region for SF_6 using their CO_2 saturation absorption laser spectrometer.[4-6] So far no hyperfine spectra has been resolved for CF_4 or SiF_4 although the latter should have resonances that can be probed by CO_2 laser. At least part of the reason for first pursuing the more complicated XY_6 molecules must be due to economic pressure from uranium isotope separation programs.

Nevertheless, the XY_4 and XY_6 molecules have enough in common that much of what is learned about one type is useful for understanding the other. In Sec. II a detailed comparison of spectral structure in the 16-μm region for SF_6 and CF_4 will be made. Examples of observed and conjectured spectral lines of SF_6 are shown in Fig. 1. These should be compared with the analogous spectra of CF_4 shown in the first figure of article I. Each successive stage 1(a), 1(b), 1(c), etc. of these figures portrays spectra which has been seen or should be seen at higher resolution than the preceding stage. Each lower stage represents a finer type of spectral structure which has generally required a breakthough in experimental technology to resolve it.

Each stage of finer structure has led to refinements in theoretical understanding, too, as the roles of various mechanisms and phenomena are defined. Finer spectral structure can generally be identified with slower motion, since the differences between energy levels are proportional to rates of time evolution. It is fortunate that these molecules have such well separated stages of spectral fineness. This allows the key mechanism

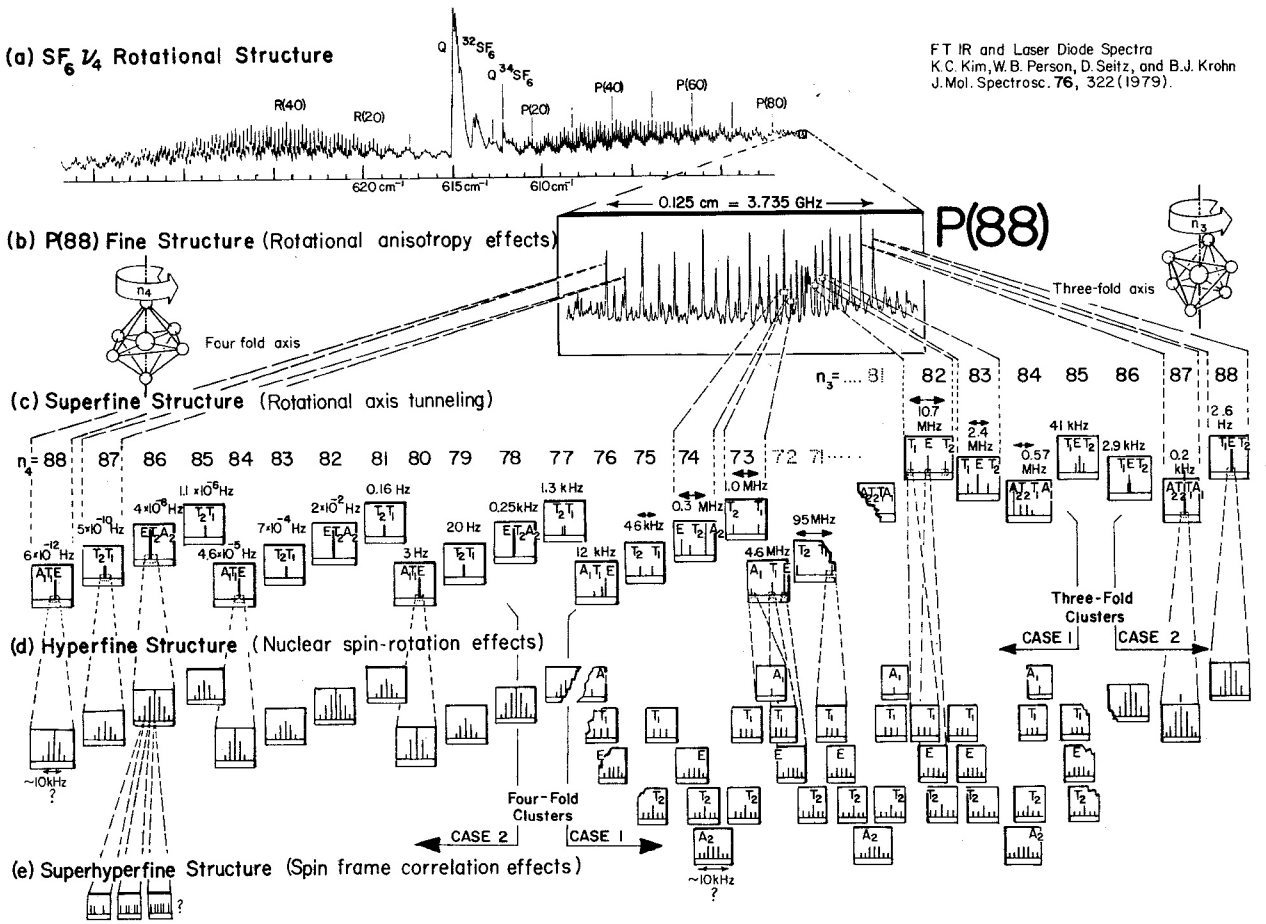

FIG. 1. Vibrational ν_4 resonance in SF_6 and $P(88)$ fine structure. The stages (a) through (e) of finer structure are discussed in Sec. II A through II E.

or motion responsible for each stage to be identified separately. This is an important feature of the analysis of nuclear spin and rotational dynamics which is being presented in these articles. The analysis also points out interesting cases where two or more different mechanisms have about the same speed and thereby tend to couple strongly.

It is probably important to point out the differences between the analysis being pursued in this article and the more conventional molecular spectroscopic approach.[7-10] The two approaches complement each other, and some details of their similarities and differences will be given as the various stages of spectral structure are reviewed in Sec. II. However, there are some general points of comparison which can be made now.

The conventional approach usually requires modern electronic computers. Often, the results are extremely accurate eigenvalues of large molecular Hamiltonian matrices. By adjusting molecular constants within a Hamiltonian one obtains a best fit to an observed spectrum using least squares or some other trial method. It is even possible, as Krohn, Bordé, and others have shown, to program experimental line shapes and make the computer draw copies of the spectra coming from the laser laboratory. The ability to synthesize completely and accurately a complex spectrum is one of the advantages of the conventional approach.

The present articles describe an approach which sets out to analyze[11] rather than synthesize spectral structures, i.e., it reduces the problem into simpler components. The analytic approach makes use of the observed breakup of complex molecular spectrum into various stages of finer structure. This structure suggests ways to represent the Hamiltonian so that the main contributions are diagonal, and off-diagonal contributions are small enough to be neglected or else treated as perturbations. Two immediate advantages of the analytical approach are simplification of computation, and probably more important, improvement of physical understanding.

Numerical computation is simpler in the analytic

approach since it does not require large numbers of numerical coefficients to be tabulated for each value of the molecular angular momentum J. The analytic approach yields approximate formulas for eigenvalues and eigenvectors in terms of J and other quantum numbers which become more accurate as J increases. In the synthetic approach each successive J value corresponds to a new and more difficult computing job than the preceding one. This approach was developed for light molecules such as methane (CH_4) which usually have low J ($J<15$), and exact solutions could be obtained before computers began to be used widely. A synthetic approach to a complicated molecular problem may use up allotted computer memory space, time, or money before a desired high J value is reached. On the other hand, the analytic formulas are less reliable for low J but become better and better for higher J.

However, the principal advantage of an analytic approach is to obtain some physical insight into the dominant mechanisms. It is possible to explain individual details or patterns in a complex spectra in terms of various models. The synthetic approach gives an entire spectrum for a given J at once, but it is difficult to tell what is happening in the molecule or in the computer. In short, a spectral synthesis will yield the most accurate set of molecular constants, but eventually some analysis should answer the perennial question: So what? To make the most of the new developments in laser spectroscopy one must identify extraordinary phenomena and effects that are most likely to lead to understanding and applications.

Among these are the unexpectedly large effects that nuclear spins have on rotational states of XY_4 and XY_6 molecules. The unexpected clustering[7,12,13] of rotational and rovibrational levels allows small interactions to have large effects. One effect is the strong hyperfine mixing of rovibronic species which was anticipated for states belonging to nearly degenerate clusters.[14-16] The first spectra showing hyperfine mixing have recently been observed and synthesized by Bordé *et al.*[4,6] for SF_6 clusters involving symmetry species $(T_1 + T_2)$ and $(T_1 + E + T_2)$. Some of these results will be reviewed qualitatively in Sec. II. A quantitative analysis for elementary cluster bases will be given for the most common clusters throughout the remainder of this article. As in article I, the main objective will be to develop the most concise descriptions of rotation, vibration, and nuclear spin states and to derive energy matrices, transition rates, and selection rules as simply as possible for each case.

Matrix calculations in this article differ from the conventional ones. The conventional techniques involve Racah-Wigner algebra of double tensors as developed by Louck[17] and Judd[18] and applied by Michelot *et al.*[10] and others. Matrices are given in terms of Racah coefficient formulas and various computer derived numerical coefficients such as Moret-Bailly F coefficients, G coefficients, and so forth. However, these techniques are practical at high J only if the resulting matrices are to be fed back to a computer for diagonalization. The analytic approach being followed in the present articles uses permutation and unitary tableau methods. The difference is analogous to that between Racah and unitary group methods in electronic and nuclear spectral calculations.[19-23] The unitary methods are not only simpler for matrix calculations, but, in the case of molecular energy matrices, they can be used to find eigensolutions as well.[24]

II. REVIEW OF SPECTRAL STRUCTURES AND THEORY

This section will review the various stages of Fig. 1 starting with the most coarse *rotational* structure at the top [Fig. 1(a)] and ending with the finest *superfine* structure at the bottom [Fig. 1(e)]. Some differences between the conventional synthetic approach to theory and the analytic approach will be explained where the differences are significant. The analytic approach has had little new to offer to the theory of coarse structure, while the synthetic approach has had little to say about the finest structure. The remainder of this article will be devoted mostly to the superhyperfine structure.

It is also helpful to compare spectral structures of SF_6 in Fig. 1 with those of CF_4 in the first figure of article I. The coarser structures of the two molecules are quite similar, but they have very different hyperfine structures. Obviously, six spin-1/2 nuclei in SF_6 must yield more complicated patterns than four such nuclei in CF_4.

A. Rotational structure

To begin the comparison note that the rotational structure of SF_6 in Fig. 1(a) is more extensive than the corresponding structure for CF_4 in Fig. 1(b) of article I. Indeed, Kim *et al.*,[3] have been able to resolve lines corresponding to rotational momentum J values of more than one hundred and thirty in SF_6. [Note that the lines due to the isotope $^{34}SF_6$ are present in Fig. 1(b), also.] The line heights are proportional to the population ρ_J of the J levels which is given by the Boltzman distribution formula:

$$\rho_J \sim (2J+1)\rho_I e^{-E(J)/kT} .$$

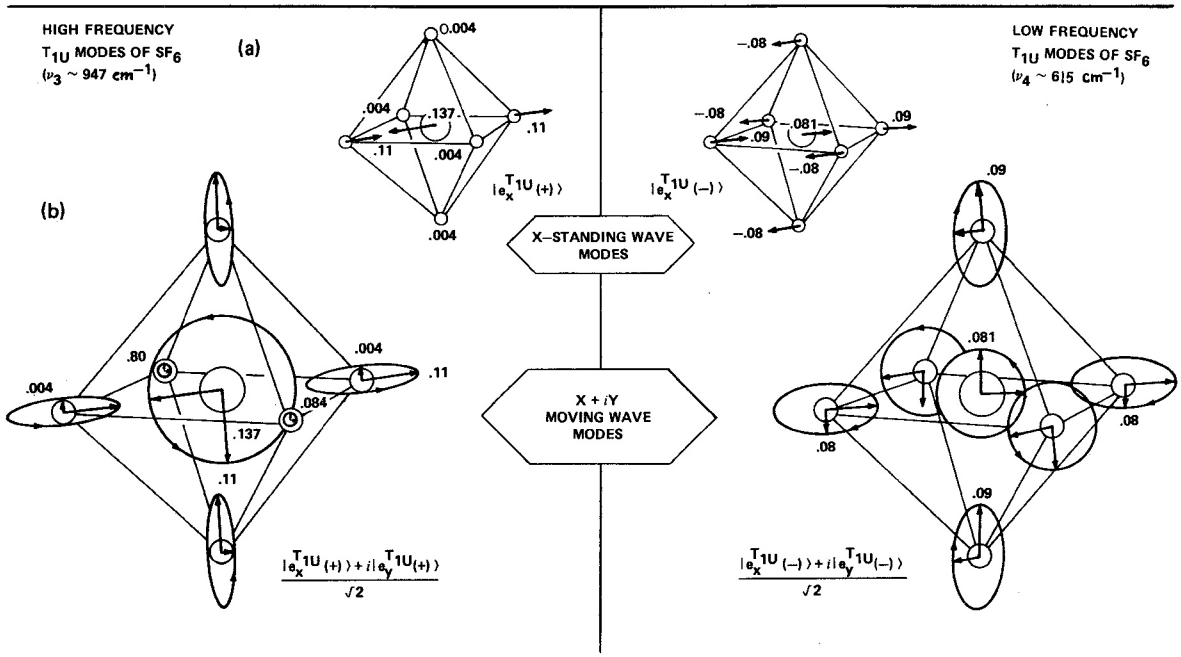

FIG. 2. Rovibrational motions of the two dipole active modes associated with the ν_3 and ν_4 resonances of SF_6.

This depends on the rotational degeneracy $(2J+1)$ and nuclear spin degeneracy ρ_I of the J level, its energy $E(J)$ and the Boltzmann temperature kT. The energy of the rotational levels is given by the eigenvalues

$$\langle H_{\rm rot}\rangle = BJ(J+1) + D[J(J+1)]^2 + \cdots \qquad (2.1)$$

of the pure rotational Hamiltonian. For approximations one can neglect the scalar centrifugal constant D which is much smaller than the rotational constant B. For SF_6, a lower rotational constant [i.e., a higher rotational inertia $(2B)^{-1}$] means greater population at higher J at the same temperature than for CF_4. (For CF_4: $B \simeq 0.131\ cm^{-1}$; for SF_6: $B \simeq 0.091\ cm^{-1}$).

The rotational structure in Fig. 1(a) arises when each SF_6 molecule starting in the $J=N$th level is excited to a state of one vibrational quantum with total angular momentum:

$$J^{\rm tot} = N^{\rm rot} + l^{\rm vib}, \qquad (2.2)$$

where the vibrational angular momentum l is taken to be unity for the ν_4 fundamental. The nuclear rotational momentum N of the rotor is often labeled R. The additional momentum l is due to nonrigid rotations of the type shown in Fig. 2. SF_6 has a low frequency (~16 $\mu m \sim cm^{-1}$) ν_4-normal mode and a high frequency (~10 $\mu m \sim 947\ cm^{-1}$) ν_3-normal mode. Both these modes are dipole active, i.e., they have vector or T_{1u} symmetry. One linear x-polarized component and one circular $(x+iy)$-polarized component are drawn for each mode in Fig. 2. When the angular momentum associated with the circular motion is added the total excited momentum can be $J=N+1$, N, or $N-1$ according to dipole selection rules. The three possibilities correspond to lines in Fig. 1(a) labeled $R(N)$ (for raising the momentum), $Q(N)$ (for status quo), and $P(N)$ (for plummet), respectively.

The excited levels are determined approximately by adding the pure vibrational energy and the scalar Coriolis vibration-rotation term to give the scalar Hamiltonian:

$$H_{\rm scalar} = H_{\rm rot} + \nu_{\rm vib} - 2B\zeta \vec{J}\cdot\vec{l}. \qquad (2.3)$$

The eigenvalues are found by writing $2\vec{J}\cdot\vec{l} = J^2 - (J-l)^2 + l^2 = J^2 - N^2 + l^2$ so that excited energy levels are given by the following (the D term is deleted here):

$$\langle H_{\rm rot}\rangle + \nu_{\rm vib} - 2B\zeta\langle\vec{J}\cdot\vec{l}\rangle = \nu_{\rm vib} + BJ(J+1) - B\zeta[J(J+1) - N(N+1) + l(l+1)]$$
$$= \nu_{\rm vib} - 2B\zeta + BN(N+1) + \begin{cases} 2B(1-\zeta)(N+1) & \text{for } J=N+1 \\ 0 & \text{for } J=N \\ -2B(1-\zeta)N & \text{for } J=N-1. \end{cases} \qquad (2.4)$$

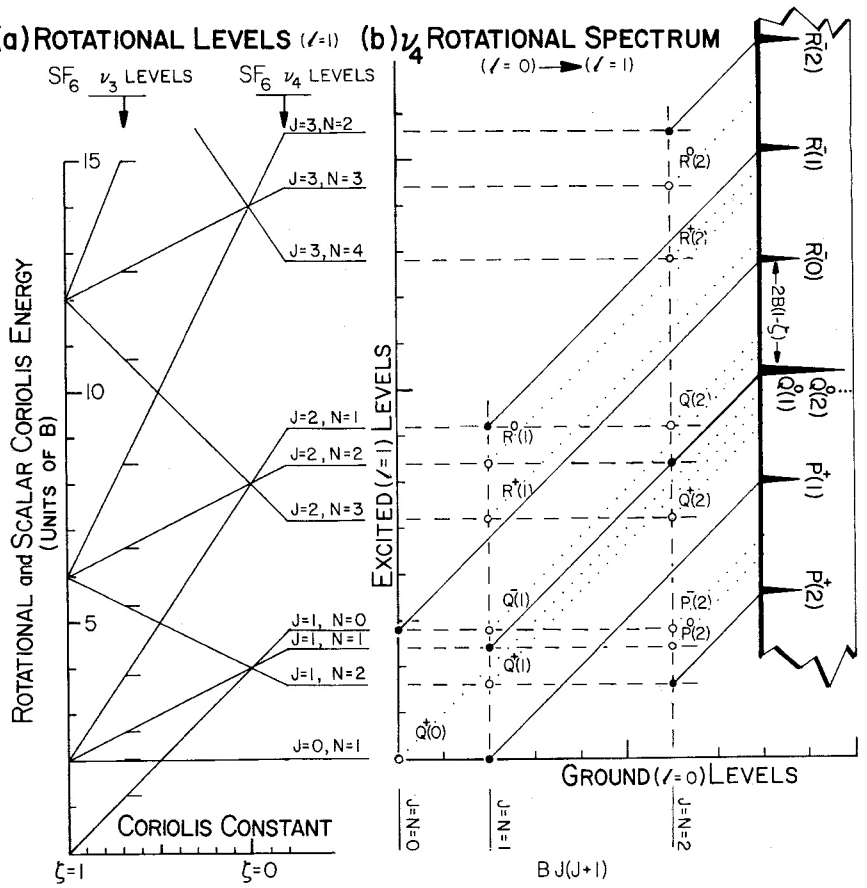

FIG. 3. Plots of levels and spectra for SF_6 rotational structure. (a) Levels for ($l=1$) rotation-vibration are plotted versus Coriolis constant (ζ). Levels for states ν_3 ($\zeta_3=0.69$) and ν_4 ($\zeta_4=-0.22$) are indicated. (b) Spectra for ν_4 transitions between ground ($l=0$) and excited ($l=1$) states are plotted using a nomogram. Each dipole-allowed transition ($J\rightarrow J+1, J$, or $J-1$) is indicated by a circle (●or ○) drawn at the intersection between ground and excited levels and a line of unit slope which indicates a possible spectral line on the right. Only the transitions which conserve N have been observed.

The resulting levels for $J \leq 3$ are plotted as a function of ζ in Fig. 3(a). The ν_4 Coriolis constant is $\zeta_4=-0.215$ and the ν_4 levels are shown on the right-hand side of Fig. 3(a).

The ν_4 spectrum is shown in Fig. 3(b) using a nomogram[25] which will be applied again later on. Here the excited levels are plotted against the ground rotational levels. Each allowed transition is indicated by a dot at the intersection of two levels. A line of unit slope drawn from each dot leads to the correct position of the corresponding spectral line. The strong lines belong to transitions which conserve N and they are indicated by solid lines and labeled $P^+(N)$, $Q^0(N)$, and $R^-(N)$ in Fig. 3(b). For most nonzero values of the Coriolos constant, the rotor momentum N is a good quantum number.[26] The N-changing transitions $P^-(N)$, $P^-(N)$, $Q^-(N)$, $R^0(N)$, and $R^+(N)$ are too weak to be observed with existing spectral sensitivity. Hence, the spectrum in Fig. 1(a) has lines with even spacing $2B(1-\zeta)=2.4B$ as indicated in Fig. 3(b).

Note that each $Q^0(N)$ transition leads into the same spectral line in Fig. 3. Together $Q(N)$ lines make up prominent features called Q branches as shown in Fig. 1(a). Some higher order effects cause $Q(N)$ lines to split, but there is not enough resolution in Fig. 1(a) to show them here. The morphology of Q branches has been analyzed by Brock *et al.*[27]

B. Fine structure

When a $P(N)$, $Q(N)$, or $R(N)$ line is examined at higher resolution a fine structure such as Fig. 1(b) emerges. The $P(88)$ fine structure for SF_6 is shown in Fig. 1(b) and should be compared to that of $P(54)$ in CF_4 in Fig. 1(c) of article I. The SF_6 diode spectra of Kim *et al.*, in Fig. 1(b), shows one type of cyclic pattern on the left-hand side and a different type of pattern on the right-hand side. The SF_6 patterns are more obvious than the ones for CF_4. The left-hand pattern

cycles after the first four lines whose height ratios are approximately 4:3:6:3, respectively. It repeats that pattern three more times before it runs into the right-hand pattern three quarters of the way through the fine-structure spectrum. The right-hand quarter of the spectrum is composed of two and a third cycles of three lines each with approximate height ratios of 5:6:5, respectively. These height ratios are due to hidden finer structures as will be explained in Secs. IIC and IID.

Fine-structure patterns such as Fig. 1(b) are due to anisotropic rotational or Coriolis effects. These are generally called "tensor" effects since they can be modeled by Racah vibration-rotation tensor Hamiltonians such as the following:

$$H^{\text{tensor}} = \sum_{k_1 k_2} t_{k_1 k_2 K} [v^{k_1}(\text{vib}) \times v^{k_2}(\text{rot})]^K_A$$
$$= t_{044}[v^4(\text{rot})]^4_A + t_{224}[v^2(\text{vib}) \times v^2(\text{rot})]^4_A + \cdots , \quad (2.5)$$

where two of the most important terms are written out. Here, $t_{k_1 k_2 K}$ are molecular constants and $[v^{k_1} \times v^{k_2}]^K_A$ are vibration-rotation tensors of rank K constructed to have the assumed octahedral or tetrahedral symmetry of the molecules. Tensor Coriolis Hamiltonians have been studied and applied by Louck,[17] Hecht,[28] Moret-Bailly,[29] and more recently by others.[30]

The energy spectra of one tensor, the (044) term, will be reviewed briefly now. As long as N is a good quantum number, the spectra of the most important (224) vibrational term fall into similar patterns.[31] The (044) or pure rotational term can be written in different notations:

$$[v^0 \times v^4]^4_{A1} = (\tfrac{7}{12})^{1/2} T^4_0 + (\tfrac{5}{24})^{1/2}(T^4_4 + T^4_{-4})$$
$$= (N_x)^4 + (N_y)^4 + (N_z)^4 - (\tfrac{3}{5})|\vec{N}|^4 . \quad (2.6)$$

The expression involving angular-momentum operators N_x, N_y, and N_z allows one to visualize the tensor geometry and understand its physical significance. For a fixed magnitude $|\vec{N}|$ of angular momentum one finds the classical energy varies with the direction $\hat{N}$ of the rotation axis. A three-dimensional plot in Fig. 4 of the energy assumes the anisotropic shape of a rounded octahedron congruent to the SF_6 octahedron.[32] A maximum value $\langle [v^4] \rangle = (2/5)|\vec{N}|^4$ is obtained for angular momentum $\vec{N}_> = |\vec{N}|(0,0,1)$ along a fourfold symmetry axis of the molecule. This corresponds to the direction of least centrifugal distortion for an octahedral molecule since the radial bonds are strongest. A minimum energy value $\langle [v^4] \rangle = (-4/15)|\vec{N}|^4$ is obtained for angular momentum $\vec{N} = |\vec{N}|(1/\sqrt{3}, 1/\sqrt{3}, 1/\sqrt{3})$ along a three-fold symmetry axis. Finally, an intermediate value $\langle [v^4] \rangle = (-1/10)|\vec{N}|^4$ is obtained

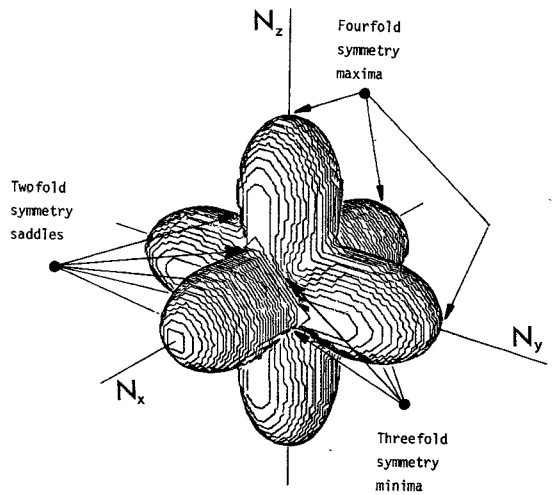

FIG. 4. Polar angle plot of energy anisotropy of fourth rank tensor ($N_x^4 + N_y^4 + N_z^4 +$ constant) for fixed magnitude of angular momentum $|\vec{N}|$. [Reprinted from W. G. Harter, and C. W. Patterson, J. Math. Phys. 20, 1453 (1978)]. The energy scale is along the radial direction.

for $\vec{N} = |\vec{N}|(0, 1/\sqrt{2}, 1/\sqrt{2})$ along a twofold symmetry axis or saddle point in Fig. 4. Note that the twofold axial energy value lies three-quarters of the way between maximum and minimum values. It corresponds to the dividing point between the fourfold and threefold patterns in Fig. 1(b). The intermediate or saddle point directions are the least constrained or localized. Starting from there, the $\vec{N}$ vector is free to roam around the surface without changing the energy.

The topography between the saddle points can be used to estimate most of the quantum energy eigenvalues of the tensor. A geometrical construction[26] is shown in Fig. 5. First the angular-momentum axis of quantization is set in the direction of a topographical maximum (or minimum). Angular-momentum uncertainty for a given state $|{}^N_n\rangle$ corresponds to the apex angle θ^N_n of cones shown centered on the axis. The slant height of the cones equals the expected length $[N(N+1)]^{1/2} \sim N + \frac{1}{2}$ of the angular-momentum $\vec{N}$ vector while the cone altitude equals the z component n as indicated in Fig. 5(a). The intersection of the cones with the topographical hill (or valley) determines approximately the fine-structure eigenvalues for that particular axis. These energy levels are indicated by circular arcs drawn through the intersections of the cones with a crossection of tensor extrema in Fig. 5(b). Hills and valleys for SF_6, CF_4, and similar molecules can be approximated by plotting just the aximuthally symmetric T^4_0 part of Eq. (2.6). The T^4_0 part is proportional to the Legendre harmonic $Y^4_0 = P_4(\cos\theta)$. The $(T^4_4 + T^4_{-4})$ part of Eq. (2.6) is negligible for small θ.

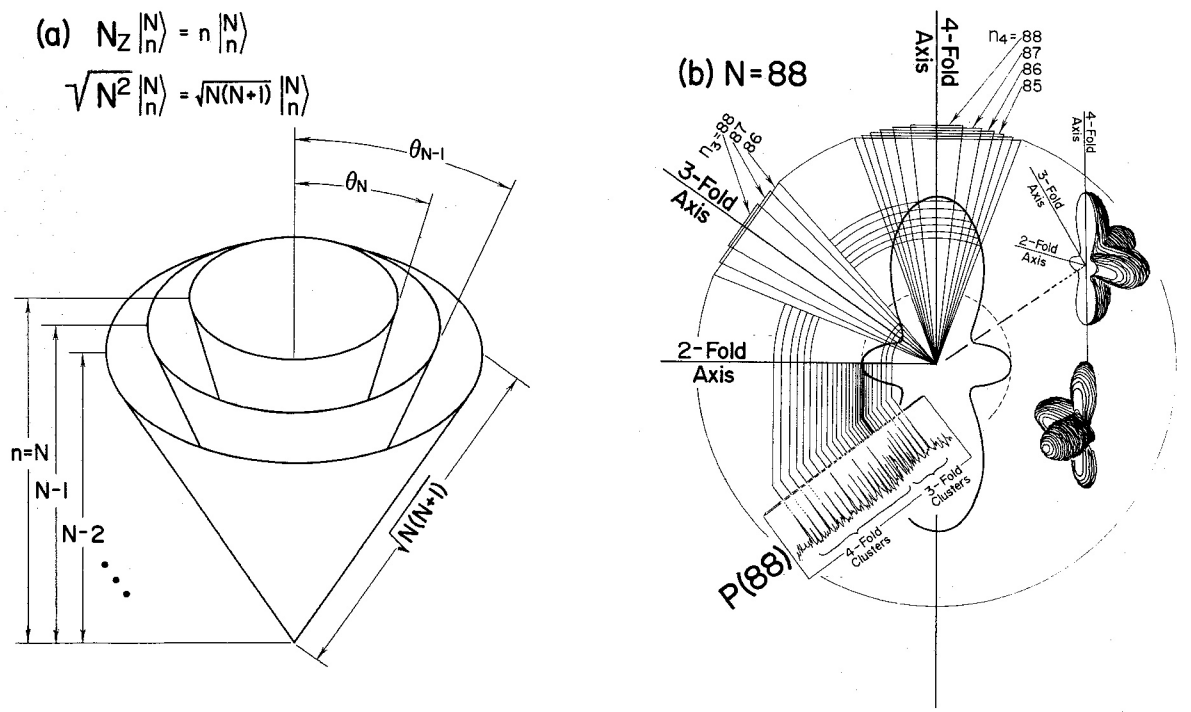

FIG. 5. Nomogram for approximating fine-structure levels due to a tensor T^k_0. (a) Angular-momentum cones for states $|{}^N_N\rangle$, $|{}^N_{N-1}\rangle$, ... have increasing uncertainty angles θ^N_N, θ^N_{N-1}, ... as z component (n) decreases. (b) Intersection of cones for ($N=88$) with tensor hill (or valley) determines the $P(88)$ fine structure according to approximate equations (2.7b) and (2.7c). These are correct to within a few percent for the highest n values near extremal axis.

The cone picture indicates how much the SF_6 molecular-rotor angular momentum N tends to be localized by energy and momentum constraints. The tensor energy expectation value is given by the Wigner-Eckart theorem:

$$t_{044}\left\langle \begin{matrix} N \\ n \end{matrix} \middle| T^4_0 \middle| \begin{matrix} N \\ n \end{matrix} \right\rangle = t_{044} \begin{pmatrix} 4 & N & N \\ 0 & n & -n \end{pmatrix} (N\|4\|N)\,. \tag{2.7a}$$

Then Edmond's asymptotic approximation[33] gives

$$\begin{pmatrix} k & N & N \\ 0 & n & -n \end{pmatrix} \simeq [P_k(\cos\theta^N_n)], \tag{2.7b}$$

where the angular-momentum cone angle is

$$\theta^N_n = \cos^{-1}\{n/[N(N+1)]^{1/2}\}, \tag{2.7c}$$

and this leads to the construction of Fig. 5. This is a good approximation[34,35] for high N *and* n.

The fact that high-angular-momentum vectors would tend to become localized first on one symmetry axis then on another is one of the more surprising results to come out of the study of tensor interactions and fine structure. As indicated in Figs. 1(b) and 5(b) the right-hand three-quarters of the $P(88)$ fine structure is due SF_6 molecules balanced on fourfold symmetry axes of rotation with a sequence $n_4 = 88, 87, 86, \ldots$ of rotational quantum components on that axis. The remaining quarter of $P(88)$ is due to molecules balanced on threefold axes with three-fold axial quanta $n_3 = 88, 87, 86, \ldots$. The angular-momentum cone for $N=88$ and N_4 (or n_3) $=88$ has angle of only $\theta^{88}_{88} = 6.1°$ according to (2.7c), and corresponds to nearly stationary energy in the maximal directions (fourfold axes) or minimal directions (threefold axes). The same is true, but to a lesser degree, for wider or less localized cones associated with lower values of n. The lowest n_4 values correspond to an angle θ^N_n of about 36° from the fourfold axes. This happens for $P(88)$ in Fig. 1(b) where the n_4 sequence ends with $n_4 = 72$ and $\theta^{88}_{72} = 35.6°$ and for $P(54)$ in Fig. 1 of article I where the fourfold sequence ends with $\theta^{54}_{44} = 36.2°$. The lowest threefold n_3 values occur when $\theta^N_{n_3}$ is around 22°.

For high N and n the SF_6 and CF_4 molecules can behave like symmetric tops.[14,34] The uncertainty angle θ^N_n is small enough so that asymmetric parts of the tensor such as $(T^4_4 + T^4_{-4})$ are small, and the symmetric (T^4_0) part traps the angular momentum N in a state for which n is a good approximate quantum number. The angle θ and quantum num-

bers n_3 and n_4 will be used in the theory of nuclear spin-rotation interactions.

The following approximate formula for pure rotational fine structure levels is a better approximation than that given by Eq. (2.7b) and is very accurate in the limit of high N and n. (It has slightly different forms for fourfold and threefold sequences.):

$$\langle H\rangle_0 = \langle H_{\text{scalar}}\rangle_0 + \langle H_{\text{tensor}}\rangle_0 = \langle H_{\text{scalar}}\rangle + \begin{cases} t(N,n_4) & \text{for fourfold sequence} \\ -\frac{2}{3}\,t(N,n_3) & \text{for threefold sequence.} \end{cases} \tag{2.8a}$$

Either form uses the fourth-degree polynomial

$$t(N,n) = (t_{044}/2)\,[3(N+2)(N+1)N(N-1) - 5n^2(6N^2+6N-5) + 35n^4], \tag{2.8b}$$

which is the numerator polynomial of the $3j$ coefficient in Eq. (2.7a). Dorney and Watson[13] noted the $3j$ dependence of computed tensor eigenvalues. Even more accurate tensor eigenvalue formulas have been given[34,35] when small n mixing is considered.

Bordé *el al.*[6] have experimentally found the very small value $t_{044} = 5.7$ Hz for the pure rotational tensor constant. Nevertheless, this small value gives quite large splittings for high N because of the fourth degree polynomial. The N-level fine-structure splitting between the highest ($n_4 = N$) fourfold rotational level and the lowest ($n_3 = N$) threefold level is given by

$$\Delta E(N) = \tfrac{5}{3}t(N,N) = (5t_{044}/3)(4N^4+2N^3+11N^2-6N). \tag{2.9}$$

This varies from 0.3 MHz for $N = 10$ to 2.2 GHz for $N = 88$.

Approximate formulas for excited rovibrational fine-structure levels and for spectra such as Fig. 1(b) involve additional constants (mainly t_{244}), but the same $t(N,n)$ polynomial. Some examples of fine structure line frequency formulas are given in Appendix A and in more detail in Galbraith *et al.*[34]

C. Superfine structure

The preceeding theory of fine structure gave a picture of SF_6 molecules balanced or localized on single rotation axes. Eighteen of the left-hand fine-structure lines in Fig. 1(b) and 1(c) are labeled by quanta $n_4 = 88, 87, \ldots, 73$, or 72 of rotation around a fourfold axis, while seven of the right-hand lines are labeled by quanta $n_4 = 88, 87, \ldots, 83$, or 82 of rotation around a threefold axis. The fourfold states correspond to momenta localized around maxima or hills of the effective energy plot in Figs. 4 and 5(b) while the threefold states correspond to momenta localized around the valleys or minima in between the hills.

However, there are six equivalent hills or fourfold axes in Fig. 4 and eight equivalent valleys or threefold axes. If a molecule is initially rotating on a single axis it is possible that the angular momentum might tunnel to one of the equivalent neighboring axes. This tunneling or precessional tumbling of the molecule is most likely if the initial momentum n is one of the lower allowed values so that the uncertainty angle θ_n^N is larger. The tunneling rate is proportional to the splitting of the fine-structure line or cluster into the superfine structure. This is indicated by prototypical spectra in Fig. 1(c).

Superfine structure usually requires sub-Doppler resolution to observe it in heavy XY_4 and XY_6 molecules. The first observations of superfine structure were made by Rabinowitz *et al.*[36] in the 10 μm region of SiF_4.[37] More recently Loete *et al.*[38] and Bordé *et al.*[4-6] have done further studies of the 10-μm region of SF_6. The spectra obtained by Bordé *et al.*[5] has the highest resolution obtained so far.

The superfine structure indicated in Fig. 1(c) is based upon theory since no sub-Doppler spectra has been taken yet in the 16-μm region. However, the predictions are similar to ones that have been observed around 10 μm. They are based upon the extremely accurate computer calculations by Krohn.[39] His calculations of superfine splittings have been correct in all cases that have been observed so far. It is important to note that superfine splitting decreases rapidly as n increases. In Fig. 1(c) it ranges from several megaHertz down to less than one cycle in forty-five centuries, i.e., 6×10^{-12} Hz for $n_4 = 88$. It may be a long time before such high-n cluster splitting is observed!

However, the phenomenological theory[40,41] is the same for cluster splittings that are large or small. A brief review of the theory of (A,T,E) clusters will be given since they have analogs which will be discussed later in connection with superhyperfine structure. The (A,T,E) cluster can be described by the eigenvectors of a tunneling pseudo-Hamiltonian matrix:

$$\langle H\rangle = \begin{array}{c} \begin{matrix} |1\rangle & |2\rangle & |3\rangle & |4\rangle & |5\rangle & |6\rangle \end{matrix} \\ \begin{bmatrix} H & 0 & -S & -S & -S & -S \\ 0 & H & -S & -S & -S & -S \\ -S & -S & H & 0 & -S & -S \\ -S & -S & 0 & H & -S & -S \\ -S & -S & -S & -S & H & 0 \\ -S & -S & -S & -S & 0 & H \end{bmatrix} \end{array} . \qquad (2.10)$$

The important parameter is the amplitude $(-S)$ for the angular momentum to tunnel between any two neighboring hills in Fig. 4. Each state corresponds to an angular-momentum coherent state in which the momentum is localized on one of the six hills. Allowing only nearest-neighbor tunneling leads to a prediction for the form of the cluster-splitting eigenvalue spectrum. The eigenvectors

$$\begin{aligned} |A_1\rangle &= (1 \quad 1 \quad 1 \quad 1 \quad 1 \quad 1)/\sqrt{6}\,, \\ |T_1,1\rangle &= (0 \quad 0 \quad 1 \quad -1 \quad 0 \quad 0)/\sqrt{2}\,, \\ |T_1,2\rangle &= (0 \quad 0 \quad 0 \quad 0 \quad 1 \quad -1)/\sqrt{2}\,, \\ |T_1,3\rangle &= (1 \quad -1 \quad 0 \quad 0 \quad 0 \quad 0)/\sqrt{2}\,, \\ |E,1\rangle &= (1 \quad 1 \quad -\tfrac{1}{2} \quad -\tfrac{1}{2} \quad -\tfrac{1}{2} \quad -\tfrac{1}{2})/\sqrt{3}\,, \\ |E,2\rangle &= (0 \quad 0 \quad \tfrac{1}{2} \quad \tfrac{1}{2} \quad \tfrac{1}{2} \quad -\tfrac{1}{2})\,, \end{aligned} \qquad (2.11)$$

correspond to the eigenvalues

$$\langle A_1|H|A_1\rangle = H - 4S,\ \langle T_1,j|H|T_1,j\rangle = H,$$

and

$$\langle E,j|H|E,j\rangle = H + 2S, \qquad (2.12)$$

where S determines the splitting and H is the energy of the fine-structure level before splitting. [Equation (2.8)] is an approximate formula for the H parameters.] A positive S parameter corresponds to an (A_1, T_1, E) ordering with a 2:1 ratio between $A_1 - T$ and $T_1 - E$ splittings. This is indicated in Fig. 1(c) for the cluster labeled by $n_4 = 76$ and 72. The total $A_1 - E$ splitting is $6S$. The magnitudes of the splittings are 12 kHz and 4.6 MHz, respectively, for these two clusters. Approximate formulas[35] have been given for the tunneling parameters S in terms of molecular constants t_{044} or t_{244}. The S formulas which have been found so far are not as accurate as the H formulas. More work is needed on the details of tunneling.

Similar tunneling pseudo-Hamiltonians may be constructed for each type of cluster.[40,41] Subgroup correlation tables may be used to determine which species A_1, A_2, T_1, T_2, or E belong to a given cluster. The subgroups which are relevant for the discussion of the clusters in Fig. 1(c) are C_3 or C_4. These are the effective symmetry subgroups of the molecule if it is stuck rotating on a single threefold or fourfold axis, respectively. Indeed, many of the high-n tunneling rates are so tiny that these symmetries can be regarded as *de facto* if not *de jure*. In this case it may be said that the octahedral molecules have undergone *spontaneous symmetry breaking* down to C_3 or C_4 symmetry.

The correlation of C_3 symmetry species 0_3, 1_3, and 2_3 or C_4 symmetry species 0_4, 1_4, 2_4, and 3_4 with octahedral species are given by the following tables:

$A_1 \downarrow C_3 =$	0_3	1_3	2_3
A_2 =	1	·	·
E =	1	·	·
T_1 =	·	1	1
T_2 =	1	1	1
	1	1	1

, (2.13a)

$A_1 \downarrow C_4 =$	0_4	1_4	2_4	3_4
A_2 =	1	·	·	·
E =	·	·	1	·
T_1 =	1	·	1	·
T_2 =	1	1	·	1
	·	1	1	1

. (2.13b)

The desired clusters correspond to columns of the correlation tables. For example, a fine-structure line labeled by $n_4 = 88 = 0 \bmod 4$ belongs to the 0_4 column which is (A_1, T_1, E). Similarly, an $n_3 = 88 = 1 \bmod 3$ cluster belongs to the 1_3 column which is (T_1, E, T_2). These two clusters form the limbs of the $P(88)$ line in Fig. 1(c).

An example of a (T_1, E, T_2) cluster in $Q(38)$ is shown in the spectrum by Bordé *et al.*, in Fig. 6. The tunneling model[41] predicts that E should fall exactly halfway between T_1 and T_2, and this is observed. The heights and structure of the T_1, E, and T_2 lines as well as the small signal between T_1 and E will be discussed in connection with hyperfine structure.

The superscripts on octahedral species (e.g., E^0, T_1^6, etc.) belong to an earlier numbering system. It was made by Moret-Bailly[29] before the significance of the cluster quantum numbers n_3 or n_4 was recognized. The numbering begins with zero and counts identical species $E^0, E^1, E^2, \ldots, E^6$, or $T_2^0, T_2^1, T_2^2, \ldots, T_2^8$, and so forth, which appear from limb to limb in a fine-structure pattern such as $Q(38)$. It is easy to see that (T_1^0, E^0, T_2^0) belongs to the $n_3 = 38$ cluster since it is the first one on the threefold limb. However, it is less conven-

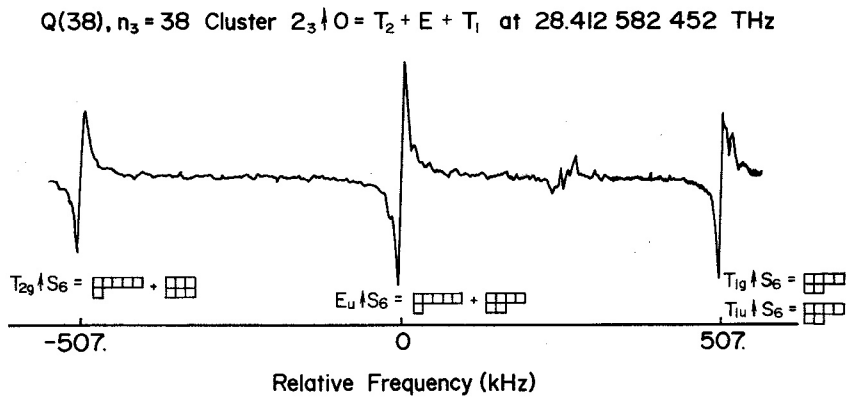

FIG. 6. Example of superfine structure in a (T_1,E,T_2) cluster. Spectra obtained by Bordé *et al.* (Refs. 4 and 6) belong to the $Q(38)$, $n_3=38$ part of the ν_3 bands of SF_6. The feature between T_1 and E was shown by Bordé *et al.* to be a crossover resonance as explained in Sec. II D.

ient to identify an inside cluster such as (A_1^2, T_1^7, E^5) with $n_4=36$. Symmetry wheels such the ones given in Fig. 8 of Ref. 14 help to convert Moret-Bailly numbers into physically meaningful quantum numbers. Note also that Moret-Bailly counting begins with threefold or fourfold limbs for N even or odd, respectively.

Finally, it is important to remember that *spectral* clusters are the result of differences or transitions between *level* clusters. Nevertheless, the spectra mimic the *form* of the levels when the rovibronic species A_1, A_2, T_1, T_2, and E are good quantum labels and are conserved along with rotor momentum N and aximuthal cluster number n_3 or n_4. This is shown by a transition nomogram for $\nu_4-P(88)$ in Fig. 7. The initial $(J=N=88)$ levels are plotted along the vertical axis of Fig. 7 as they would appear if the tensor centrifugal dis-

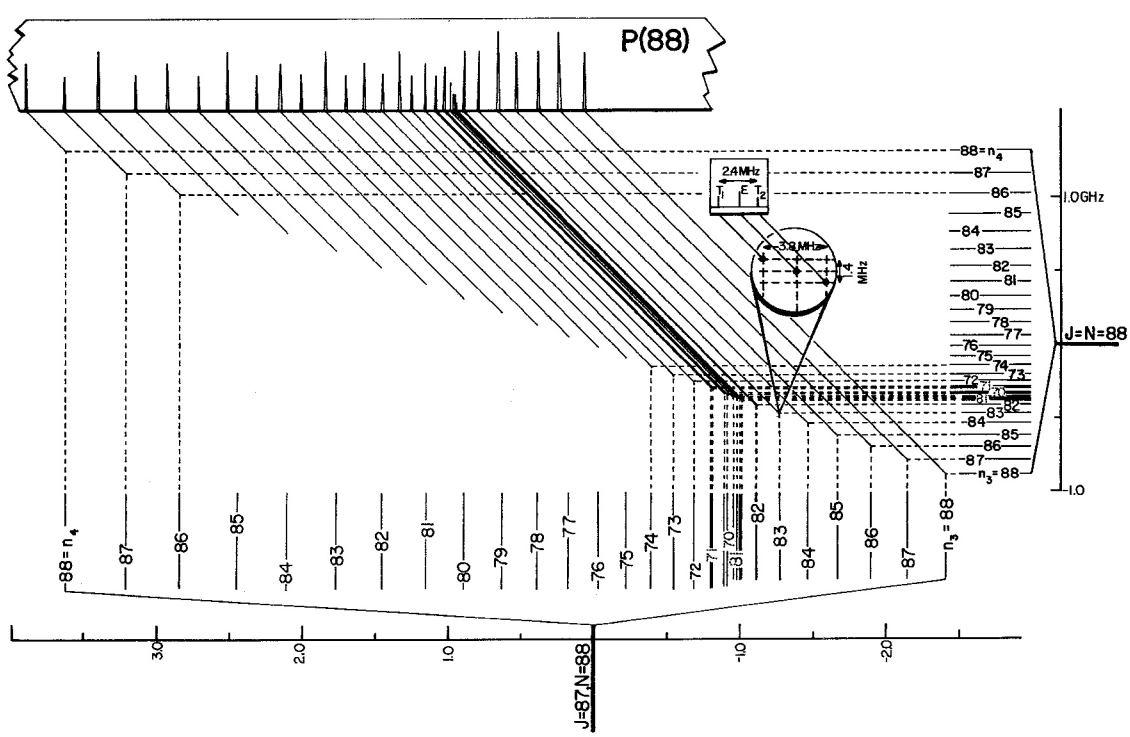

FIG. 7. Transition nomogram for the $\nu_4-P(88)$ resonances in SF_6. If cluster quantum numbers are conserved the fine structure spectrum for $P(88)$ has the same form as the initial or final level diagrams which are plotted along the lower right-hand or lower side, respectively. The same is true for the superfine spectra such as the $(n_3=83, T_1, E, T_2)$ example (see inset) as long as the individual species labels are conserved.

tortion constant was $t_{044} = 5.7$ Hz. The excited $(J = 87, N = 88)$ levels are plotted along the horizontal axis on the lower edge of Fig. 7 as they would appear if the tensor Coriolis constants were $t_{134} = 166$ Hz and $t_{224} = -6.42 \times 10^4$ Hz as given in Appendix A through Eqs. (A6) and (A8). (Note that ν_4 constants still have uncertainties of about 5%.) The transitions which give the $P(88)$ fine structure are indicated by 45° lines. Each line begins at the intersection of a pair of levels which participate in an allowed transition, and it ends on the corresponding line in the facimile spectrum along the upper edge of Fig. 7. The line heights are determined by hyperfine structure still to be discussed (Sec. II D).

One surprising thing about cluster transitions such as the $P(88)$ transitions in Fig. 7 is that relatively few take place. Only those level cluster intersections with the same n and the same *type* of n (i.e., threefold n_3 or fourfold n_4) belong to transitions with observable intensity. This is one of the results of spontaneous symmetry breaking from octahedral O_h down to D_{4h} or D_{3d}. There seem to be increased degeneracies, i.e., clusters, and there seem to be increasingly strict selection rules. In other words there are effects which might have been ascribed to a hidden *higher* symmetry. The usual octahedral symmetry rules only restrict transitions between different A, T, or E species.[14] They would allow *one-thousand two-hundred and sixty-three* transitions in $P(88)$ alone. Every level cluster intersection in Fig. 7 may belong to at least one allowed transition according to the usual O_h rules!

A comparison of the facimile $P(88)$ spectrum in Fig. 7 to the observed one in Fig. 1(b) shows that the latter has quite a number of small "extra" peaklets scattered in and around the main peaks. However, experiments have shown that these are due to "hot band" transitions from thermally excited initial states, for example, $\nu_2 \rightarrow \nu_2 + \nu_4$. (In fact it is this sort of transition in CF_4 which makes it a laser medium.) The little peaks drop much more quickly than the main ones when the temperature is lowered.

The $P(88)$ fine and superfine spectrum is a good example of the tremendous simplification resulting from the cluster superdegeneracies and superselection rules. However, it should be remembered that the degeneracies and selection rules resulting from spontaneous symmetry breaking are only approximate.[41,35] The tiny superfine splittings such as the (T_1, E, T_2) splitting indicated in Fig. 7 or Fig. 1(c) are always present. However, the superfine splittings and the transitions prohibited by superselection rules decrease exponentially with n.[35] The latter decrease very quickly; even $P(7)$ in CH_4 seems to obey superselection rules.[32] (See for example, Fig. 37 in Ref. 14.)

The levels shown in Fig. 7 can be obtained by direct computer diagonalization[39] or by series of approximate formulas[34] beginning with the lowest order of approximation given in Appendix A. Higher-order approximate formulas show to what extent the states of different N and n_3 (or n_4) are mixed by the Hamiltonian.[31,34] Using these results one can calculate the tiny transitions that appear to be forbidden by superselection rules as well as by ordinary selection rules.

While the onset of spontaneous symmetry breaking seems to give more strict types of selection rules in one sense, a more detailed theory shows that quite the opposite happens. In fact, the well known selection rules prohibiting transitions between different octahedral spin species (i.e., $A_1 \rightarrow A_2, A_1 \rightarrow E, \ldots, T_1 \rightarrow T_2$) turn out to be strongly broken by nuclear spin-rotation interactions in the presence of clustering. This is discussed briefly in the following sections and computed in detail throughout the remainder of this article. The first example used will focus on the (T_1, E, T_2) cluster studied by Bordé (Fig. 6). This cluster is similar to the one shown in the inset of Fig. 7 with at least one important difference: The ground-level cluster for Bordé's spectra has much less splitting.

D. Hyperfine structure (Case 1)

Each SF_6 superfine line labeled by octahedral species A_1, A_2, T_1, T_2 or E has a hyperfine structure or nuclear spin splitting as indicated in lower center portion of Fig. 1(c) and 1(d). (This portion is labeled by case 1 in the figure.) These species are generalizations of "ortho" and "para" species of H_2, but they are more complicated since they involve the permutational symmetry of six fluorine nuclei instead of just two hydrogens. They also have more complicated hyperfine structure than is shown for CF_4 in Fig. 1(e) of article I.

An important difference between SF_6 and simpler H_2 or CF_4 molecules is that stable SF_6 fails to exercise more than a small fraction of its total permutational symmetry. There are $6! = 720$ permutations in the permutation group S_6. Instead, it remains frozen in a subgroup O of twenty-four octahedral rotations. Here spontaneous symmetry breaking occurs when the octahedral molecules is formed. Hence, each octahedral A_1, A_2, T_1, T_2, or E level may be correlated with a cluster of levels belonging to S_6 symmetry species. The S_6 symmetry species are labeled by tableaus in each of the rows of the correlation Table I. The tableaus, in turn, label the nuclear spin states of total spin $I = 3$, 2, 1, and 0.

TABLE I. Permutational - octahedral correlation table S_6+O_h. Only the last four rows are relevant for spin-$\frac{1}{2}$ nuclei.

Fermi nuclei	Bose nuclei	A_{1g}	A_{1u}	A_{2g}	A_{2u}	E_g	E_u	T_{1g}	T_{1u}	T_{2g}	T_{2u}	
		1	·	·	·	·	·	·	·	·	·	
		·	·	·	·	1	·	·	1	·	·	
		1	·		·	1	·	·	·	1	1	
		·	·	1	·	·	·	1	1	·	1	
		·	·	1	1	·	·	·	1	·	·	
		·	·	·	·	1	1	1	1	1	1	
		·	1	·	·	·	·	1	·	1	1	
		1	1	·	·	·	·	·	·	1	·	$I=0$
		·	·	·	1	·	1	1	1	·	·	$I=1$
		·	·	·	·	·	1	·	·	1	·	$I=2$
		·	·	·	1	·	·	·	·	·	·	$I=3$

Spin-$\frac{1}{2}$ nuclei

This correlation table is derived in Ref. 14. It is quite easy to compute and apply this table because one can use powerful tableau counting algorithms. An example is given in Ref. 14 in which the nuclear spin weights associated with hexachloride molecules with spin-$\frac{5}{2}$ nuclei are derived. For spin-$\frac{1}{2}$ nuclei in SF_6 only the bottom four rows of Table I are needed. (Independently, Bordé[42] has given a similar SF_6 correlation in a letter which appeared shortly after Ref. 14.)

For example, consider the A_2 column of Table I. This contains the spin $I=1$ tableau ( ) and the spin $I=3$ tableau ( ) under the odd parity A_{2u} heading. (The even parity A_{2g} column contains no spin states for SF_6.) So A_2 corresponds to a cluster of ten spin states. (A_2 could be called the "ortho" species since it has more spin states than any other species.) An A_2 cluster can be split by two effects. The first effect could be nuclear interchange tunneling, i.e., nuclear permutations outside of the rigid rotations of the octahedron. However, this is astronomically small in the lower states of SF_6. The second effect involves the nuclear spin rotation interaction. This splits the $I=3$ septet on top of the $I=1$ triplet as shown in spectra by Bordé *et al.*,[5] in Fig. 8. There the central triplet is twice as high as the other peaks in the septet. Four A_2 septet-triplets are

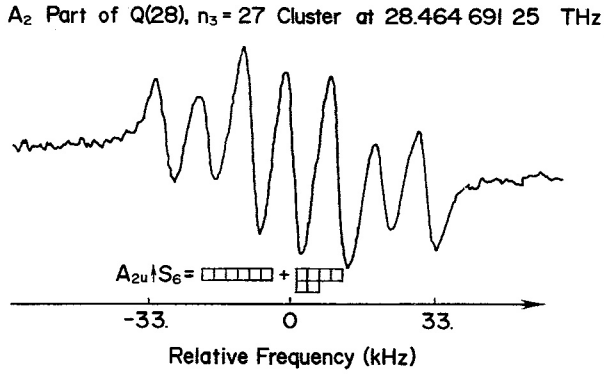

FIG. 8. Example of case-1 hyperfine structure in an A_{2u} line. Spectra obtained by Bordé *et al.*[5] belongs to an $R(28)$, $n_3=27$ cluster (A_1,T_1,T_2,A_2). The other lines in the cluster are off scale since the superfine splitting ($S\sim 88$ kHz) is greater than the hyperfine splitting shown by the figure. Hyperfine multiplets for $I=3$ and $I=1$ are clearly visible.

sketched in the bottom central portion of Fig. 1(d).

The next largest number of spin states is contained under the E (actually E_u) column of Table I. This is drawn as a quintet plus a triplet in Fig. 1(d). Under T_2 (actually T_{2g}) there is a quintet plus a singlet. The last two species T_1 and A_1 each contain both even and odd parity states, i.e., inversion doublets. T_{1u} and T_{1g} each correspond to an $I=1$ triplet. A_{1u} and A_{1g} each correspond to an $I=0$ singlet.

The ratios of line heights for clusters in the fine structure of Fig. 1(b) were mentioned earlier. They are obtained by summing up the number of spin states for each octahedral species in the cluster. One should note the differences between CF_4 and SF_6 fine structure. For example, the spin weights in the $0_4 \updownarrow O \sim A_1 + T_1 + E$ and $2_4 \updownarrow O \sim A_2 + T_2 + E$ clusters are 16 and 24, respectively, for SF_6 while they are both ten for CF_4. The first correct SF_6 spin weight calculation to be published is probably that of Cantrell and Galbraith.[43] The procedure given there is more laborious than the $S_6 \updownarrow O_h$ correlation, and it does not lead as easily into analysis of other hyperfine effects or higher spin nuclei. Also, the $S_6 \updownarrow O_h$ correlation procedure is based upon an unambiguous parity analysis which was not made explicit in Cantrell and Galbraith's calculations.

Parity assignments turn out to be extremely important for hyperfine spectroscopy which contains so called "crossover" resonances. An example of a crossover resonance appears between the E and T_1 lines in the spectrum of a (T_2, E, T_1) cluster in Fig. 6. However, there does not appear to be a resonance between T_2 and E. This is due to the fact that these two SF_6 species have opposite parity. (Recall discussion of Table I.)

Bordé *et al.*[4,6] have shown that the crossover resonance is due to hyperfine mixing of the E_u and T_{1u} species in the cluster. This is probably the first evidence of the anticipated mixing of rovibronic species in clusters.[14-16] The mixing occurs in the ground-state ($N=38$, $n_3=38$) cluster. The fine-structure splitting between the $n_3=38$ and 37 cluster [also a (T_1, E, T_2)] is over 7 MHz as derived from Eq. (2.8) or Krohn's tables.[39] However, the superfine structure splitting between E_u and T_{1u} within the $n_3=38$ cluster is only about 4 kHz. This is less than the splitting caused by the hyperfine interactions (recall Fig. 8) which indicates that they can strongly perturb or mix the clustered species.

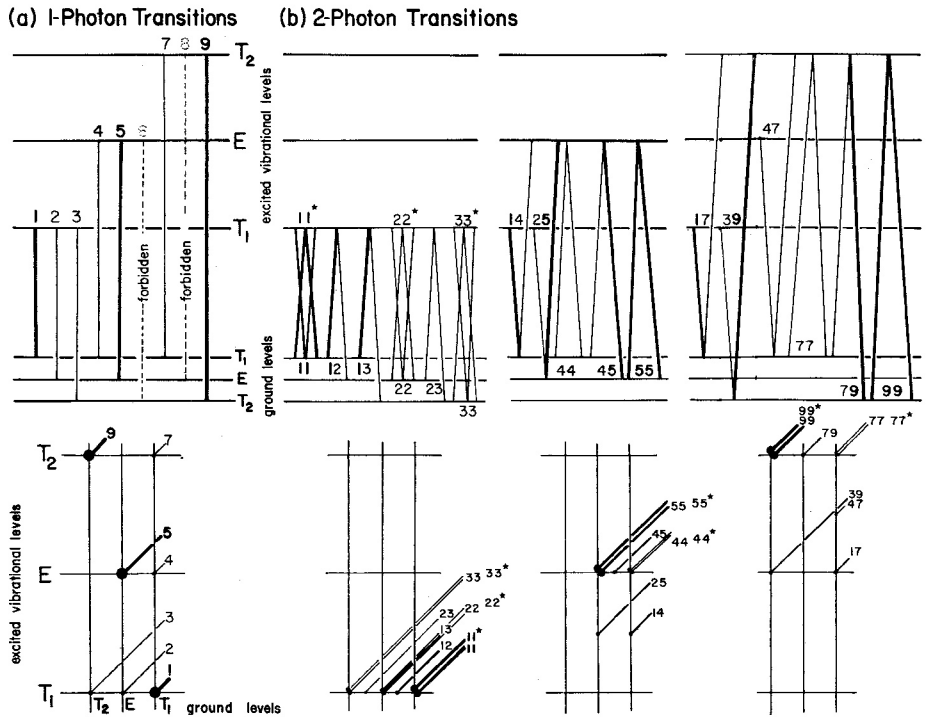

FIG. 9. Levels, transitions, and transition nomograms for displaying saturation absorption spectra. (a) Allowed one-photon transitions between fictitious (T_1, E, T_2) clusters are numbered. Each transition corresponds to a dot at the lower end of a 45° line in the nomogram. The 45° lines correspond to spectral lines. (b) The possible two-photon transitions are labeled by pairs (mn) of numbers. Each pair of equal numbers corresponds to a recoil doublet (nn) and $(nn)^*$. Each pair of unequal numbers corresponds to a crossover resonance (mn) very nearly halfway between any (m) point and (n) point which *share the same level line* in the nomogram.

Since the spectroscopic evidence of species mixing comes in the form of crossover resonances, it is helpful to find convenient ways to picture this phenomenon.[44] This may be done using spectroscopic nomograms as shown in Fig. 9. A sketch of (T_1, E, T_2) cluster levels in the ground and vibrationally excited states are drawn in the upper portion of Fig. 9(a). The scale of the superfine or cluster splittings are greatly exaggerated particularly for the lower cluster, and the hyperfine splittings are suppressed. Otherwise, the drawing would be too complicated to be of much pedagogical value for explaining crossover resonances. Nomograms showing superfine and hyperfine structure are given in Figs. 18 and 19.

Single-phonon transitions are indicated in the usual manner by lines connecting levels in the upper portion of Fig. 9(a). Transitions numbered 1, 5, and 9 correspond to heavy lines since only they would be allowed if rovibronic species were not mixed. The light lines correspond to transitions numbered 2, 3, 4, and 7 which may occur due to hyperfine mixing. Transitions 6 and 8 are forbidden by parity. In the lower portion of Fig. 9(a), the cluster of excited levels intersects the ground-level cluster, and each allowed transition corresponds to a point of intersection. Lines drawn at 45° from the intersections gives a scale model of the spectral lines as in Fig. 7. Now suppose the vertical ground-state levels are much more closely clustered than the excited levels in Fig. 9(a), i.e., let the ground splitting be ~8 kHz while the excited splitting is ~1 MHz as in $Q(38)$. Then there would be just three main spectral lines spread over a megahertz. There would be a T_1 line with transitions 1, 2, and 3 all within a few kilohertz of each other, an E line containing closely spaced transitions 4 and 5, and finally a T_2 line made up of transitions 7 and 9. However, the crossovers and other hyperfine effects will not appear unless a two-photon process such as saturation absorption spectroscopy is used.

The first hyperfine spectra of CH_4 was obtained by Hall and Bordé[45] using He-Ne laser saturation spectroscopy. Saturation spectroscopy involves two oppositely propagating beams of light with the same frequency. One beam is called the *saturating* beam since it can saturate transitions that would have otherwise absorbed part of the so-called *probing* beam going the other way. As the frequency of each beam draws near a molecular resonance there is a abrupt dip in the probing beam absorption. (This is called the "Lamb dip.") Then the saturating beam is in resonance with the same Doppler population of molecules as the probing beam. Since the beams are counterpropagating they will have opposite Doppler shifts with respect to any molecule moving with nonzero momentum k along the beam axis. Ordinary saturation spectroscopy eliminates Doppler broadening by probing the population around $k \cong 0$. Crossover spectroscopy uses Doppler shifts for $|k| \gg 0$ to saturate one transition while probing a different one. These are all done with a single laser.

If one plots the energy levels from Fig. 1(a) as a function of molecular momentum k,

$$\omega_j(k) = \omega_j + \hbar k^2/2m ,$$

it is easier to visualize the effects of Doppler shifts. In Fig. 10 an exaggerated plot of energy levels shows transitions as slanted lines. The vertical component of a slanted line is the photon frequency ω while the horizontal component is its momentum $k = \omega/c$. The slope $\omega/k = c$ is positive or negative depending on whether the transition is caused by the saturating or probing beam. (Bordé *et al*[46] have used Feynman-like energy-momentum diagrams in density-matrix treatments of laser spectra.)

Suppose the laser is tuned so that some molecules are in resonance for transition 1 $(T_1 \leftarrow T_1)$ with both the saturating beam propagating along $+k$ and the probing beam propagating along $-k$.

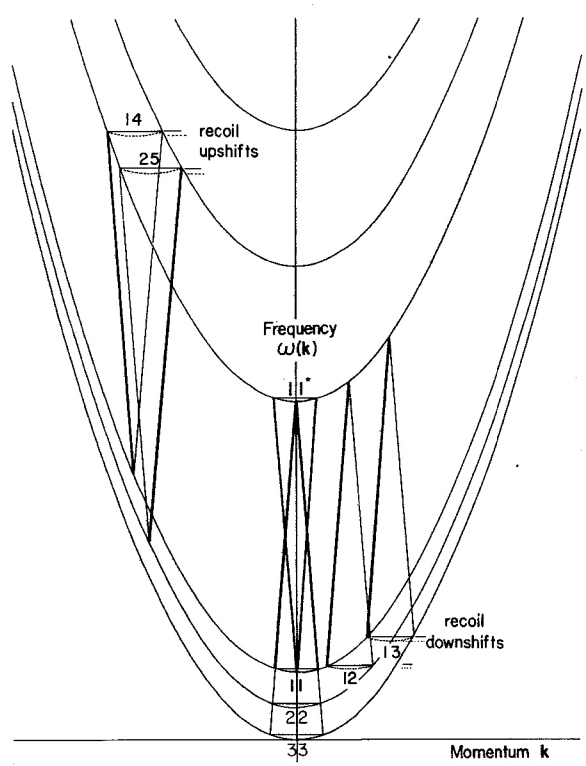

FIG. 10. Energy versus momentum plot for fictitious (T_1, E, T_2) clusters. Doppler shifts are depicted graphically so that the positions of crossovers and the magnitudes of recoil shifts can be visualized.

These conditions are met for two frequency tunings that are slightly shifted above and below the one-photon transition frequency ω_1 by $\pm\hbar k_1^2/2m = \pm\hbar\omega_1^2/2mc^2$. The resulting two-photon transitions involve $k=0$ molecules and are indicated by triangles labeled 11 and 11* in Fig. 10, and in the upper left-hand portion of Fig. 9(b). The resulting spectra is called a recoil doublet.[47] It is labeled 11 and 11* in the lower lefthand portion of Fig. 9(b).

Now suppose that the laser is tuned so that some molecules are in resonance for transition 2 ($E \leftarrow T_1$) with the probe beam ($-k$) but still in resonance with the saturating beam ($+k$) for transition 1. These conditions are met for a frequency tuning that is slightly less than the average $\omega_{12} = (\omega_1 + \omega_2)/2$ of the two one-photon transition frequencies. This is the frequency,

$$\omega_{12}(\text{crossover}) = \omega_{12} - \hbar\omega_{12}^2/2mc^2$$

of the two-photon crossover process involving ($+k$) moving molecules. It is indicated by a triangle labeled 12 in Figs. 10 and 9(b). The 12 line is the next one above the 11 doublet in the lower portion of Fig. 9(b).

All the other possible two-photon transitions are indicated in Fig. 9(b). A simple rule for drawing the saturation spectral nomogram is evident. Besides the main transitions (ii) at the intersections of levels there can be a crossover line (ij) originating halfway between each allowed intersection (ii) and (jj). It is then easy to remember which way the recoil shifts go. Imagine the 45° lines that represent saturation spectra are strings that can slide a little bit on their levels. If the strings are pulled the attachment points always slide in the direction of the recoil shifts. For example, the crossovers (14) and (25) would be upshifted from their respective halfway points in the lower central portion of Fig. 9(b). The upshifts are indicated in Fig. 10.

In SF_6 spectra the recoil shifts are too small to observe. They have been seen by Hall[45] and Bordé[46] in CH_4 and I_2 spectra. The structure of crossovers (14) and (25) which is visible in Fig. 6 halfway between the (11) or T_1 line and the (55) or E line is due to hyperfine structure. Fig. 9(b) indicates that the crossover (47) in the lower right-hand portion of Fig. 9(b) would appear by itself halfway between the (55) or E and (99) or T_2 lines when the ground cluster (T_2, E, T_1) is nearly degenerate (i.e., ~8 kHz). However, SF_6 saturation line (47) will not occur since the one-photon transitions numbered 4 ($E_u \leftarrow T_{1u}$) and 7 ($T_{2g} \leftarrow T_{1g}$) have no species in common since T_1 is a parity doublet (T_{1u}, T_{1g}). This shows one way that saturation spectroscopy can give information about structure that it might not resolve directly. Crossovers (23) and (17) would be missing, too, but their absence might not be noticed if lines near (11) and (55) could not be resolved.

E. Superhyperfine structure (Case 2)

The cluster tunneling parameters (S) and resulting superfine splitting of level clusters decreases exponentially with increasing cluster quantum numbers n_3 or n_4. Meanwhile, the principal nuclear spin-rotation interaction or hyperfine splitting increases with n_3 or n_4. When the superfine S amplitude in negligible in comparison to hyperfine energies for a given level cluster, then that cluster belongs to case 2. This is the case in which rovibronic species may be strongly mixed and the labels A_1, A_2, T_1, T_2, or E or the total nuclear spin quantum number I may not be good. In this case the eigenstates, the levels, and the spectra fall into much different groupings or clusters as indicated in Fig. 1(d) and 1(e). The details of these still unexplored clusters will be called *superhyperfine structures*. Most of the following sections of this article will be devoted to correlating the case-2 level cluster states with the separate species which belong to the better known case-1 clusters.

Cluster splitting and hyperfine level structure of an excited state may belong to different case than the vibronic ground state or pure rotational levels. The $Q(38)$; $n_3 = 38$ transition (Fig. 6) starts from a near case-2 ground-state cluster ($E^{T_1} - E^{T_2} \sim 8$ kHz), but it ends in a case-1 excited state ($E^{T_1} - E^{T_2} \sim 1$ MHz). The ground-state splittings vary approximately as $\sim t_{044}N^4$ while the excited splittings vary roughly as $\sim t_{224}N^2$. This is true for fine structure (see Eq. (2.8) and Appendix A) as well as superfine structure; however, superfine structure also has an *exponential* dependence on n_3 or n_4. The number of case-2 clusters depends much more strongly on having high n_3 or n_4 than on having low t_{ijk} constants.

Despite the small value of t_{044} (~5.6 Hz) in SF_6 the overall fine structure splitting in the ground rotational ($N=88$) level is over 2.2 GHz according to Eq. 29. This is the same order of magnitude as the 3.7-GHz splitting of the fine spectrum in Fig. 1(b), or the 6-GHz splitting of the ($J=87$, $N=88$) excited levels as shown in Fig. 7. Nevertheless, the predominance of high n_4 and n_3 values means more case-2 clusters. For $N=88$ the ground and vibrationally excited P and R manifolds have about the same number of case-2 clusters. In Fig. 1(d), there are eleven or twelve case-2 fourfold spectral clusters and two or three of the threefold variety.

In the case-2 limit, when the axis tunneling is negligible ($S \sim 0$), the angular momentum can be

regarded as localized on one axis either a fourfold or threefold axis. In addition, if n_4 (or n_3) is near maximum ($n \sim N$) then the angular uncertainty is minimum. In this limit the rotor axis of rotation is fixed in the laboratory and it behaves like a classical spinning top. There is little distinction between lab-coupled and body-coupled momentum states.[14] Then the nuclear spins tend to align or antialign with a more or less fixed axis and resultant internal magnetic fields.

The case-2 situation is analogous to that which occurs in magnetic resonance experiments involving several coupled spins. A dominant fixed-field perturbation splits the energy levels into clusters according to the number of up and down spins, i.e., n spin-up in the first cluster, $n-1$ spin-up and one spin-down in the second cluster, and so forth. Then the local environment and spin-couplings cause additional shifts and splittings, and this will determine, the superhyperfine structure indicated in Fig. 1(e).

The analysis of superhyperfine (shf) structure in the remaining sections will be similar to that of superfine (sf) structure. Various tunneling amplitudes and other parameters will be defined for approximate pseudo-Hamiltonians for each type of cluster. The shf parameters will be analogous to the sf parameters H and $(-S)$ introduced in Eqs. (2.10)–(2.12). [Also, the sf parameters enter in the correlation between case 1 (S large) and case 2 ($S=0$).] These phenomenological parameters can be related to a smaller set of conventional molecular constants just as the H's and S's for all the clusters can be related to a single set of tensor (t_{044}, t_{224}, etc.) constants.

The use of multiple sets of phenomenological parameters is one thing which distinguishes the analytic approach. The parameters correspond to energies and tunneling amplitudes of fundamental collective phenomena, and different spectral cluster patterns can be associated with different parameters. In this way small pieces of a spectrum (which is all one should expect for awhile) can be made to yield significant qualitative as well as quantitative information. It is also possible to determine the molecular tensor constants with minimum amount of data and reduce the labor of repeated computer synthesis trials. However, more complete and accurate relations between phenomenological constants and molecular tensor constants are needed for extremely accurate quantitative applications.

In the meantime it is important to look for new qualitative (shfs)-related effects. Since it is analogous to nuclear magnetic resonance (NMR) generalizations of those effects should be examined. NMR spectra is sensitive to molecular structure and dynamics, and it may be that (shfs) results even more so. One should expect rotational "chemical shifts" associated with different spin environments. For example, the octahedral molecule shown rotating on the fourfold axis in Fig. 1(b) has four equatorial nuclei in a different environment than the two nonrotating nuclei on the axis. The same is true for SF_6 nuclear rovibrations around the fourfold axis as shown in Fig. 2. The fourfold rotational shifts will be discussed in Sec. IV along with spin-spin exchange effects.

The difference in environment does not play so much a role for SF_6 molecules rotating on threefold axes since all six nuclei occupy equivalent rotational sites. However, the spin-spin exchange effects become more important. Threefold clusters will be examined in Sec. V. Note that for CF_4 it is the fourfold cluster states which put all the nuclei in equivalent rotational positions.

Several things can make SF_6 superhyperfine structure more complicated and potentially more rich than the analogous NMR spectra of a fixed octahedron. For one thing there is the quantum angular uncertainty of the molecular frame. This will be discussed briefly in Sec. IV and was introduced in article I and elsewhere.[14] In this article detailed solutions will be considered only for the elementary cluster bases with high ($N \sim n$) where this is not so important. Also, there is the Pauli exclusion principle which assigns certain spin states to certain clusters. The analysis of this begins in the following Sec. III for fourfold clusters.

III. SYMMETRY DEFINITION OF TETRAGONAL CLUSTER BASES

The definition of the basis of XY_6 molecular spin-rotation states begins as it did in article I with the cluster states $\left|{}^{Np}_{mn}\right\rangle$. Quantum number m is the component of the nuclear rotor momentum N on a laboratory fixed z axis, while $n=n_4$ is the component on body-fixed fourfold symmetry axis appropriate for defining tetragonal cluster bases. In addition let the cluster bases have definite inversion parity p (=+ or −) associated with the full O_3 orthogonal rotational symmetry.[48] Then, as in I, the internal octahedral symmetry $\overline{O}_h$ or the more general permutational S_6 symmetry is used to define cluster eigenstates. In this section S_6-defined octahedral projection operators will be used. In later sections a more elegant tableau derivation will be discussed.

The problem is to compute efficiently and to interpret the permutational symmetry projected cluster eigenstates:

$$\left| \begin{matrix} N^P\{\mu\} \\ mn\{i\}\{j\} \end{matrix} \right\rangle = \mathbf{P} \begin{matrix} \{\mu\} \\ \{i\}\{j\} \end{matrix} \left| \begin{matrix} N^P \\ mn \end{matrix} 1 \right\rangle . \tag{3.1}$$

The first step involves choosing the tableaus $\{\mu\}$ from the set of S_6 frames which have one or two columns and satisfy the Pauli principle for SF_6. These are the only ones which can be matched later with spin-$\frac{1}{2}$ tableaus $\{\tilde{\mu}\}$ to make states of definite total nuclear spin I. (Recall Table I.) The allowed tableau combinations are the following:

$$\left| \begin{matrix} \{\mu\}\{\tilde{\mu}\} \\ I \end{matrix} \right\rangle = \left| \; I=0 \right\rangle \left| \; I=1 \right\rangle \left| \; I=2 \right\rangle \left| \; I=3 \right\rangle , \tag{3.2}$$

where

$\{\tilde{\mu}\}=$ $\{3,3\}$ $\{4,2\}$ $\{5,1\}$ $\{6\}$

respectively.

A. Tableau defintion of nuclear rotational states

For each tableau one should choose combinations of substates so that the inside tableau $\{j\}$ index in Eq. (3.1) is appropriate for a given cluster base state $\left| \begin{matrix} N^P \\ mn_4 \end{matrix} 1 \right\rangle$. Since the tetragonal cluster states will be discussed first it will be convenient to construct tableau states of S_6 to be compatible with tetragonal symmetry subgroups $D_{4h} \supset D_{2h}$ of subgroup $O_h \subset S_6$. (Hence forward, the usual overline designation $(\overline{D}_{4h})$ for molecular fixed or body defined symmetry groups and operators will be deleted.) The transformation is made easier if the full octahedral-tetragonal symmetry chain $S_6 \supset O_h \supset D_{4h} \supset D_{2h}$ is exploited one link at a time. Some of the symmetry operators in these subgroups are listed in Fig. 11 and related to the permutations of the six nuclei $\{a,b,c,d,e,f\}$. The numbers $(1,2,\ldots,6)$ in Fig. 11 label states in which the nuclei reside, as in article I.

The first link in the chain involves 180° rotations and rotation-inversions (plane reflections) involving the octahedral coordinate axes and planes.

$$D_{2h}=\{1,R_1^2,R_2^2,R_3^2,I,IR_1^2,IR_2^2,IR_3^2\} . \tag{3.3}$$

According to the notation of Ref. 41 the opera-

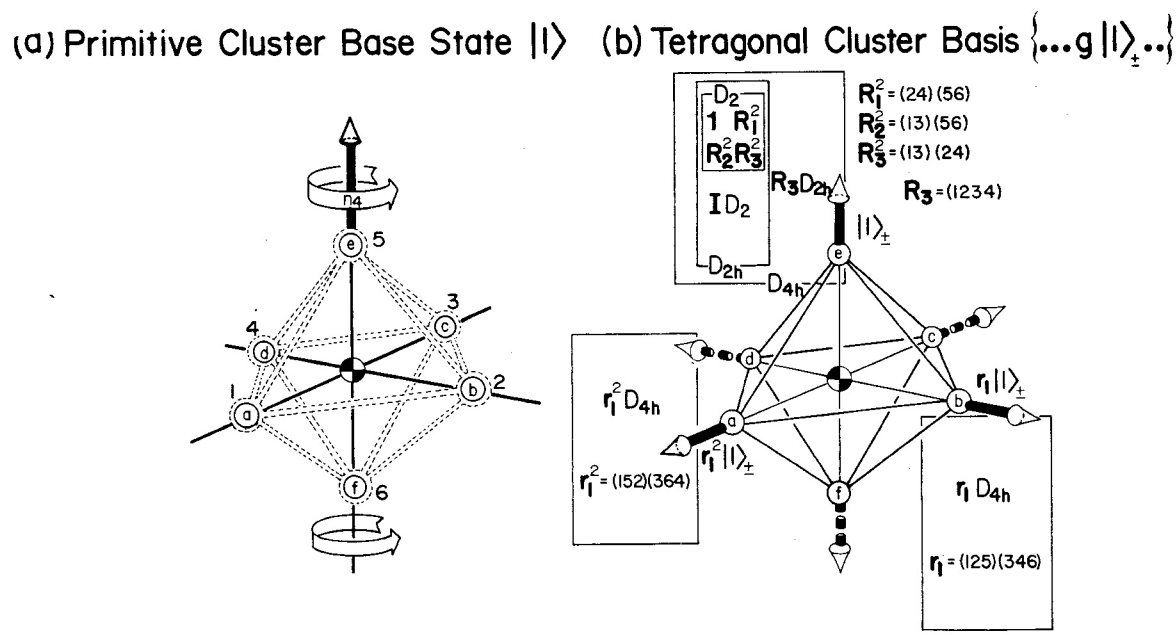

FIG. 11. XY_6 molecule rotating on fourfold symmetry axes and coset structure appropriate for tetragonal cluster bases. Labeling of cluster states depends upon which nuclei $\{a, b, \ldots, f\}$ are in which single particle states $\{1, 2, \ldots, 6\}$. (a) Laboratory view of the first cluster base state $|1\rangle$; (b) Body view of the six positions of the rotor momentum N for the six cluster base states $g|1\rangle$.

tions R_1^2, R_2^2, and R_3^2 are 180° rotations around the first (x), second (y), and third (z) octahedral fourfold axes. The effect of the y flip is given by

$$\mathbf{R}_2^2 \left| \begin{matrix} N^p \\ mn \end{matrix} 1 \right\rangle = (-1)^{N-n} \left| \begin{matrix} N^p \\ m-n \end{matrix} 1 \right\rangle , \tag{3.4}$$

while a 90° z rotation gives

$$\mathbf{R}_3 \left| \begin{matrix} N^p \\ mn \end{matrix} 1 \right\rangle = e^{\pi n i/2} \left| \begin{matrix} N^p \\ mn \end{matrix} 1 \right\rangle , \tag{3.5}$$

and the effect of inversion depends on the parity (p):

$$\mathbf{I} \left| \begin{matrix} N^p \\ mn \end{matrix} 1 \right\rangle = (-1)^p \left| \begin{matrix} N^p \\ mn \end{matrix} \right\rangle . \tag{3.6}$$

It is convenient to convert the primitive octahedral clusters states $|1\rangle$ to states $|1\rangle_\pm$ which are eigenstates of the D_{2h} operators. The D_{2h} eigenvectors are the following combination:

$$\left| \begin{matrix} N^p \\ m|n| \end{matrix} 1 \right\rangle_+ \equiv \left(\left| \begin{matrix} N^p \\ mn \end{matrix} 1 \right\rangle + \left| \begin{matrix} N^p \\ m-n \end{matrix} 1 \right\rangle \right) \Big/ \sqrt{2}$$
$$\equiv |1\rangle_+ , \tag{3.7a}$$

$$\left| \begin{matrix} N^p \\ m|n| \end{matrix} 1 \right\rangle_- \equiv i \left(\left| \begin{matrix} N^p \\ mn \end{matrix} 1 \right\rangle - \left| \begin{matrix} N^p \\ m-n \end{matrix} 1 \right\rangle \right) \Big/ \sqrt{2}$$
$$\equiv |1\rangle_- . \tag{3.7b}$$

The eigenvalues of R_2^2, R_3^2, and I determine the D_{2h} symmetry properties completely (note that $R_1^2 = R_2^2 R_3^2$):

$$\mathbf{R}_2^2 |1\rangle_\pm = \pm (-1)^{N-n} |1\rangle_\pm , \tag{3.8}$$

$$\mathbf{R}_3^2 |1\rangle_\pm = (-1)^n |1\rangle_\pm . \tag{3.9}$$

Furthermore, the D_{4h} symmetry properties are determined by (3.8) and (3.9) and the following relation involving the 90° rotation R_3:

$$\begin{aligned} \mathbf{R}_3 |1\rangle_+ &= \cos(\pi n/2) |1\rangle_+ + \sin(\pi n/2) |1\rangle_- , \\ \mathbf{R}_3 |1\rangle_- &= -\sin(\pi n/2) |1\rangle_+ + \cos(\pi n/2) |1\rangle_- . \end{aligned} \tag{3.10}$$

The D_{4h} states are labeled A or B if they are eigenstates of R_3 with eigenvalues (+1) or (−1), respectively. The states $|1\rangle_\pm$ are A states if $n = 0$ mod 4 and B states if $n = 2$ mod 4. For ($n = 1$ mod 4) and ($n = 3$ mod 4) the pair of states $|1\rangle_\pm$ become an E doublet with respect to D_{4h}. The D_{2h} operators R_1^2 and R_2^2 can be used to complete the state labeling.

An A (B) state is labeled A_1 (B_1) or A_2 (B_2) if the eigenvalue of both R_1^2 and R_2^2 is (1) or (−1), respectively. The E states are labeled E_x and E_y if they imitate the D_4 transformation behavior of coordinate vectors x and y, respectively. Table II gives a complete listing of the $D_{4h} \supset D_{2h}$ labeling of the primitive states. Note that the D_{2h} label is A or B depending on whether the eigenvalue of R_3^2 is (1) or (−1), respectively. The D_{2h} subscript is (1) or (2) depending on whether the eigenvalue of R_1^2 is (1) or (−1), respectively.

The subgroup chain labels make it much easier

TABLE II. Tetragonal D_{4h} symmetry representations and labels for primitive cluster bases. N^p is rotor angular momentum and parity, and n is the body component of momentum modulo four.

	$n=0$ $\|1\rangle_+$ $\|1\rangle_-$	$n=1$ $\|1\rangle_+$ $\|1\rangle_-$	$n=2$ $\|1\rangle_+$ $\|1\rangle_-$	$n=3$ $\|1\rangle_+$ $\|1\rangle_-$
$\langle(-1)^N R_2^2\rangle =$	(1) (−1)	(−1) (1)	(1) (−1)	(−1) (1)
$\langle R_3 \rangle =$	$\begin{pmatrix} 1 & 0 \\ 0 & 1 \end{pmatrix}$	$\begin{pmatrix} 0 & -1 \\ 1 & 0 \end{pmatrix}$	$\begin{pmatrix} -1 & 0 \\ 0 & -1 \end{pmatrix}$	$\begin{pmatrix} 0 & 1 \\ -1 & 0 \end{pmatrix}$
N^+ – even:	A_{1g} A_{2g}	E_g E_g x y	B_{1g} B_{2g}	E_g E_g x $-y$
N^- – even:	A_{1u} A_{2u}	E_u E_u x y	B_{1u} B_{2u}	E_u E_u x $-y$
N^+ – odd:	A_{2g} A_{1g}	E_g E_g y x	B_{2g} B_{1g}	E_g E_g y $-x$
N^- – odd:	A_{2u} A_{1u}	E_u E_u y x	B_{2u} B_{1u}	E_u E_u y $-x$

to reduce the tableau representations of S_6 to tetragonally defined representations of the octahedral subgroup. The D_{2h} can be factored to the form

$$\mathbf{P}^6 = (1 \pm R_1^2)(1 \pm R_3^2)(1 \pm I)/8 \tag{3.11}$$

where the permutation definitions of the symmetry operators are given by

$$R_1^2 = (24)(56), \quad R_3^2 = (13)(24), \quad I = (13)(24)(56) \tag{3.12}$$

according to Figure 11. The tableau representations of the D_{2h} generators are found using the Yamanouchi formula (See Appendix A of article I) for the elementary transpositions (12), (23), (45), and (56). The generator transpositions are the following products:

$$(13) = (12)(23)(12), \quad (24) = (23)(34)(23). \tag{3.13}$$

Any of the eight D_{2h} labels $\delta = \{A_{1g} A_{1u} B_{1g} \cdots B_{2u}\}$ are obtained by a given choice of signs in (3.11).

To find which $D_{2h} \subset D_{4h} \subset O_h$ irreps are appearing in each tableau reduction one must correlate the irreps. This is easily done using characters[14] and the results are as follows:

$$\begin{aligned}
\{\widetilde{3,3}\} &\downarrow O_h \sim \mathbf{T}_{2g} \qquad \oplus \mathbf{A}_{1u} \oplus \mathbf{A}_{1g} \\
&\downarrow D_{4h} \sim E_g \qquad \oplus B_{2g} \oplus A_{1u} \oplus A_{1g} \\
&\downarrow D_{2h} \sim B_{1g} \oplus B_{2g} \oplus A_{2g} \oplus A_{1u} \oplus A_{1g}
\end{aligned} \tag{3.14}$$

$$\begin{aligned}
\{\widetilde{4,2}\} &\downarrow O_h \sim \mathbf{T}_{1u} \qquad \oplus \mathbf{T}_{1g} \qquad \oplus \mathbf{E}_u \qquad \oplus \mathbf{A}_{2u} \\
&\downarrow D_{4h} \sim E_u \qquad \oplus A_{2u} \oplus E_g \qquad \oplus A_{2g} \oplus A_{1u} \oplus B_{1u} \oplus B_{1u} \\
&\downarrow D_{2h} \sim B_{1u} \oplus B_{2u} \oplus A_{2u} \oplus B_{1g} \oplus B_{2g} \oplus A_{2g} \oplus A_{1u} \oplus A_{1u} \oplus A_{1u}
\end{aligned} \tag{3.15}$$

$$\begin{aligned}
\{\widetilde{5,1}\} &\downarrow O_h \sim \mathbf{T}_{2g} \qquad \oplus \mathbf{E}_u \\
&\downarrow D_{4h} \sim E_g \qquad \oplus B_{2g} \oplus A_{1u} \oplus B_{1u} \\
&\downarrow D_{2h} \sim B_{1g} \oplus B_{2g} \oplus A_{2g} \oplus A_{1u} \oplus A_{1u} \ .
\end{aligned} \tag{3.16}$$

Each $\{\widetilde{3,3}\}$ tableau state is determined uniquely to within a phase by D_{2h} labels. The other tableaus have two or three A_{1u} states that require the operators from the higher symmetries D_{4h} and O_h to label completely the projection. One additional operation such as R_3 will determine the D_{4h} transformation properties once and for all. Any operation in the coset $R_3 D_{2h}$ serves to extend D_{2h} labeling to the next higher D_{4h} link in the subgroup chain. Finally, subgroup D_{4h} and the cosets $r_1 D_{4h}$ and $r_1^2 D_{4h}$ complete the full octahedral O_h symmetry. These subgroups and cosets are indicated in Fig. 11. So the permutation representations of the 90° z rotation R_3 and the 120° (111) rotation r_1 are all that one needs to complete the projection. The permutation expressions for these key operators are

$$\begin{aligned}
R_3 &= (14)(13)(12)\,, \\
r_1 &= (15)(12)(36)(34)\,.
\end{aligned} \tag{3.17}$$

Note that $r_1^2 = r_1^\dagger$ is the transpose of r_1. The tetragonally defined octahedral (O) irreducible representations of those generators are defined by the following:

Subgroup O: $\mathbf{T}_1$ · · $\mathbf{T}_2$ · ·

D_4: E · A_2 E · B_2

D_2: B_1 B_2 A_2 B_1 B_2 A_2

$$\mathfrak{D}^{\mathbf{T}_1}(R_3) = \begin{pmatrix} 0 & -1 & 0 \\ 1 & 0 & 0 \\ 0 & 0 & 1 \end{pmatrix} \quad \mathfrak{D}^{\mathbf{T}_2}(R_3) = \begin{pmatrix} 0 & -1 & 0 \\ 1 & 0 & 0 \\ 0 & 0 & -1 \end{pmatrix}$$

$$\mathfrak{D}^{\mathbf{T}_1}(r_1) = \begin{pmatrix} 0 & 0 & 1 \\ 1 & 0 & 0 \\ 0 & 1 & 0 \end{pmatrix} \quad \mathfrak{D}^{\mathbf{T}_2}(r_1) = \begin{pmatrix} 0 & 0 & 1 \\ -1 & 0 & 0 \\ 0 & -1 & 0 \end{pmatrix} \tag{3.18}$$

$$\begin{array}{c} \mathbf{E} \\ A_1 \quad B_1 \\ A_1 \quad A_1 \end{array}$$

$$\mathfrak{D}^{\mathbf{E}}(R_3) = \begin{pmatrix} 1 & 0 \\ 0 & -1 \end{pmatrix}$$

$$\mathfrak{D}^{\mathbf{E}}(r_1) = \begin{pmatrix} -\frac{1}{2} & -\sqrt{3}/2 \\ \sqrt{3}/2 & -\frac{1}{2} \end{pmatrix}. \tag{3.19}$$

TABLE III. Transformations between XY_6 tableau bases and octahedral-tetragonally defined bases. The octahedral labeling is done using the subgroup chain

$O_h \supset D_{4h} \supset D_{2h}$.

(a)

A_{2u}	: D_h
B_{1u}	: D_{4h}
A_{1u}	: D_{2h}
1	

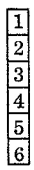

(b)

T_{2g} E_g B_{1g}	B_{2g}	B_{2g} A_{2g}	E_u A_{1u} A_{1u}	B_{1u} A_{1u}	: O_h : D_{4h} : D_{2h}
1/2	1/2	0	$\sqrt{2}/2$	0	
$-\sqrt{3}/2$	$\sqrt{3}/6$	0	$\sqrt{6}/6$	0	
0	$-\sqrt{6}/3$	0	$\sqrt{3}/3$	0	
0	0	$\sqrt{10}/5$	0	$-\sqrt{15}/5$	
0	0	$\sqrt{15}/5$	0	$\sqrt{10}/5$	

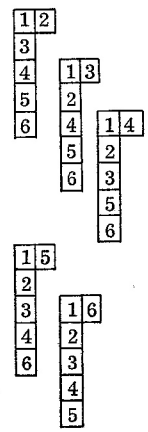

(c)

T_{1u} E_u B_{1u}	B_{2u}	A_{2u} A_{2u}	T_{1g} E_g B_{1g}	B_{2g}	A_{2g} A_{2g}	E_u A_{1u} A_{1u}	B_{1u} A_{1u}	A_{2u} B_{1u} A_{1u}	: O_h : D_{4h} : D_{2h}
0	0	−1/2	0	0	0	0	$-\sqrt{3}/3$	$\sqrt{15}/6$	
0	0	$\sqrt{3}/2$	0	0	0	0	−1/3	$\sqrt{5}/6$	
$\sqrt{3}/6$	$-\sqrt{3}/6$	0	$\sqrt{6}/6$	$\sqrt{6}/6$	$-\sqrt{6}/6$	$\sqrt{3}/3$	0	0	
1/6	1/2	0	$-\sqrt{2}/2$	$\sqrt{2}/6$	$-\sqrt{2}/6$	1/3	0	0	
$-\sqrt{2}/3$	0	0	0	−2/3	−1/3	$\sqrt{2}/3$	0	0	
$\sqrt{6}/6$	$-\sqrt{6}/6$	0	$-\sqrt{3}/6$	$-\sqrt{3}/6$	$-\sqrt{3}/3$	$-\sqrt{6}/6$	0	0	
$\sqrt{2}/6$	$\sqrt{2}/2$	0	1/2	−1/6	−1/3	$-\sqrt{2}/6$	0	0	
−2/3	0	0	0	$\sqrt{2}/3$	$-\sqrt{2}/3$	−1/3	0	0	
0	0	0	0	0	0	0	$-\sqrt{5}/3$	−2/3	

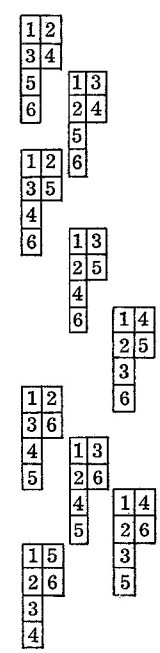

The transformation matrices which accomplish the reductions (3.14), (3.15), and (3.16) are given in Table III. They are analogous to the transformation which was needed to bring the trigonal T_1 or $\{3,1\}$ tableau basis to a form which was useful for tetragonal cluster analysis of XY_4 molecules. (See Appendix B of article I.)

B. Tableau definition of nuclear spin states and Slater determinants

The orbital-spin assembly formula given in Fig. 5 of article I may be applied to the XY_6 tableau states. The calculation is the same as it was for the XY_3 and XY_4 examples except that now one

TABLE III. *(Continued.)*

(d)

T_{2g} E_g B_{1g}	B_{2g}	B_{2g} A_{2g}	A_{1u} A_{1u} A_{1u}	A_{1g} A_{1g} A_{1g}	: O_h : D_{4h} : D_{2h}
0	0	$-\sqrt{3}/2$	0	1/2	1 2 / 3 4 / 5 6
0	0	$-1/2$	0	$-\sqrt{3}/2$	1 3 / 2 4 / 5 6
1/2	1/2	0	$\sqrt{2}/2$	0	1 2 / 3 5 / 4 6
$-\sqrt{3}/2$	$\sqrt{3}/6$	0	$\sqrt{6}/6$	0	1 3 / 2 5 / 4 6
0	$-\sqrt{6}/3$	0	$\sqrt{3}/3$	0	1 4 / 2 5 / 3 6

deals with four times as many spin states. It is helpful to use the recursive properties of the tableau states to minimize the computation. The XY_6 results are shown in Tables IV (a)–IV (c).

For example, one should note that the first two or three columns of the XY_6 Table IV (a) are equal to the first two columns of the XY_3 table in Fig. 5 of I or the first three columns of the XY_4 Table III (a) of I, respectively. In fact wherever there are four or six states having identical spin configurations on states (5) and (6) there will be a repeat of the I Tables III (a) and III (b), respectively, except for an overall factor. Calculation of one element is all that is needed to determine this factor. The Tables IV (a)–IV (c) do not have the Slater determinant states ordered so this recursion is obvious at a glance for all cases.

Instead, the Slater states are ordered according to binary counting as though the XY_6 molecule were a six-bit digital register. Spin down (↓) corresponds to binary 1, while binary 0 or spin up (↑) is indicated by a bar (|) in Table IV. This makes it possible to exploit the spin up-down symmetry. Note that columns of Table IV (c) are either symmetric or antisymmetric to reflection around the horizontal bisector of the table. This reflection amounts to the reversal of up and down spins in the Slater bases. The tableau columns which change sign are just the ones associated with an odd number of spin pairs. These include state $\{\tilde{3},3\}$ belonging to total spin ($I=0$) state which contains three antisymmetric paired singlets represented by three columns of the tableau:

$$\left|\begin{array}{|c|c|c|}\hline \uparrow & \uparrow & \uparrow \\ \hline \downarrow & \downarrow & \downarrow \\ \hline \end{array}\right\rangle = - \left|\begin{array}{|c|c|c|}\hline \downarrow & \downarrow & \downarrow \\ \hline \uparrow & \uparrow & \uparrow \\ \hline \end{array}\right\rangle . \tag{3.20}$$

The states $\{\tilde{5},1\}$ belonging to total spin ($I=2$) state contain one pair and are antisymmetric, too:

$$\left|\begin{array}{|c|c|c|c|c|}\hline \uparrow & \uparrow & \uparrow & \downarrow & \downarrow \\ \hline \downarrow \\ \cline{1-1} \end{array}\right\rangle = - \left|\begin{array}{|c|c|c|c|c|}\hline \downarrow & \downarrow & \downarrow & \uparrow & \uparrow \\ \hline \uparrow \\ \cline{1-1} \end{array}\right\rangle . \tag{3.21}$$

The other tableau states $\{\tilde{4},2\}$ and $\{\tilde{6}\}$ are symmetric to mirror reflection:

$$\left|\begin{array}{|c|c|c|c|}\hline \uparrow & \uparrow & \uparrow & \downarrow \\ \hline \downarrow & \downarrow \\ \cline{1-2} \end{array}\right\rangle = \left|\begin{array}{|c|c|c|c|}\hline \downarrow & \downarrow & \downarrow & \uparrow \\ \hline \uparrow & \uparrow \\ \cline{1-2} \end{array}\right\rangle \tag{3.22}$$

$$\left|\begin{array}{|c|c|c|c|c|c|}\hline \uparrow & \uparrow & \uparrow & \downarrow & \downarrow & \downarrow \\ \hline \end{array}\right\rangle = \left|\begin{array}{|c|c|c|c|c|c|}\hline \downarrow & \downarrow & \downarrow & \uparrow & \uparrow & \uparrow \\ \hline \end{array}\right\rangle \tag{3.23}$$

The simple behavior of these states under mirror reflection makes it unnecessary to compute tables for states with more than half of the spins turned down.

A remarkably convenient numerical property is evident in Tables IV (a)–IV (c) which was not pointed out in article I: A normalization factor can be removed from each column so that only integers remain. Even more remarkable is the preservation of this integer property in Tables V (a)–V (c) in which tetragonal tableau states are related to Slater states. These tables are obtained by combining the columns of Table IV according to the transformation in Table III. The presence of integers in columns (in fact, there are mostly one's and zero's) expedites the Hamiltonian matrix calculations which may involve sums over individual columns of Table V (a)–V (c). Of course, if one chooses to evaluate the Hamiltonians using a calculating machine, then this arithmetic nicety will not be appreciated as much.

TABLE IV. XY_6 tableau states expressed in terms of Slater determinants. The notation $|\,|\,|\downarrow|\,|$, for example, is a shorthand version for the Slater state ($1\uparrow, 2\uparrow, 3\uparrow, 4\downarrow, 5\uparrow, 6\downarrow$). Factors which normalize each column are placed below the tables.

(a)

1 2 3 4 5 6	1 2 / 3 4 / 5 6	1 3 / 2 4 / 5 6	1 4 / 2 5 / 3 6	1 5 / 2 3 / 4 6	1 6 / 2 3 / 4 5	1 / 2 / 3 / 4 / 5 / 6
$\|\,\|\,\|\,\|\,\|\downarrow$	0	0	0	0	5	1
$\|\,\|\,\|\,\|\downarrow\|$	0	0	0	−4	1	1
$\|\,\|\,\|\downarrow\|\,\|$	0	0	3	1	−1	1
$\|\,\|\downarrow\|\,\|\,\|$	0	−2	−1	1	−1	1
$\|\downarrow\|\,\|\,\|\,\|$	1	1	−1	1	−1	1
$\downarrow\|\,\|\,\|\,\|\,\|$	−1	1	−1	1	−1	1
	$1/\sqrt{2}$	$1/\sqrt{6}$	$1/2\sqrt{3}$	$1/2\sqrt{5}$	$1/\sqrt{30}$	$1/\sqrt{6}$

TABLE IV. *(Continued.)*

(b)

1 2 3 4 5 6	[1 2 / 3 4 / 5 / 6]	[1 3 / 2 4 / 5 / 6]	[1 2 / 3 5 / 4 / 6]	[1 3 / 2 5 / 4 / 6]	[1 4 / 2 5 / 3 / 6]	[1 2 / 3 6 / 4 / 5]	[1 3 / 2 6 / 4 / 5]	[1 4 / 2 6 / 3 / 5]	[1 5 / 2 6 / 3 / 4]	[1 2 / 3 / 4 / 5 / 6]	[1 3 / 2 / 4 / 5 / 6]	[1 4 / 2 / 3 / 4 / 6]	[1 5 / 2 / 3 / 4 / 6]	[1 6 / 2 / 3 / 4 / 5]	[1 / 2 / 3 / 4 / 5 / 6]
↓ ↓ | | | |	0	0	0	0	0	0	0	0	−12	0	0	0	−4	2	1
↓ ↓ | | | ↓	0	0	0	0	0	0	0	9	3	0	0	3	1	2	1
↓ ↓ | | ↓ |	0	0	0	0	−3	0	0	−3	3	0	0	3	−3	−1	1
↓ ↓ | ↓ | ↓	0	0	0	0	0	0	−6	−3	3	0	−2	−1	1	2	1
↓ ↓ | ↓ | |	0	0	0	4	1	0	2	1	3	0	−2	−1	−3	−1	1
↓ ↓ | ↓ ↓ | |	0	−2	0	−2	1	0	2	−2	−2	0	−2	2	2	−1	1
↓ | ↓ | | ↓	0	0	0	0	0	3	3	−3	3	1	1	−1	1	2	1
↓ | ↓ | ↓ |	0	0	−2	−2	1	−1	−1	1	3	1	1	−1	−3	−1	1
↓ | ↓ | | |	1	1	1	1	1	−1	−1	−2	−2	1	1	2	2	−1	1
↓ | ↓ ↓ | | |	−1	1	1	−1	−1	−1	1	2	−2	1	−1	−2	2	−1	1
↓ | | | | ↓	0	0	0	0	0	−3	3	−3	3	−1	1	−1	1	2	1
↑ | | | ↓ |	0	0	2	−2	1	1	−1	1	3	−1	1	−1	−3	−1	1
↓ | | ↓ | |	−1	1	−1	1	1	1	−1	−2	−2	−1	1	2	2	−1	1
↓ | ↓ | | |	1	1	−1	−1	−1	1	1	2	−2	−1	−1	−2	2	−1	1
↓ ↓ | | | |	0	−2	0	2	−1	0	−2	2	−2	0	2	−2	2	−1	1
	1/2	1/2√3	1/2√3	1/6	1/3√2	1/2√6	1/6√2	1/12	1/4√15	1/2√2	1/2√6	1/4√3	1/4√5	1/√30	1/√15

TABLE IV. *(Continued.)*

(c)

1 2 3 4 5 6	$\begin{array}{\|c\|c\|}\hline 1&2\\\hline 3&4\\\hline 5&6\\\hline\end{array}$	$\begin{array}{\|c\|c\|}\hline 1&3\\\hline 2&4\\\hline 5&6\\\hline\end{array}$	$\begin{array}{\|c\|c\|}\hline 1&2\\\hline 3&5\\\hline 4&6\\\hline\end{array}$	$\begin{array}{\|c\|c\|}\hline 1&3\\\hline 2&5\\\hline 4&6\\\hline\end{array}$	$\begin{array}{\|c\|c\|}\hline 1&4\\\hline 2&5\\\hline 3&6\\\hline\end{array}$	$\begin{array}{\|c\|c\|}\hline 1&2\\\hline 3&4\\\hline 5\\\cline{1-1} 6\\\cline{1-1}\end{array}$	$\begin{array}{\|c\|c\|}\hline 1&3\\\hline 2&4\\\hline 5\\\cline{1-1} 6\\\cline{1-1}\end{array}$	$\begin{array}{\|c\|c\|}\hline 1&2\\\hline 3&5\\\hline 4\\\cline{1-1} 6\\\cline{1-1}\end{array}$	$\begin{array}{\|c\|c\|}\hline 1&3\\\hline 2&5\\\hline 4\\\cline{1-1} 6\\\cline{1-1}\end{array}$	$\begin{array}{\|c\|c\|}\hline 1&4\\\hline 2&5\\\hline 3\\\cline{1-1} 6\\\cline{1-1}\end{array}$	$\begin{array}{\|c\|c\|}\hline 1&2\\\hline 3&6\\\hline 4\\\cline{1-1} 5\\\cline{1-1}\end{array}$	$\begin{array}{\|c\|c\|}\hline 1&3\\\hline 2&6\\\hline 4\\\cline{1-1} 5\\\cline{1-1}\end{array}$	$\begin{array}{\|c\|c\|}\hline 1&4\\\hline 2&6\\\hline 3\\\cline{1-1} 5\\\cline{1-1}\end{array}$	$\begin{array}{\|c\|c\|}\hline 1&5\\\hline 2&6\\\hline 3\\\cline{1-1} 4\\\cline{1-1}\end{array}$	$\begin{array}{\|c\|c\|}\hline 1&2\\\hline 3\\\cline{1-1} 4\\\cline{1-1} 5\\\cline{1-1} 6\\\cline{1-1}\end{array}$	$\begin{array}{\|c\|c\|}\hline 1&3\\\hline 2\\\cline{1-1} 4\\\cline{1-1} 5\\\cline{1-1} 6\\\cline{1-1}\end{array}$	$\begin{array}{\|c\|c\|}\hline 1&4\\\hline 2\\\cline{1-1} 3\\\cline{1-1} 5\\\cline{1-1} 6\\\cline{1-1}\end{array}$	$\begin{array}{\|c\|c\|}\hline 1&5\\\hline 2\\\cline{1-1} 3\\\cline{1-1} 4\\\cline{1-1} 6\\\cline{1-1}\end{array}$	$\begin{array}{\|c\|c\|}\hline 1&6\\\hline 2\\\cline{1-1} 3\\\cline{1-1} 4\\\cline{1-1} 5\\\cline{1-1}\end{array}$	$\begin{array}{\|c\|c\|}\hline 1\\\hline 2\\\cline{1-1} 3\\\cline{1-1} 4\\\cline{1-1} 5\\\cline{1-1} 6\\\cline{1-1}\end{array}$
|||↓↓↓	0	0	0	0	−3	0	0	0	0	−3	0	0	3	−3	0	0	3	−3	1	1
||↓|↓↓	0	0	0	4	1	0	0	0	4	1	0	−2	−1	−3	0	−2	−1	−3	1	1
||↓↓|↓	0	−2	0	−2	1	0	−2	0	−2	1	0	−2	2	2	0	−2	2	2	1	1
||↓↓↓|	0	2	0	−2	1	0	−2	0	2	−1	0	2	−2	2	0	−2	2	−2	−1	1
|↓||↓↓	0	0	−2	−2	1	0	0	−2	−2	1	1	1	−1	−3	1	1	−1	−3	1	1
|↓|↓|↓	1	1	1	1	1	1	1	1	1	1	1	1	2	2	1	1	2	2	1	1
|↓|↓↓|	−1	−1	1	1	1	1	1	−1	−1	−1	−1	−1	−2	2	1	1	2	−2	−1	1
|↓↓||↓	−1	1	1	−1	−1	−1	1	1	−1	−1	1	−1	−2	2	1	−1	−2	2	1	1
|↓↓|↓|	1	−1	1	−1	−1	−1	1	−1	1	1	−1	1	2	2	1	−1	−2	−2	−1	1
|↓↓↓||	0	0	−2	2	−1	0	0	2	−2	1	−1	1	−1	−3	1	−1	1	3	−1	1
↓||↓↓↓	0	0	2	−2	1	0	0	2	−2	1	−1	1	−1	−3	−1	1	−1	−3	1	1
↓||↓|↓	−1	1	−1	1	1	−1	1	−1	1	1	−1	1	2	2	−1	1	2	2	1	1
↓||↓↓|	1	−1	−1	1	1	−1	1	1	−1	−1	1	−1	−2	2	−1	1	2	−2	−1	1
↓|↓||↓	1	1	−1	−1	−1	1	1	−1	−1	−1	−1	−1	−2	2	−1	−1	−2	2	1	1
↓|↓|↓|	−1	−1	−1	−1	−1	1	1	1	1	1	1	1	2	2	−1	−1	−2	−2	−1	1
↓|↓↓||	0	0	2	2	−1	0	0	−2	−2	1	1	1	−1	−3	−1	−1	1	3	−1	1
↓↓|||↓	0	−2	0	2	−1	0	−2	0	2	−1	0	2	−1	2	0	2	−2	2	1	1
↓↓||↓|	0	2	0	2	−1	0	−2	0	−2	1	0	−2	2	2	0	2	−2	−2	−1	1
↓↓|↓||	0	0	0	−4	−1	0	0	0	4	1	0	−2	−1	−3	0	2	1	3	−1	1
↓↓↓|||	0	0	0	0	3	0	0	0	0	−3	0	0	3	−3	0	0	−3	3	−1	1
	$1/\sqrt{8}$	$1/2\sqrt{6}$	$1/2\sqrt{6}$	$1/6\sqrt{2}$	$1/6$	$1/\sqrt{8}$	$1/2\sqrt{6}$	$1/2\sqrt{6}$	$1/6\sqrt{2}$	$1/6$	$1/2\sqrt{3}$	$1/6$	$1/6\sqrt{2}$	$1/2\sqrt{30}$	$1/2\sqrt{3}$	$1/6$	$1/6\sqrt{2}$	$1/2\sqrt{30}$	$1/2\sqrt{3}$	$1/2\sqrt{5}$

TABLE V. XY_6 octahedral-tetragonal cluster states expressed in terms of Slater determinants.

(a)

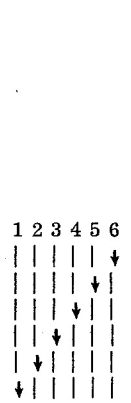

T_{2g} E_g B_{1g}	B_{2g}	B_{2g} A_{2g}	E_u A_{1u} A_{1u}	B_{1u} A_{1u}	A_{2u} B_{1u}	$=O_h$ labels $=D_{4h}$ $=D_{2h}$
0	0	1	0	2	1	
0	0	−1	0	2	1	
0	−1	0	1	−1	1	
1	0	0	−1	−1	1	
0	1	0	1	−1	1	
−1	0	0	−1	−1	1	
$1/\sqrt{2}$	$1/\sqrt{2}$	$1/\sqrt{2}$	$1/2$	$1/2\sqrt{3}$	$1/\sqrt{6}$	

(b)

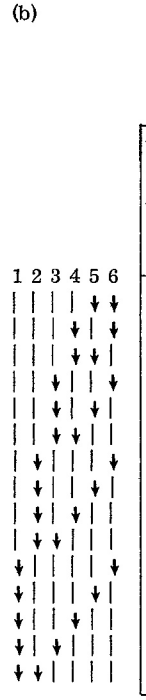

T_{1u} E_u B_{1u}	B_{2u}	A_{2u} A_{2u}	T_{1g} E_g B_{1g}	B_{2g}	A_{2g} A_{2g}	E_u A_{1u} A_{1u}	B_{1u} A_{1u}	A_{2u} B_{1u} A_{1u}	T_{2g} E_g B_{1g}	B_{2g}	B_{2g} A_{1g}	E_u A_{1u} A_{1u}	B_{1u} A_{1u}	A_{2u} B_{1u}
0	0	0	0	0	0	0	4	4	0	0	0	0	4	1
−1	0	0	0	1	−1	−1	−1	−1	0	−1	1	1	1	1
1	0	0	0	1	1	−1	−1	−1	0	−1	−1	1	1	1
0	−1	0	−1	0	1	1	−1	−1	1	0	1	−1	1	1
0	1	0	−1	0	−1	1	−1	−1	1	0	−1	−1	1	1
0	0	−1	1	−1	0	0	2	−1	1	−1	0	0	−2	1
1	0	0	0	−1	−1	−1	−1	−1	0	1	1	1	1	1
−1	0	0	0	−1	1	−1	−1	−1	0	1	−1	1	1	1
0	0	0	0	0	0	2	−2	4	0	0	0	2	−2	1
0	0	1	1	1	0	0	2	−1	1	1	0	0	−2	1
0	1	0	1	0	1	1	−1	−1	−1	0	1	−1	1	1
0	−1	0	1	0	−1	1	−1	−1	−1	0	−1	−1	1	1
0	0	1	−1	−1	0	0	2	−1	−1	−1	0	0	−2	1
0	0	0	0	0	0	−2	−2	4	0	0	0	−2	−2	1
0	0	−1	−1	1	0	0	2	−1	−1	1	0	0	−2	1
$1/2$	$1/2$	$1/2$	$1/2\sqrt{2}$	$1/2\sqrt{2}$	$1/2\sqrt{2}$	$1/4$	$1/4\sqrt{3}$	$1/2\sqrt{15}$	$1/2\sqrt{2}$	$1/2\sqrt{2}$	$1/2\sqrt{2}$	$1/4$	$1/4\sqrt{3}$	$1/\sqrt{15}$

TABLE V. *(Continued.)*

(c)

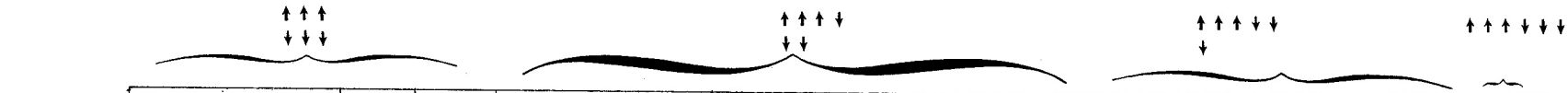

1 2 3 4 5 6	T_{2g} E_g B_{1g}	B_{2g}	B_{2g} A_{2g}	A_{1u} A_{1u} A_{1u}	A_{1g} A_{1g} A_{1g}	T_{1u} E_u B_{1u}	B_{2u}	A_{2u} A_{2u}	T_{1g} E_g B_{1g}	B_{2g}	A_{2g} A_{2g}	E_u A_{1u} A_{1u}	A_{1u} A_{1u}	A_{2u} B_{1u} A_{1u}	T_{2g} E_g B_{1g}	B_{2g}	B_{2g} A_{2g}	E_u A_{1u} A_{1u}	B_{1u} A_{1u}	A_{2u} B_{1u} A_{1u}
↑ ↑ ↑ ↓ ↓ ↓	0	2	0	−1	0	0	0	0	0	1	0	−1	1	2	0	−1	0	1	1	1
↑ ↑ ↓ ↑ ↓ ↓	−2	0	0	1	0	0	0	0	−1	0	0	1	1	2	1	0	0	−1	1	1
↑ ↑ ↓ ↓ ↑ ↓	1	−1	1	0	1	−1	−1	−1	0	0	0	0	0	−3	1	−1	1	0	0	1
↑ ↑ ↓ ↓ ↓ ↑	1	−1	−1	0	−1	1	1	−1	0	0	0	0	0	−3	1	−1	−1	0	0	1
↑ ↓ ↑ ↑ ↓ ↓	0	−2	0	−1	0	0	0	0	0	−1	0	−1	1	2	0	1	0	1	1	1
↑ ↓ ↑ ↓ ↑ ↓	0	0	−2	1	0	0	0	0	0	0	−1	0	−2	2	0	0	1	2	0	1
↑ ↓ ↑ ↓ ↓ ↑	0	0	2	1	0	0	0	0	0	0	1	0	−2	2	0	0	−1	2	0	1
↑ ↓ ↓ ↑ ↑ ↓	1	1	1	0	−1	1	−1	1	0	0	0	0	0	−3	1	1	1	0	0	1
↑ ↓ ↓ ↑ ↓ ↑	1	1	−1	0	1	−1	1	1	0	0	0	0	0	−3	1	1	−1	0	0	1
↑ ↓ ↓ ↓ ↑ ↑	−2	0	0	−1	0	0	0	0	1	0	0	1	1	2	1	0	0	1	−1	1
↓ ↑ ↑ ↑ ↓ ↓	2	0	0	1	0	0	0	0	1	0	0	1	1	2	−1	0	0	−1	1	1
↓ ↑ ↑ ↓ ↑ ↓	−1	−1	1	0	−1	−1	1	1	0	0	0	0	0	−3	−1	−1	1	0	0	1
↓ ↑ ↑ ↓ ↓ ↑	−1	−1	−1	0	1	1	−1	1	0	0	0	0	0	−3	−1	−1	−1	0	0	1
↓ ↑ ↓ ↑ ↑ ↓	0	0	−2	−1	0	0	0	0	0	0	1	0	−2	2	0	0	1	−2	0	1
↓ ↑ ↓ ↑ ↓ ↑	0	0	2	−1	0	0	0	0	0	0	−1	0	−2	2	0	0	−1	−2	0	1
↓ ↑ ↓ ↓ ↑ ↑	0	2	0	1	0	0	0	0	0	−1	0	−1	1	2	0	−1	0	−1	−1	1
↓ ↓ ↑ ↑ ↑ ↓	−1	1	1	0	1	1	1	−1	0	0	0	0	0	−3	−1	1	1	0	0	1
↓ ↓ ↑ ↑ ↓ ↑	−1	1	−1	0	−1	−1	−1	−1	0	0	0	0	0	−3	−1	1	−1	0	0	1
↓ ↓ ↑ ↓ ↑ ↑	2	0	0	−1	0	0	0	0	−1	0	0	1	1	2	−1	0	0	1	−1	1
↓ ↓ ↓ ↑ ↑ ↑	0	−2	0	1	0	0	0	0	0	1	0	−1	1	2	0	1	0	−1	−1	1
	$1/2\sqrt{6}$	$1/2\sqrt{6}$	$1/2\sqrt{6}$	$1/2\sqrt{3}$	$1/2\sqrt{2}$	$1/2\sqrt{2}$	$1/2\sqrt{2}$	$1/2\sqrt{2}$	$1/2$	$1/2$	$1/2$	$1/2\sqrt{2}$	$1/2\sqrt{6}$	$1/2\sqrt{30}$	$1/2\sqrt{3}$	$1/2\sqrt{3}$	$1/2\sqrt{3}$	$1/2\sqrt{6}$	$1/2\sqrt{2}$	$1/2\sqrt{5}$

IV. MODEL HAMILTONIAN REPRESENTATIONS IN THE TETRAGONAL CLUSTER BASIS

The effects of spin and rotation on the XY_6 molecules can be modeled in the elementary-cluster approximation (ECA). Here we shall treat the scalar and tensor-spin-rotation Hamiltonian for the ground vibrational levels explicitly as one example, but will model other effects such as spin-spin, spin-vibration, etc. using various phenomenalogical tunneling parameters. The spin rotation Hamiltonian is the sum

$$H_{sr} = H_{ssr} + H_{tsr}\,, \tag{4.1a}$$

where

$$H_{ssr}(\mathrm{ECA}) = \sigma N_{\bar{g}}\left[I_{\bar{g}}(1) + I_{\bar{g}}(2) + \cdots + I_{\bar{g}}(6)\right] \tag{4.1b}$$

and

$$H_{tsr}(\mathrm{ECA}) = \tau N_{\bar{g}}\left\{(6a+4)\left[I_{\bar{g}}(1) + I_{\bar{g}}(2) + I_{\bar{g}}(3) + I_{\bar{g}}(4)\right] + 4\left[I_{\bar{g}}(5) + I_{\bar{g}}(6)\right]\right\} \tag{4.1c}$$

are the scalar and tensor parts, respectively, and the latter follows from Eq. (2.24) of article I. The octahedral symmetry and the cluster approximation reduces the Hamiltonian to this simple form. When one ignores $N_{\bar{x}}$ or $N_{\bar{y}}$ terms which would raise or lower between different clusters then the $I_{\bar{x}}$ and $I_{\bar{y}}$ terms disappear as well. This reflects the fact that spins will tend to align or antialign perfectly to the rotation axis if XY_6 is stuck on a tetragonal axis. There are no terms which tend to give canted spins.

The σ and τ spin-rotation parameters can be related to the conventional parameters of the hyperfine Hamiltonians such as have been given by Michelot *et al.*[10] In Michelot *et al.*,[10] the two spin rotation operators are the scalar given by

$$\alpha_a\left[\left[l^{(0,1)} \times D^{(1,1)}\right]^{(1,0A_{1g})} \times I^{(1,A_{1g})}\right]^{(0,A_{1g})} \sim \alpha_a N_{\bar{g}}\left[I_{\bar{g}}(1) + I_{\bar{g}}(2) + I_{\bar{g}}(3) + I_{\bar{g}}(4) + I_{\bar{g}}(5) + I_{\bar{g}}(6)\right]/\sqrt{3} \tag{4.2a}$$

and the tensor given by

$$\alpha_d\left[\left[l^{(0,1)} \times D^{(1,1)}\right]^{(1,2E_g)} \times I^{(1,E_g)}\right]^{(0,A_{1g})} \sim \alpha_d N_{\bar{g}}\left[I_{\bar{g}}(1) + I_{\bar{g}}(2) + I_{\bar{g}}(3) + I_{\bar{g}}(4) - 2I_{\bar{g}}(5) - 2I_{\bar{g}}(6)\right]/\sqrt{3}\,. \tag{4.2b}$$

The right-hand side of the above equations contain only those parts of each operator which survive in the ECA. Comparing with the pseudo-Hamiltonian (4.1) one obtains

$$\alpha_a = \sqrt{3}[\sigma + 4\tau(a+1)]\,, \quad \alpha_d = \sqrt{3}\tau a/2 \\ = -\sqrt{3}hc_a \qquad\qquad = \sqrt{2/3}hc_d\,. \tag{4.3}$$

The parameters c_a and c_d are those of Ozier *et al.*[8] as quoted by Michelot *et al.*[10]

Symmetry differences between Hamiltonians and cluster pseudo-Hamiltonians are important. Both the Hamiltonians on the left-hand side of (4.2) have double scalar (O, A_{1g}) symmetry, i.e., scalar or $J=0$ for the lab-based O_3 symmetry and scalar or A_{1g} for the molecule-based O_h symmetry. However, cluster pseudo-Hamiltonians may reflect the spontaneously broken molecular symmetry, which is $D_{4h} \subset O_h$ for tetragonal clusters. The pseudo-Hamiltonians in (4.2) are both A_{1g} invariants for D_{4h}, but they have different O_h symmetry. The first one belongs to A_{1g} of O_h while the second

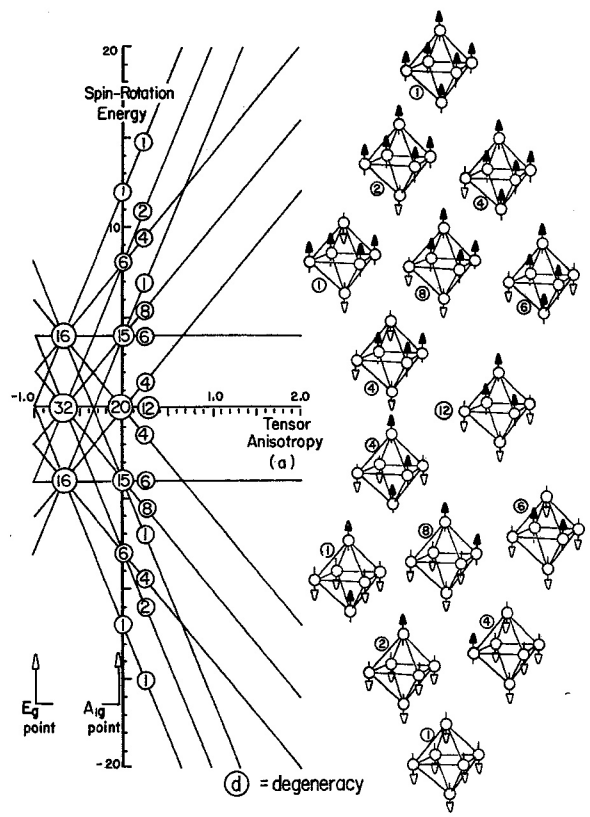

FIG. 12. Plot of semiclassical tensor spin-rotation levels for tetragonal case-2 cluster states. The quantity (a) is a measure of the relative strength of tensor versus scalar interaction. The value $(a=-1)$ corresponds to a pure E-type tensor operator. For $(a>0)$ tensor interactions there is more spin (↑) vs (↓) energy difference for equatorial nuclei (states 1 through 4) than for polar nuclei (states 5 and 6).

one belongs to the first component of E_g. The value ($\alpha_a = 0$) yields pure E_g spin-rotation interaction if α_d is nonzero.

It is instructive to see what forms the eigenvalue spectrum of the spin-rotation operators (4.1) can take in the extreme case (2) limit for tetragonal XY_6 clusters. It is sufficient to examine the tensor spin-rotation Hamiltonian H_{tsr}(ECA) since it reduces to the scalar spin-rotation operator H_{ssr}(ECA) when (a) is zero. In Fig. 12 the limiting eigenvalues are plotted as a function of (a) for $\sigma = 0$ and $\langle \tau N_{\bar{z}} \rangle = 1$. With $\sigma = 0$ the parameter (a) serves as a measure of the difference between the effective magnetic field on the octahedral fourfold axis and the field on the octahedral equator. The value ($a = -1$) corresponds to a pure E_g spin-rotation interaction according to Eq. (4.3). The nuclei on the equator are in states numbered 1 through 4 while the ones on the axis are in states numbered 5 and 6 as given by Fig. 11. The equatorial nuclei are being flung around a great deal more than the axial ones, and their four spins should be more strongly coupled to the rotation than the two spins on the axis. Therefore a change of the equatorial spins should make more difference in energy than the same change of the axial spins. This is indicated in Fig. 12 where it is supposed that the highest state has all six spins up. The next state below it has one axial spin down. The number (2) on that energy trajectory gives the degeneracy of the level, i.e., either the nucleus in axial state 5 or 6 can have spin down. (No spin-tunneling is assumed here.) Similarly, the number (4) on the next line gives the degeneracy of the level in which one of the equatorial nuclei has spin down. For low values of the anisotropy parameter ($a < \frac{2}{3}$) this level lies above the singly degenerate one in which both axial spins are down. For $a = 0$ the levels collapse into seven levels having the binomial coefficient degeneracies 1, 6, 15, 20, 15, 6, and 1, respectively. This situation is a familiar one in NMR studies of symmetric complexes. The sum of all the degeneracies is $2^6 = 64$ which is the total number of Slater states.

A comparison between spin-spin Hamiltonians and their pseudo-Hamiltonians can also be made; however it is more difficult. Here we will consider phenomenological spin-spin pseudo-Hamiltonians which describe exchange of spins between pairs of nuclei. Let us define an elementary tunneling operator by

$$T(i \rightleftharpoons j) = a^{\dagger}_{i\uparrow} a^{\dagger}_{j\downarrow} a_{i\downarrow} a_{j\uparrow} + a^{\dagger}_{i\downarrow} a^{\dagger}_{j\uparrow} a_{i\uparrow} a_{j\downarrow} , \qquad (4.4)$$

so that it interchanges the spins of nuclei in states i and j if they are oppositely oriented. Then let a D_{4h}-symmetric spin tunneling Hamiltonian be

$$H_{\mathrm{ss}} = s[T(1 \rightleftharpoons 2) + T(2 \rightleftharpoons 3) + T(3 \rightleftharpoons 4) + T(4 \rightleftharpoons 1)]$$
$$+ s' \sum_{j=5,6} [T(1 \rightleftharpoons j) + T(2 \rightleftharpoons j) + T(3 \rightleftharpoons j) + T(4 \rightleftharpoons j)] + t[T(1 \rightleftharpoons 3) + T(2 \rightleftharpoons 4)] + t' T(5 \rightleftharpoons 6) . \qquad (4.5)$$

The tunneling amplitudes s, s', t, and t' are analogous to the cluster tunneling amplitude ($-S$) in Eq. (2.10). In fact the representation of the hyperfine pseudo-Hamiltonian in the Slater basis for $\langle I_{\bar{z}} \rangle = 2$ (one-spin-down states) is a broken symmetry analogy for (2.10). The $\langle I_{\bar{z}} \rangle = 3$ and $\langle I_{\bar{z}} \rangle = 2$ Slater representation is the following:

$$\langle H_{\mathrm{sr}} + H_{\mathrm{ss}} \rangle_{I_{\bar{z}}=3,2} = \begin{array}{c|cccccc} & 1 & 2 & 3 & 4 & 5 & 6 \\ \hline |\,|\,|\,|\,|\,|\,| & A & & & & & & I_{\bar{z}} = 3 \\ |\,|\,|\,|\,|\,\downarrow & B & t' & s' & s' & s' & s' & I_{\bar{z}} = 2 \\ |\,|\,|\,|\,\downarrow\,| & t' & B & s' & s' & s' & s' & \\ |\,|\,|\,\downarrow\,|\,| & s' & s' & C & s & t & s & \\ |\,|\,\downarrow\,|\,|\,| & s' & s' & s & C & s & t & \\ |\,\downarrow\,|\,|\,|\,| & s' & s' & t & s & C & s & \\ \downarrow\,|\,|\,|\,|\,| & s' & s' & s & t & s & C & \end{array} \qquad (4.6a)$$

One can imagine that a single spin-down is a quasi-particle and call it a "downon". The downon can tunnel around to six different locations in the SF_6 octahedron which explains the analogy between (4.6) and (2.10). However, (2.10) starts with an O_h symmetric octahedron whereas for (4.6) that symmetry may be broken to D_{4h}. Hence, two different kinds of nearest neighbor tunneling amplitudes s and s' may be needed. In addition there are next-nearest neighbor tunneling amplitudes t and t' which actually may be dominant because of electronic bonding. (Non-nearest amplitudes do not appear in rotational tunneling analogs except for extraordinary tensors.[32]) Finally, instead of H in (2.2) there are different diagonal energies:

$$A = 3\sigma n_4 + 12\tau n_4(a+1),$$
$$B = 2\sigma n_4 + 4\tau n_4(3a+2), \qquad (4.6b)$$
$$C = 2\sigma n_4 + 2\tau n_4(3a+4).$$

Here, we will assume the difference between B and C energies is primarily due to the tensor spin-rotation (4.1c). However, diagonal terms can contain tensor spin-spin contributions, as well.[10]

The Slater representation for two-downon states, i.e., $\langle I_{\bar{z}}\rangle = 1$ is given by the following:

$\langle H_{sr} + H_{ss}\rangle_{I_{\bar{z}}=1} =$

123456																														
||||↓↓	D	s'	s'	s'	s'	·	s'	s'	·	·	s'	s'	·	·	·															
|||↓|↓	s'	E	t'	s	·	s'	t	·	s'	·	s	·	s'	·	·															
|||↓↓|	s'	t'	E	·	s	s'	·	t	s'	·	·	s	s'	·	·															
||↓||↓	s'	s	·	E	t'	s'	s	·	·	s'	t	·	·	s'	·															
||↓|↓|	s'	·	s	t'	E	s'	·	s	·	s'	·	t	·	s'	·															
||↓↓||	·	s'	s'	s'	s'	F	·	·	s	t	·	·	t	s	·															
|↓||↓	s'	t	·	s	·	·	E	t'	s'	s'	s	·	·	·	s'															
|↓||↓|	s'	·	t	·	s	·	t'	E	s'	s'	·	s	·	·	s'															
|↓|↓||	·	s'	s'	·	·	s	s'	s'	F	s	·	·	s	·	s															
|↓↓|||	·	·	·	s'	s'	t'	s'	s'	s	F	·	·	·	s	t															
↓||||↓	s'	·	·	t	·	·	s	·	·	·	E	t'	s'	s'	s'															
↓|||↓|	s'	·	·	·	t	·	·	s	·	·	t'	E	s'	s'	s'															
↓||↓||	·	s'	s'	·	·	t	·	·	s	·	s'	s'	F	s	t															
↓|↓|||	·	·	·	s'	s'	s	·	·	·	s	s'	s'	s	F	s															
↓↓||||	·	·	·	·	·	·	s'	s'	s	t	s'	s'	t	s	F															

(4.7a)

Here the diagonal spin-rotation terms are the following:

$$D = \sigma n_4 + 4\tau n_4(3a+1),$$
$$E = \sigma n_4 + 2\tau n_4(3a+2), \qquad (4.7b)$$
$$F = \sigma n_4 + 4\tau n_4.$$

Finally, the Slater representation for the $I_{\bar{z}} = 0$ or three-down states is given for the first half of the rows:

$\langle H_{s} + H_{ss}\rangle_{I_{\bar{z}}=0} =$

123456																														
|||↓↓↓	G	s	s'	s'	t	s'	s'	·	·	·	s	s'	s'	·	·	·	·	·	·	·										
||↓|↓↓	s	G	s'	s'	s	·	·	s'	s'	·	t	·	·	s'	s'	·	·	·	·	·										
||↓↓|↓	d'	d'	0	t	·	s	·	t	·	s'	·	t	·	s	·	s'	·	·	·	·										
||↓↓↓|	s'	s'	t'	0	·	·	s	·	t	s'	·	·	t	·	s	s'	·	·	·	·										
|↓||↓↓	t	s	·	·	G	s'	s'	s'	s'	·	s	·	·	·	·	·	s'	s'	·	·										
|↓|↓|↓	s'	·	s	·	s'	0	t'	s	·	s'	·	s	·	·	·	·	s	·	s'	·										
|↓|↓↓|	s'	·	·	s	s'	t'	0	·	s	s'	·	·	s	·	·	·	·	s	s'	·										
|↓↓||↓	·	s'	t	·	s'	s	·	0	t'	s'	·	·	·	s	·	·	t	·	·	s'										
|↓↓|↓|	·	s'	·	t	s'	·	s	t'	0	s'	·	·	·	·	s	·	·	t	·	s'										
|↓↓↓||	·	·	s'	s'	·	s'	s'	s'	s'	$-G$	·	·	·	·	·	·	s	·	·	t	s										

(4.8a)

All matrices are symmetric to diagonal transposition. However, the $(I_z=0)$ matrix is also symmetric to antidiagonal transposition for all components except the diagonal components

$$G=6\tau n_4 a\,, \tag{4.8b}$$

which change sign upon transposition. This gives the second half of (4.8a). The $(\uparrow\text{-}\downarrow)$ symmetry mentioned in Sec. III B is being used here. This gives the $\langle I_z\rangle=-1$, -2, and -3 matrices as anti-diagonal transpositions of (4.7a), and (4.6a), respectively.

The preceeding analysis is an incomplete treatment of hyperfine interactions. There are other possible phenomenological parameters, but there are also relations between the phenomenological pseudo-Hamiltonian parameters and the more fundamental molecular parameters such as α_a, α_b, and others which are defined in Ref. 10. However, the main objective of this article is to study the cluster representations and approximate eigensolutions for different cases involving simple model Hamiltonians. Later, a more judicious choice of parameters can be easily inserted and interpreted.

Now the Slater determinant cluster representations (4.6) to (4.8) will be transformed to the octahedral bases using the transformations listed in Tables V(a)–V(c). Each type of tetragonal cluster will be represented in turn in Secs. IV A–IV C below.

A. Type $O_4\uparrow O=A_1\oplus T_1\oplus E$ clusters

The bases chosen for (A, T, E) clusters are just those whose D_{4h} labels correspond to cluster momentum components with $n=0$ modulo 4 in Table II. This means only those bases in Table V for which the D_{4h} label is A_{1g}, A_{2g}, A_{1u}, or A_{2u} need be considered. This gives rise to octahedral A_{1g}, A_{1u}, T_{1g}, T_{1u}, and two kinds of E_u states in the $A_1\oplus T_1\oplus E$ cluster.

Among these there are no states with total body spin component $\langle I_{\bar z}\rangle=3$. There is one E_u state with $\langle I_{\bar z}\rangle=2$ for the O_4 cluster in Table V(a):

$$\langle H_{\rm sr}+H_{\rm ss}\rangle^{E_u\,\bar\uparrow\uparrow\uparrow\uparrow\uparrow}_{\quad\bar\downarrow\quad A_{1u}\,I_{\bar z}=2}=[2\sigma+(6a+8)\tau]n_4+t-2s\,. \tag{4.9}$$

This $(E_u, I=2)$ state is joined by another E_u state in the $I_{\bar z}=1$ matrix. There are two E_u's and a (T_{1g}, T_{1u}) doublet for the O_4 cluster in Table V(b):

$$\langle H_{\rm sr}+H_{\rm ss}\rangle_{I_{\bar z}=1}=$$

$E_u\ \bar\uparrow\uparrow\uparrow\uparrow\uparrow$, $A_{1u}\ \bar\downarrow$	$E_u\ \bar\uparrow\uparrow\uparrow\uparrow$, $A_{1u}\ \bar\downarrow\downarrow$	$T_{1g}\ \bar\uparrow\uparrow\uparrow\uparrow$, $A_{2g}\ \bar\downarrow\downarrow$	$T_{1u}\ \bar\uparrow\uparrow\uparrow\uparrow$, $A_{2u}\ \bar\downarrow\downarrow$
$[\sigma+(3a+4)\tau]n_4$ $+(t+t')/2-s+2s'$	$-3a\tau n_4+$ $s-(t+t')/2$		
$-3a\tau n_4+$ $s-(t+t')/2$	$[\sigma+(3a+4)\tau]n_4$ $+(t+t')/2-s-2s'$		
		$[\sigma+(6a+4)\tau]n_4$ $+t-t'-2s$	
			$(\sigma+4\tau)n_4-2t$

. (4.10)

Finally the $\langle I_{\bar z}\rangle=0$ matrix is represented in the basis of states given by columns of Table V(c) with A-type D_{4h} labels:

$\langle H_{sr}+H_{ss}\rangle_{I_{\bar z}=0}=$

E_u $\bar{\uparrow}\bar{\uparrow}\bar{\uparrow}\uparrow\uparrow\uparrow$ $\downarrow$	E_u $\bar{\uparrow}\bar{\uparrow}\uparrow\uparrow$ $\downarrow\downarrow$	A_{1u} $\bar{\uparrow}\bar{\uparrow}\uparrow$ $\downarrow\downarrow\downarrow$
A_{1u}	A_{1u}	A_{1u}
$2(4s'-s)/3$ $+(t+2t')/3$	$-2\sqrt{3}\,a\tau n$	$2\sqrt{2}\,(s-s')/3$ $+\sqrt{2}\,(t'-t)/3$
$-2\sqrt{3}\,a\tau n$	$t-2s$	$2\sqrt{6}\,a\tau n$
$2\sqrt{2}(s-s')/3$ $+\sqrt{2}(t'-t)/3$	$2\sqrt{6}\,a\tau n$	$-4(s-2s')/3$ $+(t'+2t)/3$

(4.11)

T_{1g} $\bar{\uparrow}\bar{\uparrow}\uparrow\uparrow$ $\downarrow\downarrow$	T_{1u} $\bar{\uparrow}\bar{\uparrow}\uparrow\uparrow$ $\downarrow\downarrow$	A_{1g} $\bar{\uparrow}\bar{\uparrow}\uparrow$ $\downarrow\downarrow\downarrow$
A_{2g}	A_{2u}	
$-t'$	$t'-2t$	$-t'-2t$

Tetragonal symmetry of the cluster pseudo-Hamiltonian causes body-defined matrix components to vanish if they involve different D_{4h} labels. Furthermore, all components which connect different values of body component $\langle I_{\bar z}\rangle=\bar n_I$ of spin are missing since the Hamiltonian contains no $I_{\bar x}$ or $I_{\bar y}$ operators. Therefore, there are fewer terms to consider in matrix components involving the eigenstates of total angular momentum $F=N\pm\Delta$, where $\Delta=I, I-1, \ldots, -I$ and I is the total spin quantum number. The theory of frame transformations between states of definite $\bar n_I$ and states of definite total rotor momentum N were treated in article I, and in Ref. 14. The states with definite $\bar n_I$ quantum numbers have the spins quantized in the body fixed or molecular frame, (these are overlined, e.g., $\bar{\uparrow}\bar{\uparrow}\bar{\uparrow}$), while the states with definite N have the spins quantized in the lab fixed frame.

In the (A_1T_1E) cluster only the $[\{5,1\}E_u]$ states have $I=2$. The frame transformation coefficients $d_{\Delta\bar n}$ from Table VI of article I may be used to produce lab coupled states of definite rotor momentum N:

$$\left|\begin{matrix} N & \{\widetilde{5,1}\} & F=N+\Delta \\ n_4 & E_u & \end{matrix}\right\rangle=\sum_{\bar n_I=-2}^{2} d_{\Delta\bar n_I}\left|\begin{matrix} \{\widetilde{5,1}\} \\ E_u\ \ \bar n_I \end{matrix}\right\rangle. \tag{4.12}$$

It should be remembered that the kets on either side of a frame transformation such as (4.12) have definite total nuclear spin I, definite total angular momentum $F=N+I, N+I-1,\ldots,$ or $|N-I|$, and definite cluster momentum component n_4. There are three sets of states $[\{\widetilde{4,2}\}E_u]$, $[\{\widetilde{4,2}\}T_{1u}]$ and $[\{\widetilde{4,2}\}T_{1g}]$ which have $I=1$. The frame transformation coefficients $c_{\Delta\bar n}$ from Table V of Article I may be used for each of these sets for $\nu=E_u, T_u$, and T_{1g} to give lab defined momentum eigenstates:

$$\left|\begin{matrix} N & \{\widetilde{4,2}\} & F=N+\Delta \\ n & \nu & \end{matrix}\right\rangle=\sum_{\bar n_I=-1}^{1} c_{\Delta\bar n_I}\left|\begin{matrix} \{\widetilde{4,2}\} \\ \nu\ \ n_I \end{matrix}\right\rangle. \tag{4.13}$$

Finally, the $(I=0)$ states $[\{\widetilde{3,3}\}A_{1g}]$ and $[\{\widetilde{3,3}\}A_{1u}]$ do not require frame transformations.

The diagonal components $c_{\Delta\bar n_I}$ and $d_{\Delta\bar n_I}$ for $\Delta=\bar n_I$ become nearly equal to unity and much larger than the off-diagonal components in the strong cluster limit of high N and n_4. Then the uncertainty or deviation of the body axis of quantization from the axis becomes small. In the same limit the tunneling amplitude S for rotational clusters is becoming small. This means that the energies $(H-4S)$ for A_1 levels, H for T_1 levels, and $(H+2S)$ for E levels become nearly equal. Then it is possible to ignore the frame transformations. One obtains the lab-coupled representation of the total Hamiltonian $\langle H_{\text{scalar}}+H_{\text{tensor}}+H_{sr}+H_{ss}\rangle$ simply by adding $(H-4S)$, H, or $(H+2S)$ to the diagonals of matrices (4.9) to (4.11), labeled by A_1, T_1, or E octahedral species, respectively.

It is instructive to investigate the extreme limit of case 2 or strong clusters in which one ignores the tunneling coefficient S and the off-diagonal c and d coefficients. Then the Hamiltonian representations given in Eqs. (4.9)–(4.11) are all that one has to solve. The interpretation of some of those will be considered now. The overlines on the spins will be deleted since the distinction between lab- and body-fixed axes disappears in the strong case-2 limit.

Consider first the highest-angular-momentum state $(I=2)$ which is not involved in a matrix with any others:

$$\left|\begin{matrix} N & \{\widetilde{5,1}\} & F^{\flat}=(N+2)^{-} \\ n & E_u & \end{matrix}\right\rangle \cong \left|\begin{matrix} \{5,1\} & \uparrow\uparrow\uparrow\uparrow\uparrow \\ E_u & \downarrow \end{matrix}\right\rangle \tag{4.14}$$

$$= \begin{pmatrix} +(\uparrow\uparrow\uparrow\downarrow\uparrow\uparrow) \\ -(\uparrow\uparrow\downarrow\uparrow\uparrow\uparrow) \\ +(\uparrow\downarrow\uparrow\uparrow\uparrow\uparrow) \\ -(\downarrow\uparrow\uparrow\uparrow\uparrow\uparrow) \end{pmatrix} \Big/ 2 \ .$$

The Slater representation is written using the (E_u, A_{1u}) column of Table V(a). This can be written in broken tableau form as

$$\left|\begin{matrix} \{\widetilde{5,1}\} & \uparrow\uparrow\uparrow\uparrow\uparrow \\ E_u & \downarrow \end{matrix}\right\rangle = \left|\begin{matrix} \chi & \\ & \end{matrix}\ \begin{matrix} \uparrow\uparrow\uparrow \\ \downarrow \end{matrix}\right\rangle \left|\begin{matrix} 5 \\ 6 \end{matrix}\ \uparrow\uparrow\right\rangle , \tag{4.15}$$

where, it is convenient to define a χ tableau as explained in Appendix B. A similar definition was made in Table IV(a) of article I:

$$\left|\begin{matrix} \chi & \\ & \end{matrix}\ \begin{matrix} \uparrow\uparrow\uparrow \\ \downarrow \end{matrix}\right\rangle = \Big([(\uparrow\uparrow\uparrow\downarrow) - (\uparrow\uparrow\downarrow\uparrow) + (\uparrow\downarrow\uparrow\uparrow) - (\downarrow\uparrow\uparrow\uparrow)] \Big) \Big/ 2$$

$$= \left[(1/\sqrt{2}) \begin{matrix} 1 & 2 \\ 3 & \\ 4 & \end{matrix} + (1/\sqrt{6}) \begin{matrix} 1 & 3 \\ 2 & \\ 4 & \end{matrix} + (1/\sqrt{3}) \begin{matrix} 1 & 4 \\ 2 & \\ 3 & \end{matrix} \right] \begin{matrix} \uparrow\uparrow\uparrow \\ \downarrow \end{matrix} \ . \tag{4.16}$$

The E_u states having the next-highest angular momentum $F = N+1$ become mixed. With $(s'=0)$, the eigenvectors of the 2×2 matrix (4.10) are positive and negative combinations. The positive combination

$$\left(\left|\begin{matrix} \{\widetilde{4,2}\} & \uparrow\uparrow\uparrow\uparrow \\ E_u & \downarrow\downarrow \end{matrix}\right\rangle + \left|\begin{matrix} \{\widetilde{5,1}\} & \uparrow\uparrow\uparrow\uparrow\uparrow \\ E_u & \downarrow \end{matrix}\right\rangle \right) \Big/ \sqrt{2} = \begin{pmatrix} (\uparrow\downarrow\uparrow\uparrow\downarrow\uparrow) \\ -(\downarrow\uparrow\uparrow\uparrow\uparrow\downarrow) \end{pmatrix} \Big/ \sqrt{2}$$

$$= \left|\begin{matrix} \chi & \\ & \end{matrix}\ \begin{matrix} \uparrow\uparrow\uparrow \\ \downarrow \end{matrix}\right\rangle \left|\begin{matrix} 5 \\ 6 \end{matrix}\ \uparrow\uparrow\right\rangle \tag{4.17a}$$

has eigenvalue

$$e^{+} = (\sigma + 4\tau) n_4 , \tag{4.17b}$$

while the negative combination

$$\left(- \left|\begin{matrix} \{\widetilde{4,2}\} & \uparrow\uparrow\uparrow\uparrow \\ E_u & \downarrow\downarrow \end{matrix}\right\rangle + \left|\begin{matrix} \{\widetilde{5,1}\} & \uparrow\uparrow\uparrow\uparrow\uparrow \\ E_u & \downarrow \end{matrix}\right\rangle \right) \Big/ \sqrt{2} = \begin{pmatrix} (\uparrow\uparrow\uparrow\downarrow\uparrow\uparrow) + (\uparrow\uparrow\uparrow\uparrow\downarrow\uparrow) \\ -(\uparrow\uparrow\uparrow\uparrow\downarrow\uparrow) - (\uparrow\uparrow\uparrow\uparrow\uparrow\downarrow) \\ +(\uparrow\uparrow\downarrow\uparrow\uparrow\uparrow) + (\uparrow\uparrow\uparrow\downarrow\uparrow\uparrow) \\ -(\uparrow\downarrow\uparrow\uparrow\uparrow\uparrow) - (\downarrow\uparrow\uparrow\uparrow\uparrow\uparrow) \end{pmatrix} \Big/ \sqrt{8}$$

$$= \left|\begin{matrix} \chi & \\ & \end{matrix}\ \begin{matrix} \uparrow\uparrow\uparrow \\ \downarrow \end{matrix}\right\rangle \left|\begin{matrix} 5 \\ 6 \end{matrix}\ \uparrow\downarrow\right\rangle \tag{4.18a}$$

has eigenvalue

$$[\sigma + (6a+4)\tau] n_4 - 2s + t' + t . \tag{4.18b}$$

This is an example where two different tableaus or S_6 symmetry species have been mixed by hyperfine interactions. Total spin I is no longer a good quantum number. Instead, the system factors into "equatorial" nuclei in states 1, 2, 3, and 4, and "polar" nuclei in states 5 and 6. Without tunneling $(s = s' = t = t' = 0)$ the eigenvalues (4.17b) and (4.18b) correspond to the circles marked 6 and 8 in Fig. 12.

The factoring of Slater representations in Eqs. (4.15) to (4.18) is done here in the same way as it was for the XY_4 states in article I. However, this procedure can become impractical for some of the more complicated cluster states of XY_6. It is much easier to obtain these results by directly inspecting the tableau representations of the states. For example, the $S_6 \downarrow O_h$ transformation in Table III(a) gives the following:

$$\left|\begin{matrix}\{\widetilde{5,1}\}\\ E_u, A_{1u}\end{matrix}\right\rangle = (\sqrt{2}/2)\begin{array}{|c|c|}\hline 1&2\\\hline 3\\\cline{1-1}4\\\cline{1-1}5\\\cline{1-1}6\\\cline{1-1}\end{array} + (\sqrt{6}/6)\begin{array}{|c|c|}\hline 1&3\\\hline 2\\\cline{1-1}4\\\cline{1-1}5\\\cline{1-1}6\\\cline{1-1}\end{array} + (\sqrt{3}/3)\begin{array}{|c|c|}\hline 1&4\\\hline 2\\\cline{1-1}3\\\cline{1-1}5\\\cline{1-1}6\\\cline{1-1}\end{array} . \tag{4.19}$$

The $\begin{array}{|c|}\hline 5\\\hline 6\\\hline\end{array}$ tableau is in the same position in each of the three component tableaus of the $[\{5,1\}E_u]$ state, and it may be factored to give the following form:

$$\left|\begin{matrix}\{\widetilde{5,1}\}\\ E_u, A_{1u}\end{matrix}\right\rangle = \left|(\sqrt{2}/2)\begin{array}{|c|c|}\hline 1&2\\\hline 3\\\cline{1-1}4\\\cline{1-1}\end{array} + (\sqrt{6}/6)\begin{array}{|c|c|}\hline 1&3\\\hline 2\\\cline{1-1}4\\\cline{1-1}\end{array} + (\sqrt{3}/3)\begin{array}{|c|c|}\hline 1&4\\\hline 2\\\cline{1-1}3\\\cline{1-1}\end{array}\right\rangle \left|\begin{array}{|c|}\hline 5\\\hline 6\\\hline\end{array}\right\rangle$$

$$= \left|\begin{array}{|c|c|}\hline \chi&\\\hline &\\\cline{1-1}&\\\cline{1-1}\end{array}\ \begin{array}{|c|}\hline 5\\\hline 6\\\hline\end{array}\right\rangle . \tag{4.20}$$

The definition of the χ tableau from Eq. (4.16) has been used again. The spin states belonging to the separate factors may be coupled using Clebsch-Gordan coefficients $C^{S_1 S_2 S}_{m_1 m_2 m_I}$ to give any of the allowed total-spin states. The tableau $\{5.1\}$ has $S=2$ while the factors $\begin{array}{|c|c|}\hline \chi&\\\hline &\\\cline{1-1}&\\\cline{1-1}\end{array}$ and $\begin{array}{|c|}\hline 5\\\hline 6\\\hline\end{array}$ have $S_1=1$ and $S_2=1$, respectively. With $n_I=2$ one rederives Eq. (4.15):

$$\left|\begin{matrix}\{\widetilde{5,1}\}\ \uparrow\uparrow\uparrow\uparrow\uparrow\ S=2\\ E_u, A_{1u}\ \ \downarrow\ \ \ \ \ n_I=2\end{matrix}\right\rangle = \sum_{m_1 m_2} C^{S_1 S_2 S}_{m_1 m_2 m_I} \left|\begin{array}{|c|c|}\hline \chi&\\\hline &\\\cline{1-1}&\\\cline{1-1}\end{array}\ S_1\ \begin{array}{|c|}\hline 5\\\hline 6\\\hline\end{array}\ S_2\right\rangle_{m_1\ m_2}$$

$$= \left|\begin{array}{|c|c|}\hline \chi&\\\hline &\\\cline{1-1}&\\\cline{1-1}\end{array}\ \uparrow\uparrow\uparrow\ \begin{array}{|c|}\hline 5\\\hline 6\\\hline\end{array}\ \uparrow\uparrow\right\rangle . \tag{4.21}$$

With $n_I=1$ one rederives the sum of Eqs. (4.17a) and (4.18a):

$$\left|\begin{matrix}\{\widetilde{5,1}\}\ \uparrow\uparrow\uparrow\uparrow\downarrow\ S=2\\ E_u, A_{1u}\ \ \downarrow\ \ \ \ \ n_I=1\end{matrix}\right\rangle = (\sqrt{2}/2)\left|\begin{array}{|c|c|}\hline \chi&\\\hline &\\\cline{1-1}&\\\cline{1-1}\end{array}\ \uparrow\uparrow\uparrow\ \begin{array}{|c|}\hline 5\\\hline 6\\\hline\end{array}\ \downarrow\right\rangle + (\sqrt{2}/2)\left|\begin{array}{|c|c|}\hline \chi&\\\hline &\\\cline{1-1}&\\\cline{1-1}\end{array}\ \uparrow\uparrow\downarrow\ \begin{array}{|c|}\hline 5\\\hline 6\\\hline\end{array}\ \uparrow\right\rangle . \tag{4.22}$$

With $n_I=0$ a new state is derived which will be considered shortly:

$$\left|\begin{matrix}\{\widetilde{5,1}\}\ \uparrow\uparrow\uparrow\uparrow\downarrow\ S=2\\ \ \ \ \ \ \downarrow\ \ \ \ \ n_I=0\end{matrix}\right\rangle$$

$$= (\sqrt{6}/6)\left|\begin{array}{|c|c|}\hline \chi&\\\hline &\\\cline{1-1}&\\\cline{1-1}\end{array}\ \uparrow\uparrow\uparrow\ \begin{array}{|c|}\hline 5\\\hline 6\\\hline\end{array}\ \downarrow\downarrow\right\rangle + (\sqrt{6}/3)\left|\uparrow\uparrow\uparrow\ \downarrow\downarrow\right\rangle + (\sqrt{6}/6)\left|\uparrow\uparrow\downarrow\ \uparrow\downarrow\right\rangle . \tag{4.23}$$

For now we turn our attention to the other part of Eqs. (4.17-18) which involves the $\{4,2\}$ tableau state.

The factoring of the $\{4,2\}$ states requires some more general tableau mathematics. The $S_6 \downarrow O_h$ transformation in Table III(b) gives the following combination.

$$\left|\begin{matrix}\{\widetilde{4,2}\}\\ E_u, A_{1u}\end{matrix}\right\rangle = (\sqrt{3}/3)\begin{array}{|c|c|}\hline 1&2\\\hline 3&5\\\cline{1-2}4\\\cline{1-1}6\\\cline{1-1}\end{array} - (\sqrt{6}/6)\begin{array}{|c|c|}\hline 1&2\\\hline 3&6\\\cline{1-2}4\\\cline{1-1}5\\\cline{1-1}\end{array} + (1/3)\begin{array}{|c|c|}\hline 1&3\\\hline 2&5\\\cline{1-2}4\\\cline{1-1}6\\\cline{1-1}\end{array} - (\sqrt{2}/6)\begin{array}{|c|c|}\hline 1&3\\\hline 2&6\\\cline{1-2}4\\\cline{1-1}5\\\cline{1-1}\end{array} + (\sqrt{2}/3)\begin{array}{|c|c|}\hline 1&4\\\hline 2&5\\\cline{1-2}3\\\cline{1-1}6\\\cline{1-1}\end{array} - (1/3)\begin{array}{|c|c|}\hline 1&4\\\hline 2&6\\\cline{1-2}3\\\cline{1-1}5\\\cline{1-1}\end{array} . \tag{4.24}$$

Here the tableaus have been paired so that those with the same $\{1234\}$ arrangement are next to each other. There are three such pairs: one for each S_4 tableau $\begin{array}{|c|c|}\hline 1&2\\\hline 3\\\cline{1-1} 4\\\cline{1-1}\end{array}$, $\begin{array}{|c|c|}\hline 1&3\\\hline 2\\\cline{1-1} 4\\\cline{1-1}\end{array}$, and $\begin{array}{|c|c|}\hline 1&4\\\hline 2\\\cline{1-1} 3\\\cline{1-1}\end{array}$, respectively. The question remains. How does one factor the $\{56\}$ part when it is not itself a standard tableau?

In general a two-column tableau can be factored according to the formulas given in Fig. 13. This formula was originally designed to transform multiple-shell or mixed-configuration electronic states of atoms and molecules.[49] To use the formula one simply removes one number at a time from the tableau being factored and from the tableau of the second factor. The tableau of the first factor is fixed for each transformation. Each number that is removed will be taken from either the first or second column of the smaller factor tableau and from either the first or second column of the larger original tableau. The four possibilities (A) first-and-first, (b) first-and-second, (C) second-and-first, and (D) second-and-second each give a different factor in the transformation matrix element according to Fig. 13. [The possibility (E) for which *both* first and second columns contain a given number will not occur in this article.] For example, the $\{\widetilde{4,2}\}$ to $\{\widetilde{3,1}\}\times\{\bar{2}\}$ factoring transformation matrix elements are calculated as follows:

$$\left\langle \begin{array}{|c|c|}\hline 1&2\\\hline 3\\\cline{1-1} 4\\\cline{1-1}\end{array}\ \boxed{5}\ \boxed{6}\ \middle|\ \begin{array}{|c|c|}\hline 1&2\\\hline 3&5\\\cline{1-2} 4\\\cline{1-1} 6\\\cline{1-1}\end{array}\right\rangle = \left\langle \begin{array}{|c|}\hline \\\cline{1-1} \\\cline{1-1} \\\cline{1-1} \\\cline{1-1}\end{array}\ \boxed{6}\ \middle|\ \begin{array}{|c|}\hline \\\cline{1-1} \\\cline{1-1} \\\cline{1-1} 6\\\cline{1-1}\end{array}\right\rangle \left\langle \begin{array}{|c|}\hline \\\cline{1-1} \\\cline{1-1} \\\cline{1-1}\end{array}\ \boxed{5}\ \middle|\ \begin{array}{|c|}\hline \\\cline{1-1} \\\cline{1-1} \\\cline{1-1} 5\\\cline{1-1}\end{array}\right\rangle$$

$$(A)\colon S_1=1, S_2=1, S=1 \quad (B)\colon S_1=1, S_2=1/2, S=1/2$$

$$=\left(\frac{4\cdot 1}{2\cdot 3}\right)^{1/2} \quad -\left(\frac{1\cdot 2}{1\cdot 2}\right)^{1/2}$$

$$=-(2/3)^{1/2}\ , \tag{4.25a}$$

$$\left\langle \begin{array}{|c|c|}\hline 1&2\\\hline 3\\\cline{1-1} 4\\\cline{1-1}\end{array}\ \boxed{5}\ \boxed{6}\ \middle|\ \begin{array}{|c|c|}\hline 1&2\\\hline 3&6\\\cline{1-2} 4\\\cline{1-1} 5\\\cline{1-1}\end{array}\right\rangle = \left\langle \begin{array}{|c|c|}\hline \\\cline{1-2} \\\cline{1-2} \\\cline{1-2}\end{array}\ \boxed{6}\ \middle|\ \begin{array}{|c|c|}\hline \\\cline{1-2} \\\cline{1-2} 6\\\cline{1-2}\end{array}\right\rangle \left\langle \begin{array}{|c|c|}\hline \\\cline{1-2} \\\cline{1-2} \\\cline{1-2}\end{array}\ \boxed{5}\ \middle|\ \begin{array}{|c|c|}\hline \\\cline{1-2} \\\cline{1-2} \\\cline{1-2} 5\\\cline{1-2}\end{array}\right\rangle$$

$$(B)\colon S_1=1,\ S_2=1,\ S=1 \quad (A)\colon S_1=1,\ S_2=1/2,\ S=3/2$$

$$=\left(\frac{1\cdot 2}{2\cdot 3}\right)^{1/2}\cdot\left(\frac{4\cdot 1}{1\cdot 4}\right)^{1/2}$$

$$=(1/3)^{1/2}. \tag{4.25b}$$

This transformation can be expressed as follows:

$$\left|\begin{array}{|c|c|}\hline 1&2\\\hline 3\\\cline{1-1} 4\\\cline{1-1}\end{array}\ \begin{array}{|c|}\hline 5\\\hline 6\\\cline{1-1}\end{array}\right\rangle = -(2/3)^{1/2}\left|\begin{array}{|c|c|}\hline 1&2\\\hline 3&5\\\cline{1-2} 4\\\cline{1-1} 6\\\cline{1-1}\end{array}\right\rangle + (1/3)^{1/2}\left|\begin{array}{|c|c|}\hline 1&2\\\hline 3&6\\\cline{1-2} 4\\\cline{1-1} 5\\\cline{1-1}\end{array}\right\rangle . \tag{4.26a}$$

The same methods yield the orthogonal combination:

$$\left|\begin{array}{|c|c|}\hline 1&2\\\hline 3\\\cline{1-1} 4\\\cline{1-1}\end{array}\ \begin{array}{|c|c|}\hline 5&6\\\hline\end{array}\right\rangle = (1/3)^{1/2}\left|\begin{array}{|c|c|}\hline 1&2\\\hline 3&5\\\cline{1-2} 4\\\cline{1-1} 6\\\cline{1-1}\end{array}\right\rangle + (2/3)^{1/2}\left|\begin{array}{|c|c|}\hline 1&2\\\hline 3&6\\\cline{1-2} 4\\\cline{1-1} 5\\\cline{1-1}\end{array}\right\rangle . \tag{4.26b}$$

This is an example of a unitary transformation for the reduction of $U(6)\downarrow U(4)\times U(2)$ representations. Other examples of this sort of transformation are given in Table VII(a), and these will be used to help complete the tetragonal cluster analysis. The trigonal cluster analysis in Sec. V will require reduction of $U(6)\downarrow U(3)\times U(3)$ representations which are shown in Table VII(b). These $U(m+n)\downarrow U(m)\times U(n)$ reductions should be contrasted with $U(m\cdot n)\downarrow U(m)\times U(n)$ reductions. For example, a $U(6)\downarrow U(3)\times U(2)$ reduction was given by the spin-orbital assembly formula in Fig. 5 of article I. For spin-$\frac{1}{2}$ particles the

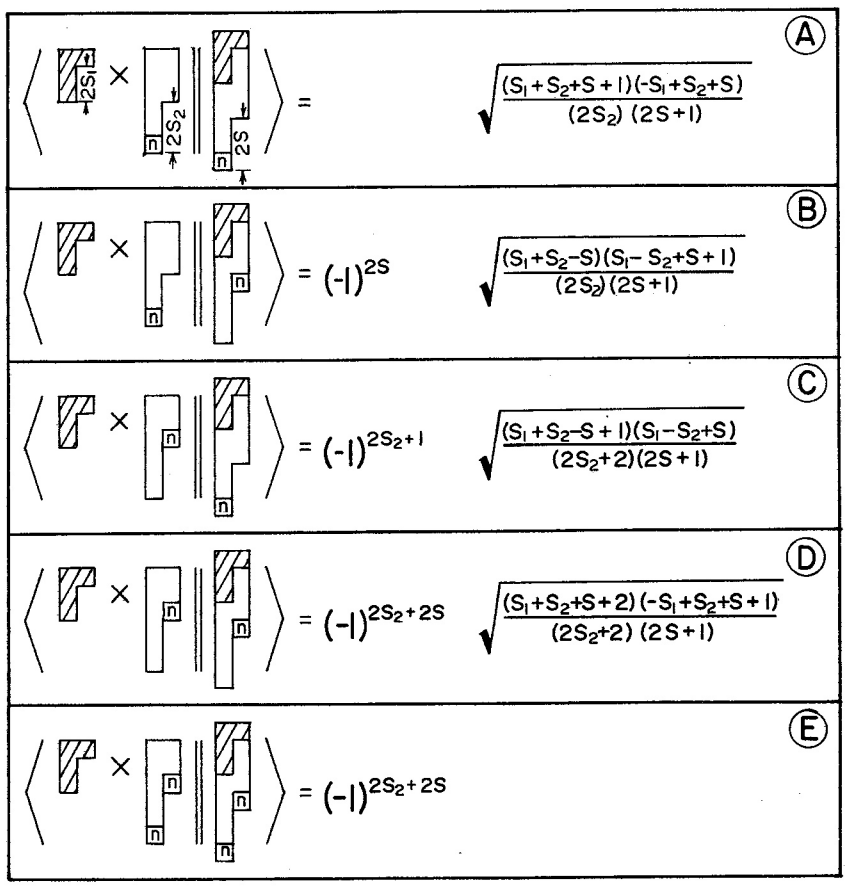

FIG. 13. Orbital tableau assembly or factoring formula. [Reprinted from C. W. Patterson, and W. G. Harter, Phys. Rev. A 15, 2372 (1977)]. Subduction coefficients for $[\mu] \downarrow [\mu_1] \times [\mu_2]$ are found by successive removal of boxes with highest state numbers from tableaus $[\mu_2]$ and $[\mu]$. Each "removal" gives a factor in terms of conjugate total spins S_1, S_2, and S, depending on where the highest states n are located (case A–E). All of the numbers in the formulas refer to the condition of the tableaus just before the boxes containing n are removed. Subduction coefficient is zero unless the tableau of $[\mu]$ contains the bableau of $[\mu_1]$ as indicated by the shaded area.

spin-orbital assembly coefficients can be related to SU(2) Clebsch-Gordan coefficients as shown by Drake and Schlesinger.[22] Similarily, the coefficients in Fig. 13 can be related to SU(2) recoupling coefficients. Higher-spin nuclei will require the same type of coefficients for higher unitary groups. Methods are available for these derivations.[19, 22, 50, 51]

Returning to complete the factorization of the $\{4,2\}$ state (4.24) one finds that each pair of states with the same U(4) labeling has the following factored form:

$$\left|\begin{matrix}\{\widetilde{4,2}\}\\ E_u, A_{1u}\end{matrix}\right\rangle = -(\sqrt{2}/2)\left|\begin{array}{|c|c|}\hline 1&2\\\hline 3\\\cline{1-1}4\\\cline{1-1}\end{array}\ \begin{array}{|c|}\hline 5\\\hline 6\\\hline\end{array}\right\rangle - (\sqrt{6}/6)\left|\begin{array}{|c|c|}\hline 1&3\\\hline 2\\\cline{1-1}4\\\cline{1-1}\end{array}\ \begin{array}{|c|}\hline 5\\\hline 6\\\hline\end{array}\right\rangle - (\sqrt{3}/3)\left|\begin{array}{|c|c|}\hline 1&4\\\hline 2\\\cline{1-1}3\\\cline{1-1}\end{array}\ \begin{array}{|c|}\hline 5\\\hline 6\\\hline\end{array}\right\rangle$$

$$= -\left|\begin{array}{|c|c|}\hline \chi&\\\hline &\\\hline\end{array}\ \begin{array}{|c|}\hline 5\\\hline 6\\\hline\end{array}\right\rangle . \tag{4.27}$$

The χ tableau state notation (4.16) is used again. The result looks the same as the $\{\widetilde{5,1}\}$ state in Eq. (4.20) except for the phase. However, the $\{\widetilde{4,2}\}$ state is associated only with total spin $I=1$ while the $\{\widetilde{5,1}\}$ states has $I=2$. Spin angular-momentum coupling gives the following $\{\widetilde{4,2}\}$ tableau state labeling:

$$\left|\begin{matrix}\{\widetilde{4,2}\}\\ E_u, A_{1u}\end{matrix}\ \begin{matrix}\uparrow\uparrow\uparrow\uparrow\\ \downarrow\downarrow\end{matrix}\ \begin{matrix}S=1\\ n_I=1\end{matrix}\right\rangle = -(\sqrt{2}/2)\left|\begin{array}{|c|}\hline \chi\\\hline\\\cline{1-1}\end{array}\ \begin{matrix}\uparrow\uparrow\uparrow\\ \downarrow\end{matrix}\ \begin{array}{|c|}\hline 5\\\hline 6\\\hline\end{array}\ \uparrow\downarrow\right\rangle + (\sqrt{2}/2)\left|\begin{array}{|c|}\hline \chi\\\hline\\\cline{1-1}\end{array}\ \begin{matrix}\uparrow\uparrow\uparrow\\ \downarrow\end{matrix}\ \begin{array}{|c|}\hline 5\\\hline 6\\\hline\end{array}\ \uparrow\uparrow\right\rangle , \tag{4.28}$$

$$\left|\begin{matrix}\{\widetilde{4,2}\}\\ E_u, A_{1u}\end{matrix}\ \begin{matrix}\uparrow\uparrow\uparrow\uparrow\\ \downarrow\downarrow\end{matrix}\ \begin{matrix}S=1\\ n_I=0\end{matrix}\right\rangle = -(\sqrt{2}/2)\left|\begin{array}{|c|}\hline \chi\\\hline\\\cline{1-1}\end{array}\ \begin{matrix}\uparrow\uparrow\uparrow\\ \downarrow\end{matrix}\ \begin{array}{|c|}\hline 5\\\hline 6\\\hline\end{array}\ \uparrow\downarrow\right\rangle + (\sqrt{2}/2)\left|\begin{array}{|c|}\hline \chi\\\hline\\\cline{1-1}\end{array}\ \begin{matrix}\uparrow\uparrow\uparrow\\ \downarrow\end{matrix}\ \begin{array}{|c|}\hline 5\\\hline 6\\\hline\end{array}\ \uparrow\uparrow\right\rangle . \tag{4.29}$$

The state (4.28) is consistent with the result obtained by subtracting state (4.18a) from (4.17a). The state (4.29) is involved in an analogous transformation with each of the $(n_I=0)$ states that have the same D_{4h} label (A_{1u}). These include the $\{5,1\}$ state (4.23) and a $\{\widetilde{3,3}\}$ state:

$$\left|\begin{matrix}\{\widetilde{3,3}\}\\ A_{1u}, A_{1u}\end{matrix}\right\rangle = (\sqrt{2}/2)\begin{array}{|c|c|}\hline 1&2\\\hline 3&5\\\hline 4&6\\\hline\end{array} + (\sqrt{6}/6)\begin{array}{|c|c|}\hline 1&3\\\hline 2&5\\\hline 4&6\\\hline\end{array} + (\sqrt{3}/3)\begin{array}{|c|c|}\hline 1&4\\\hline 2&5\\\hline 3&6\\\hline\end{array} .$$

The factoring of Fig. 13 or Table VII(a) gives the following for the $\{\widetilde{3,3}\}$ state:

$$\left|\begin{matrix}\{\widetilde{3,3}\}\\ A_{1u}, A_{1u}\end{matrix}\right\rangle = \left|-(\sqrt{2}/2)\begin{array}{|c|c|}\hline 1&2\\\hline 3\\\cline{1-1}4\\\cline{1-1}\end{array} - (\sqrt{6}/6)\begin{array}{|c|c|}\hline 1&3\\\hline 2\\\cline{1-1}4\\\cline{1-1}\end{array} - (\sqrt{3}/3)\begin{array}{|c|c|}\hline 1&4\\\hline 2\\\cline{1-1}3\\\cline{1-1}\end{array}\right\rangle \left|\begin{array}{|c|}\hline 5\\\hline 6\\\hline\end{array}\right\rangle$$

$$= -\left|\begin{array}{|c|c|}\hline \chi&\\\hline &\\\hline\end{array}\ \begin{array}{|c|}\hline 5\\\hline 6\\\hline\end{array}\right\rangle .$$

The spin-coupling coefficients $C^{s_1 s_2 0}_{m_1 m_2 0}$ are used to write the explicit spin-tableau labeling of the $\{\widetilde{3,3}\}$ state. This is written below along with the other $(n_I=0)$ states from Eqs. (4.23) and (4.29):

$$\left|\begin{matrix}\{\widetilde{3,3}\}\\ A_{1u}, A_{1u}\end{matrix}\ \begin{matrix}\uparrow\uparrow\uparrow\\ \downarrow\downarrow\downarrow\end{matrix}\right\rangle = -(\sqrt{3}/3)\left|\begin{array}{|c|}\hline \chi\\\hline\\\cline{1-1}\end{array}\ \begin{matrix}\uparrow\uparrow\uparrow\\ \downarrow\end{matrix}\ \begin{array}{|c|}\hline 5\\\hline 6\\\hline\end{array}\ \uparrow\downarrow\right\rangle + (\sqrt{3}/3)\left|\begin{array}{|c|}\hline \chi\\\hline\\\cline{1-1}\end{array}\ \begin{matrix}\uparrow\uparrow\uparrow\\ \downarrow\end{matrix}\ \begin{array}{|c|}\hline 5\\\hline 6\\\hline\end{array}\ \uparrow\uparrow\right\rangle - (\sqrt{3}/3)\left|\begin{array}{|c|}\hline \chi\\\hline\\\cline{1-1}\end{array}\ \begin{matrix}\uparrow\uparrow\uparrow\\ \downarrow\end{matrix}\ \begin{array}{|c|}\hline 5\\\hline 6\\\hline\end{array}\ \uparrow\uparrow\right\rangle$$

$$\left|\begin{matrix}\{\widetilde{4,2}\}\\ E_u, A_{1u}\end{matrix}\ \begin{matrix}\uparrow\uparrow\uparrow\uparrow\\ \downarrow\downarrow\end{matrix}\right\rangle = -(\sqrt{2}/2)\left|\begin{array}{|c|}\hline \chi\\\hline\\\cline{1-1}\end{array}\ \begin{matrix}\uparrow\uparrow\uparrow\\ \downarrow\end{matrix}\ \begin{array}{|c|}\hline 5\\\hline 6\\\hline\end{array}\ \uparrow\downarrow\right\rangle + (\sqrt{2}/2)\left|\begin{array}{|c|}\hline \chi\\\hline\\\cline{1-1}\end{array}\ \begin{matrix}\uparrow\uparrow\uparrow\\ \downarrow\end{matrix}\ \begin{array}{|c|}\hline 5\\\hline 6\\\hline\end{array}\ \uparrow\uparrow\right\rangle$$

$$\left|\begin{matrix}\{\widetilde{5,1}\}\\ E_u, A_{1u}\end{matrix}\ \begin{matrix}\uparrow\uparrow\uparrow\uparrow\uparrow\\ \downarrow\end{matrix}\right\rangle = (\sqrt{6}/6)\left|\begin{array}{|c|}\hline \chi\\\hline\\\cline{1-1}\end{array}\ \begin{matrix}\uparrow\uparrow\uparrow\\ \downarrow\end{matrix}\ \begin{array}{|c|}\hline 5\\\hline 6\\\hline\end{array}\ \uparrow\downarrow\right\rangle + (\sqrt{6}/3)\left|\begin{array}{|c|}\hline \chi\\\hline\\\cline{1-1}\end{array}\ \begin{matrix}\uparrow\uparrow\uparrow\\ \downarrow\end{matrix}\ \begin{array}{|c|}\hline 5\\\hline 6\\\hline\end{array}\ \uparrow\uparrow\right\rangle + (\sqrt{6}/6)\left|\begin{array}{|c|}\hline \chi\\\hline\\\cline{1-1}\end{array}\ \begin{matrix}\uparrow\uparrow\uparrow\\ \downarrow\end{matrix}\ \begin{array}{|c|}\hline 5\\\hline 6\\\hline\end{array}\ \uparrow\uparrow\right\rangle . \tag{4.30}$$

The representation of the 3×3 submatrix in Eq. (4.11) in the factored or mixed species has a simpler form:

$$\langle H_{sr}+H_{ss}\rangle_{A_{1u},I_{\bar{z}}=0}=\begin{pmatrix} 6a\tau n_4+t-2s & 2s' & 0 \\ 2s' & t' & 2s' \\ 0 & 2s' & -6a\tau n_4+t-2s \end{pmatrix}. \tag{4.31}$$

This is another example in which the eigenstates of the spin-rotation Hamiltonian are factored tableau states. However, the spin-exchange tunneling s' between polar and equatorial positions is an off-diagonal perturbation.

To complete the (A_1T_1E) basis one needs to do the factoring analysis for the states which were already diagonal in Eqs. (4.10) and 4.11). The results for the T_{1g} states are as follows:

$$\left|\begin{matrix}\{4,2\}\\ T_{1g},A_{2g}\end{matrix}\right\rangle = -\left|\begin{array}{|c|}\hline\chi\\\hline\end{array}\right\rangle\left|\begin{matrix}\uparrow\uparrow\uparrow\\ \downarrow\end{matrix}\right\rangle\left|\begin{array}{|c|c|}\hline 5&6\\\hline\end{array}\right\rangle\left|\begin{matrix}\uparrow\\ \downarrow\end{matrix}\right\rangle$$

$$\left|\begin{matrix}\uparrow\uparrow\uparrow\uparrow\\ \downarrow\downarrow\end{matrix}\right\rangle = -\left|\begin{array}{|c|}\hline\chi\\\hline\end{array}\right\rangle\left|\begin{matrix}\uparrow\uparrow\uparrow\\ \downarrow\end{matrix}\right\rangle\left|\begin{array}{|c|c|}\hline 5&6\\\hline\end{array}\right\rangle\left|\begin{matrix}\uparrow\\ \downarrow\end{matrix}\right\rangle$$

$$\left|\begin{matrix}\uparrow\uparrow\uparrow\uparrow\\ \downarrow\downarrow\end{matrix}\right\rangle = -\left|\begin{array}{|c|}\hline\chi\\\hline\end{array}\right\rangle\left|\begin{matrix}\uparrow\uparrow\uparrow\\ \downarrow\end{matrix}\right\rangle\left|\begin{array}{|c|c|}\hline 5&6\\\hline\end{array}\right\rangle\left|\begin{matrix}\uparrow\\ \downarrow\end{matrix}\right\rangle. \tag{4.32}$$

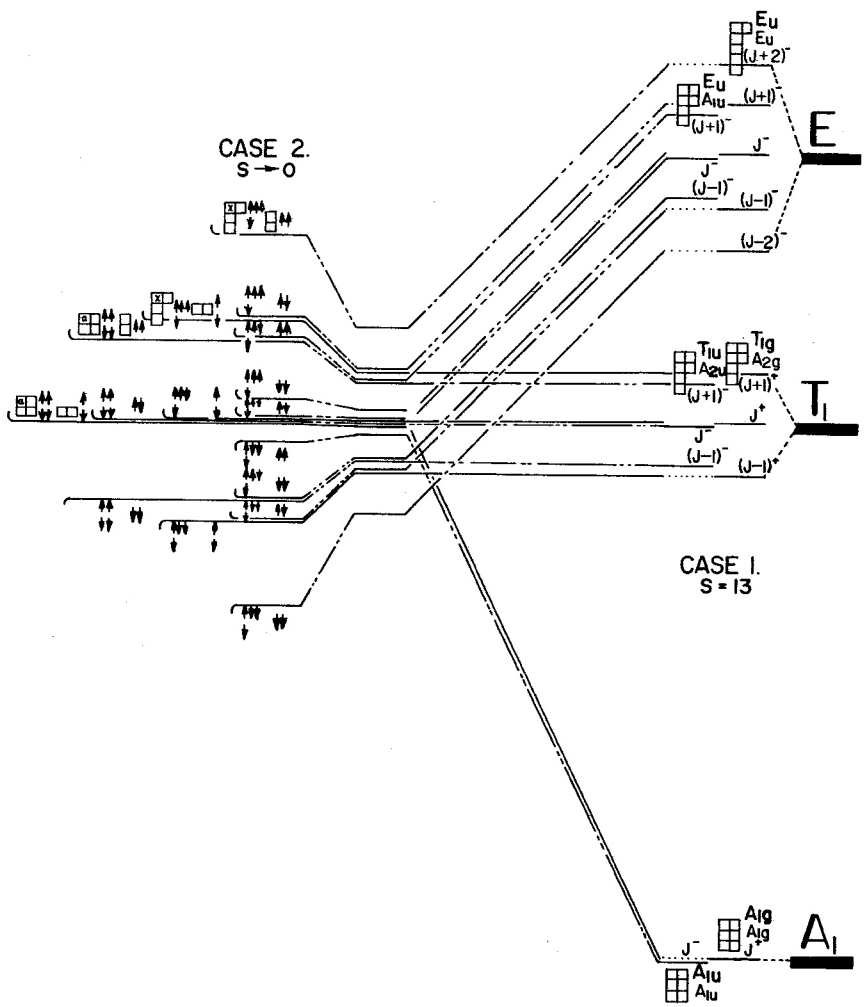

FIG. 14. Superhyperfine level correlations for the A-type tetragonal clusters ($0_4\dagger O = A_1+T_1+E$). (a) Case-1 levels are shown on the left-hand side. They are labeled by broken tableaus which are good labels when the tensor spin-rotation parameter (a) is dominant. (b) Case-1 levels are shown on the right-hand side. They are labeled by full tableaus which are good labels when the axis tunneling parameter ($-S$) is dominant.

The T_{1u} states have a different form given by

$$\left|\begin{matrix}\{4,2\}\\ T_{1u},A_{2u}\end{matrix}\ \uparrow\uparrow\uparrow\uparrow\ \downarrow\downarrow\right\rangle = \left|\begin{array}{|c|c|}\hline\alpha & \\\hline\end{array}\ \uparrow\uparrow\ \downarrow\downarrow\ \begin{array}{|c|c|}\hline 5&\\\hline 6&\\\hline\end{array}\ \uparrow\downarrow\right\rangle$$

$$\left|\ \uparrow\uparrow\uparrow\uparrow\ \downarrow\downarrow\right\rangle = \left|\begin{array}{|c|c|}\hline\alpha & \\\hline\end{array}\ \uparrow\uparrow\ \downarrow\downarrow\ \begin{array}{|c|}\hline\ \\\hline 6\\\hline\end{array}\ \uparrow\downarrow\right\rangle \qquad (4.33)$$

$$\left|\ \uparrow\uparrow\uparrow\uparrow\ \downarrow\downarrow\right\rangle = \left|\begin{array}{|c|c|}\hline\alpha & \\\hline\end{array}\ \uparrow\uparrow\ \downarrow\downarrow\ \begin{array}{|c|c|}\hline 5&\\\hline 6&\\\hline\end{array}\ \downarrow\downarrow\right\rangle .$$

Here we designate by (α) the following $\{2,2\}$ tableau combination (See Appendix B):

$$-(1/2)\begin{array}{|c|c|}\hline 1&2\\\hline 3&4\\\hline\end{array}+(\sqrt{3}/2)\begin{array}{|c|c|}\hline 1&3\\\hline 2&4\\\hline\end{array}\equiv\begin{array}{|c|c|}\hline\alpha & \\\hline\end{array}\ . \qquad (4.34)$$

Finally, the A_{1g} states are also written in terms of the (α) tableau:

$$\left|\begin{matrix}\{3,3\}\\ A_{1g},A_{1g}\end{matrix}\ \uparrow\uparrow\uparrow\ \downarrow\downarrow\downarrow\right\rangle = -\left|\begin{array}{|c|c|}\hline\alpha & \\\hline\end{array}\ \uparrow\uparrow\ \downarrow\downarrow\ \begin{array}{|c|c|}\hline 5&6\\\hline\end{array}\ \uparrow\downarrow\right\rangle . \qquad (4.35)$$

A correlation plot of (A_1T_1E) levels is drawn in Fig. 14. The case-1 levels with nonzero rotational tunneling amplitude $(S=13)$ are shown on the right-hand side. The case-2 levels for $(S=0)$ are drawn on the left-hand side according to the eigenvalues of matrices (4.9) and (4.11). In Fig. 14 the parameters are chosen to be $\sigma=0$, $n_I\tau=1$, and $a=\frac{1}{6}$. This gives easily recognizable spin-rotation clusters or super hyperfine level structure. The sixteen (A_1T_1E) case-2 levels in Fig. 14 are a subset of the $2^6=64$ levels shown in Fig. 12. For $a=\frac{1}{6}$ there are spin clusters at $H_{sr}=0,\pm1,\pm4,\pm5,\pm6,\pm9,\pm10$, and ±14 in Fig. 12, marked by degeneracy

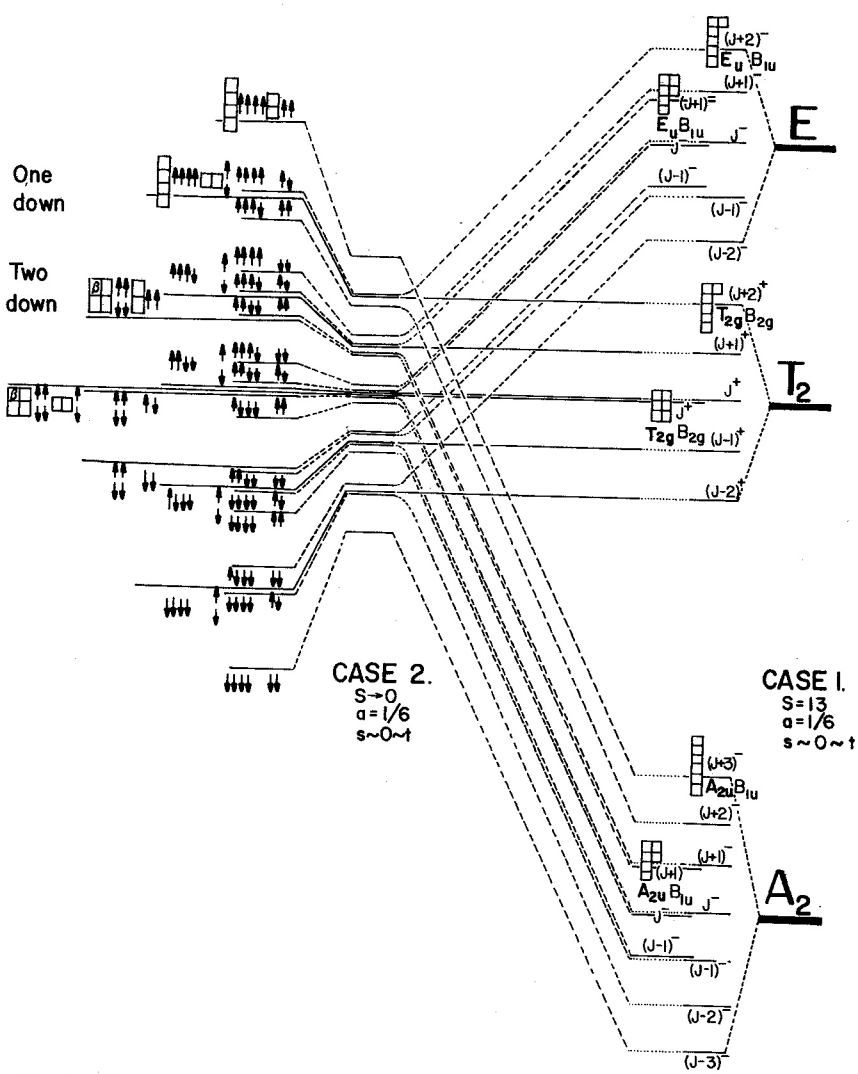

FIG. 15. Superhyperfine level correlations for the B-type tetragonal clusters $(2_4\dagger O=A_2+T_2+E)$. (a) Case-2 levels are shown on the left-hand side. They are labeled by broken tableaus which are good labels when the tensor spin-rotation parameter (a) is dominant. The one-downon and two-downon subclusters are indicated. (b) Case-1 levels are shown on the right-hand side. They are labeled by full tableaus which are good labels when the axis tunneling parameter $(-S)$ is dominant.

numbers 12, 4; 6, 8, 1; 4, 2; and 1, respectively. Of these, (A_1T_1E) uses 4, 1; 2, 2, 0; 1 0; and 0 levels, respectively.

In between the two cases the energy levels and eigenvectors vary with the rotational tunneling amplitude S. The additional cluster energies $(H-4S)$ for A_1 states, H for T_1 states, and $(H+2S)$ for E on the diagonal of (4.9) and (4.11) will affect the hyperfine mixing for some states and not others. (The parameter H stands for the cluster center of gravity and is taken to be zero here.) It is interesting to note that the splitting and mixing of the $(\{42\}, E_u, (J\pm1)^-)$ and $(\{51\}, E_u, (J\pm1)^-)$ states is independent of S. For these states hyperfine tensor spin-rotation splitting may be observable even in case (1) levels. The same may also be true for the $\{4,2\}(J\pm1)^\pm$ inversion doublets.

We will not discuss here more of the effects of the spin-spin tunneling parameters s, s, t, t', etc. or of the frame transformation coefficients c and d in Eqs. (4.12) and (4.13). Discussion of these important details will be done in future works when spectroscopic examples are treated, or when synthesized computer spectra are analyzed. Transformations between the factored case-2 (ECA) states and the case-1 octahedral species are summarized in Table VII(a).

B. Type $2_4\uparrow O = A_2 + T_2 + E$ clusters

The 2_4 or B-type clusters have the richest superhyperfine structure. Of the $2^6 = 64$ possible levels, the (A_2T_2E) cluster is allowed by the Pauli principle to have twenty-four superhyperfine levels. These levels are shown in a case-1 to -2 correlation diagram in Fig. 15. Transformations between the factored case-2 (ECA) states and octahedral species are summarized in Table VII(b). Here we will discuss the details of only the subclusters labeled "one down" in Fig. 15 or the $(n_I = 2)$ states in Table VII(b).

We have already mentioned the analogy between the tunneling model (2.10) in which rotor momentum could pick six positions, and the one-spin-down model (4.62) in which a single reversed spin or "downon" could pick six positions. Indeed, the eigenstates (2.11) of the rotor cluster have the same form as the $(n_I = 2)$ or one-down bases listed in Table V(a). There is a minor difference in labeling between the (A_1T_1E) rotor cluster states (2.11) and the $(A_{2u}T_{2g}E_u)$ downon cluster states in Table V(a) which is due to strict adherence to the Pauli principle. Otherwise the two problems have the same basic structure.

However, octahedral one-downon bases may not be eigenvectors of the tunneling Hamiltonian (4.6a) since is has only D_{4h} symmetry. Indeed, the representation of (4.6a) in the octahedral basis has a 2×2 submatrix (Here we set $\sigma = 0$ and $\tau = 1$ to simplify notation):

$$\langle H_{sr} + H_{ss}\rangle_{n_I=2} = \begin{array}{c|cc} & \widetilde{\{5,1\}} & \widetilde{\{6,0\}} \\ & T_{2g} \quad E_g \quad B_{1g} & E_u \quad A_{1u} \quad B_{2g} \quad A_{2g} \quad B_{2g} \quad A_{1u} \quad B_{1u} \quad A_{1u} \\ \hline \widetilde{\{5,1\}} & \begin{array}{c} 6a+8 \\ -t \end{array} & \\ & & \begin{array}{c} 6a+8 \\ -t \end{array} \\ & & & \begin{array}{c} 6a+8 \\ -t' \end{array} \\ & & & & \begin{array}{c} 6a+8+ \\ t'-2s \end{array} \\ & & & & & \begin{array}{c} 10a+8+ \\ (2t'+t)/3 \\ +2(s-4s')/3 \end{array} & \begin{array}{c} a\sqrt{8}+ \\ \sqrt{8}(s'-s)/3 \\ +\sqrt{2}(t'-t)/3 \end{array} \\ \widetilde{\{6,0\}} & & & & & & & \begin{array}{c} 8a+8+ \\ 4(s+2s')/3 \\ +(t'+2t)/3 \end{array} \end{array} \qquad (4.36)$$

The D_{4h} label is B_{1u} for the octahedral states E_u and A_{2u} which will be mixed by the 2×2 hyperfine matrix. The other state with a B-type D_{4h} label is the third octahedral T_{2g} component. Since states with B labels belong to the (A_2T_2E) cluster we see that the one-downon subcluster will have all three types A_{2u}, T_{2g}, and E_u of octahedral species represented. The superfine (A_2T_2E) cluster contains the basis for a miniature superhyperfine copy of itself!

However, the tensor spin-rotation perturbation can mix the A_{2u} and E_u species and give various different cluster level patterns. The tableau definition of these species are as follows from Table III(a) and III(b):

$$\begin{array}{ll} \{6,0\} & \{5,1\} \\ A_{2u} = \begin{array}{|c|}\hline 1\\\hline 2\\\hline 3\\\hline 4\\\hline 5\\\hline 6\\\hline\end{array}\,, & E_u = -(\sqrt{15}/5)\begin{array}{|c|c|}\hline 1&5\\\hline 2\\\hline 3\\\hline 4\\\hline 6\\\hline\end{array} + \sqrt{10/5}\begin{array}{|c|c|}\hline 1&6\\\hline 2\\\hline 3\\\hline 4\\\hline 5\\\hline\end{array}\,. \\ B_{1u} & B_{1u} \end{array} \tag{4.37}$$

The factor state $\left|\begin{array}{|c|}\hline 1\\\hline 2\\\hline 3\\\hline 4\\\hline\end{array}\ \begin{array}{|c|}\hline 5\\\hline 6\\\hline\end{array}\right\rangle$ is easily seen to be associated with the A_{2u} tableau. Table VI provides the factoring for the tableaus in the E_u state:

$$\begin{array}{|c|c|}\hline 1&5\\\hline 2\\\hline 3\\\hline 4\\\hline 6\\\hline\end{array} = -\sqrt{\frac{3}{5}}\begin{array}{|c|}\hline 1\\\hline 2\\\hline 3\\\hline 4\\\hline\end{array}\ \begin{array}{|c|}\hline 5\\\hline 6\\\hline\end{array} + \sqrt{\frac{2}{5}}\begin{array}{|c|}\hline 1\\\hline 2\\\hline 3\\\hline 4\\\hline\end{array}\ \begin{array}{|c|c|}\hline 5&6\\\hline\end{array}\,, \qquad \begin{array}{|c|c|}\hline 1&6\\\hline 2\\\hline 3\\\hline 4\\\hline 5\\\hline\end{array} = \sqrt{\frac{2}{5}}\begin{array}{|c|}\hline 1\\\hline 2\\\hline 3\\\hline 4\\\hline\end{array}\ \begin{array}{|c|}\hline 5\\\hline 6\\\hline\end{array} + \sqrt{\frac{3}{5}}\begin{array}{|c|}\hline 1\\\hline 2\\\hline 3\\\hline 4\\\hline\end{array}\ \begin{array}{|c|c|}\hline 5&6\\\hline\end{array}\,. \tag{4.38}$$

This shows that the A_{2u} and E_u states with same D_{4h} label have the same broken tableau structure:

$$\begin{array}{ll} \{6\} & \{5,1\} \\ A_{2u} = \begin{array}{|c|}\hline 1\\\hline 2\\\hline 3\\\hline 4\\\hline\end{array}\ \begin{array}{|c|c|}\hline 5&6\\\hline\end{array}\,, & E_u = \begin{array}{|c|}\hline 1\\\hline 2\\\hline 3\\\hline 4\\\hline\end{array}\ \begin{array}{|c|c|}\hline 5&6\\\hline\end{array}\,. \\ B_{1u} & B_{1u} \end{array} \tag{4.39}$$

It is possible to work backwards from the broken tableau labeling using Table VI. One could derive the transformations in Table III directly. The subgroup $S_6 \supset O_h \supset D_{4h}$ is compatible with the chain $S_6 \supset S_4 \times S_2$ which defines broken tableaus.

The spin tableau states are made by coupling the spin parts of the factors to total spin I:

$$\left|\begin{array}{l}\{u\}\\ \Gamma \quad I\\ B_{1u} \quad n_I=2\end{array}\right\rangle = C^{21I}_{202}\left|\begin{array}{|c|}\hline 1\\\hline 2\\\hline 3\\\hline 4\\\hline\end{array}\ \uparrow\uparrow\uparrow\uparrow\ \begin{array}{|c|}\hline 5\\\hline 6\\\hline\end{array}\ \uparrow\downarrow\right\rangle + C^{21I}_{112}\left|\begin{array}{|c|}\hline 1\\\hline 2\\\hline 3\\\hline 4\\\hline\end{array}\ \uparrow\uparrow\uparrow\downarrow\ \begin{array}{|c|}\hline 5\\\hline 6\\\hline\end{array}\ \uparrow\downarrow\right\rangle .$$

The I value depends on the tableau $\{u\}$. It is $I=3$ for $\{6,0\}$ and $I=2$ for $\{5,1\}$:

$$\left|\begin{array}{l}\{6,0\}\\ A_{2u}\\ B_{1u}\end{array}\ \uparrow\uparrow\uparrow\uparrow\uparrow\uparrow\right\rangle = \sqrt{\frac{1}{3}}\left|\begin{array}{|c|}\hline 1\\\hline 2\\\hline 3\\\hline 4\\\hline\end{array}\ \uparrow\uparrow\uparrow\uparrow\ \begin{array}{|c|}\hline 5\\\hline 6\\\hline\end{array}\ \uparrow\downarrow\right\rangle + \sqrt{\frac{2}{3}}\left|\begin{array}{|c|}\hline 1\\\hline 2\\\hline 3\\\hline 4\\\hline\end{array}\ \uparrow\uparrow\uparrow\downarrow\ \begin{array}{|c|}\hline 5\\\hline 6\\\hline\end{array}\ \uparrow\downarrow\right\rangle\,, \tag{4.40a}$$

$$\left|\begin{array}{l}\{5,1\}\\ E_u\\ B_{1u}\end{array}\ \begin{array}{l}\uparrow\uparrow\uparrow\uparrow\uparrow\\ \downarrow\end{array}\right\rangle = \sqrt{\frac{2}{3}}\left|\begin{array}{|c|}\hline 1\\\hline 2\\\hline 3\\\hline 4\\\hline\end{array}\ \uparrow\uparrow\uparrow\uparrow\ \begin{array}{|c|}\hline 5\\\hline 6\\\hline\end{array}\ \uparrow\downarrow\right\rangle - \sqrt{\frac{1}{3}}\left|\begin{array}{|c|}\hline 1\\\hline 2\\\hline 3\\\hline 4\\\hline\end{array}\ \uparrow\uparrow\uparrow\downarrow\ \begin{array}{|c|}\hline 5\\\hline 6\\\hline\end{array}\ \uparrow\downarrow\right\rangle . \tag{4.40b}$$

TABLE VI. Factoring transformation matrices for (a) tetragonal ($6 \rightarrow 4+2$), and (b) trigonal ($6 \rightarrow 3+3$) factorization.

(a)

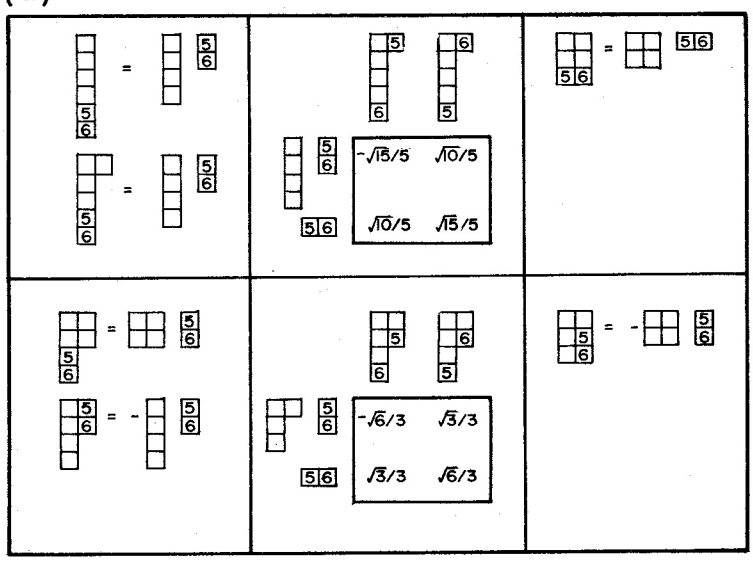

(b)

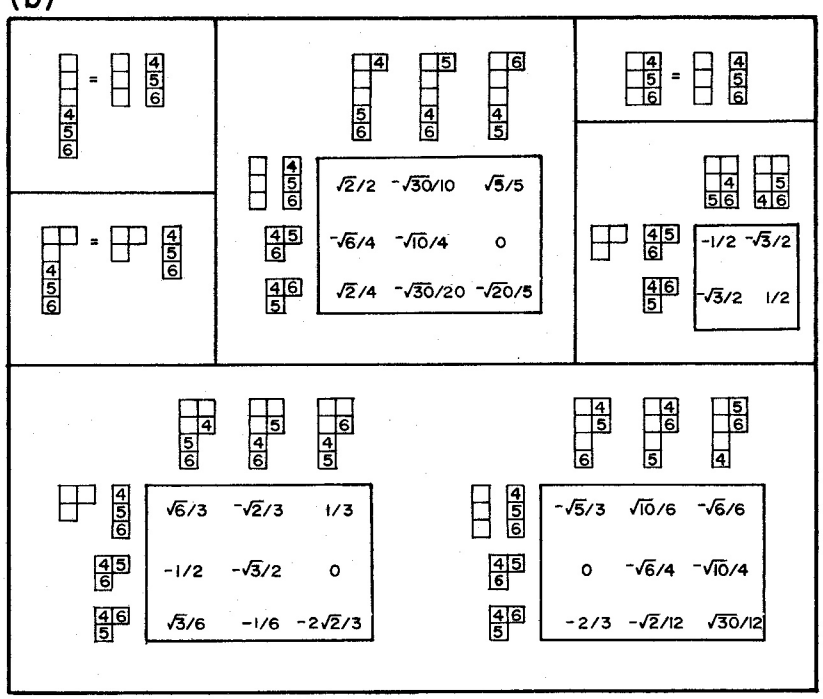

The inverse of this transformation yields the desired mixtures of A_{2u} and E_u states:

$$\left| \begin{array}{|c|}\hline 1 \\ \hline 2 \\ \hline 3 \\ \hline 4 \\ \hline \end{array} \uparrow\uparrow\uparrow\uparrow \begin{array}{|c|}\hline 5 \\ \hline 6 \\ \hline \end{array} \uparrow\uparrow \right\rangle = \sqrt{\frac{1}{3}} \left| A_{2u} \right\rangle + \sqrt{\frac{2}{3}} \left| E_u \right\rangle , \tag{4.41a}$$

$$\left|\begin{array}{|c|}\hline 1\\\hline 2\\\hline 3\\\hline 4\\\hline\end{array}\ \uparrow\uparrow\uparrow\downarrow\ \begin{array}{|c|}\hline 5\\\hline 6\\\hline\end{array}\ \uparrow\downarrow\right\rangle = \sqrt{\frac{2}{3}}\left|A_{2u}\right\rangle - \sqrt{\frac{1}{3}}\left|E_u\right\rangle . \tag{4.41b}$$

In the broken tableau basis the representation of the spin-rotation interaction becomes diagonal:

$$\langle H_{sr}+H_{ss}\rangle_{B_{1u},n_I=2} = \begin{array}{|c|c|}\hline \begin{array}{|c|}\hline 1\\\hline 2\\\hline 3\\\hline 4\\\hline\end{array}\ \uparrow\uparrow\uparrow\uparrow\ \begin{array}{|c|}\hline 5\\\hline 6\\\hline\end{array}\ \uparrow\downarrow & \begin{array}{|c|}\hline 1\\\hline 2\\\hline 3\\\hline 4\\\hline\end{array}\ \uparrow\uparrow\uparrow\downarrow\ \begin{array}{|c|}\hline 5\\\hline 6\\\hline\end{array}\ \uparrow\downarrow \\\hline 12a+8+t'+4s' & s'\sqrt{8} \\\hline s'\sqrt{8} & 6a+8+t+2s-4s' \\\hline\end{array} . \tag{4.42}$$

The spin tunneling amplitude s' between polar and equatorial positions perturbs the spin-rotation eigenstates. This was also the case in Eq. (4.31).

The extreme cases for $(n_I=2)$ or one-downon superhyperfine level structure are indicated on either side of Fig. 16. The extreme spin tensor case is shown on the right-hand side where all parameters except $(\tau=1)$ and $(a<0)$ are zero. This corresponds to the levels marked 2 and 4 near the top of Fig. 12. The extreme scalar case is shown on the left-hand side where the spin exchanges between nearest neighbors equally $(s=s'<0)$ but all other parameters are zero. This is analogous to the two-to-one splitting of the ordinary (A, T, E) cluster as given in Eq. (2.12).

In the level correlation between the two extremes of Fig. 16 we assume $s'=0$ and arbitrary values for a, s, t, and t'. The eigenvalues from Eqs. (4.36) and (4.42) are indicated for the factored eigenstates. The levels which arise in the B-type or $2_4\uparrow O=(A_2,T_2,E)$ rotational clusters are drawn in the right-hand column of Fig. 16. The single level from the A-type or $1_4\uparrow O=(A_1,T_1,E)$ cluster is drawn on the left-hand column. [Recall Eq. (4.9).] The E-type or (T_1,T_2) clusters will be discussed in the following subsection.

In the example of Eqs. (4.36) or (4.42) the factored case-2 states cannot be eigenstates in case 1. The energies of unfactored A_{2u} and E_u species are dominated by $(H-4S)$ and $(H+2S)$, respectively, due to rotational tumbling or tunneling. For large S the separate hyperfine structures of superfine levels will reassert themselves as shown on the right-hand side of Fig. 15. The two cases are each characterized by a different type of tunneling or exchange processes. In case-1 nuclei are exchanged, while in case-2 spins or downon quasiparticles are exchanged.

The structure of two-downon $(n_1=1)$ and three-downon $(n_I=0)$ states can show the effects of more complicated processes. For one thing one should include diagonal scalar and tensor spin-spin contributions which are left out of pseudo-Hamiltonians (4.7) and (4.8). This corresponds to interaction energies between quasiparticles. The detailed physics of the resulting super-hyperfine structure should be discussed in a separate work after these features have been observed in laser spectra or in computer synthesis. (See also the discussion in Appendix D.)

However, there are some mathematical features which should be pointed out here. The $\{4,2\}$ octahedral A_{2u} and E_u states are combinations of two different types of broken tableaus. From Table III(a) one obtains

$$\left|\begin{array}{c}\{\widetilde{4,2}\}\\ A_{2u}\\ B_{1u}\end{array}\right\rangle = (\sqrt{15}/6)\ \begin{array}{|c|c|}\hline 1&2\\\hline 3&4\\\hline 5\\\cline{1-1} 6\\\cline{1-1}\end{array}\ + (\sqrt{5}/6)\ \begin{array}{|c|c|}\hline 1&3\\\hline 2&4\\\hline 5\\\cline{1-1} 6\\\cline{1-1}\end{array}$$

$$-(2/3)\ \begin{array}{|c|c|}\hline 1&5\\\hline 2&6\\\hline 3\\\cline{1-1} 4\\\cline{1-1}\end{array} . \tag{4.43}$$

This factors easily according to Fig. 13 or Table VI(a):

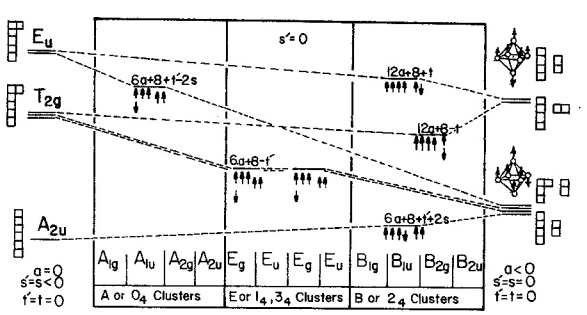

FIG. 16. Case-2 energy level correlations for a one-downon subcluster. The right-hand side corresponds to a dominant tensor spin-rotation parameter (a), while the left-hand side corresponds to dominant spin exchange tunneling parameters $(s=s')$.

TABLE VII. Factored eigenvectors for tetragonal cluster tensor spin-rotation Hamiltonian. (a) A_1+T_1+E cluster, (b) A_2+T_2+E, (c) T_1+T_2 cluster. Symbol key:

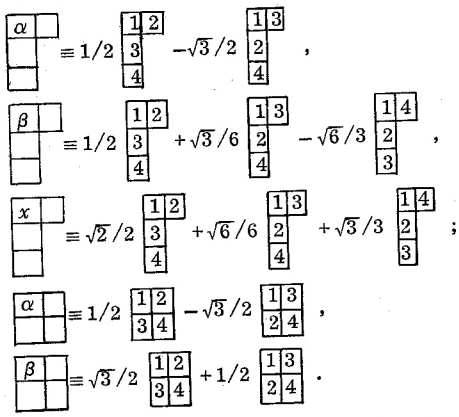

(a) A-type (A_1T_1E) clusters

	n_I	$n_I=1$		$n_I=0$		
	$\left\|\uparrow\uparrow\uparrow\downarrow\ \uparrow\uparrow\right\rangle$	$\left\|\uparrow\uparrow\uparrow\downarrow\ \uparrow\downarrow\right\rangle$	$\left\|\uparrow\uparrow\downarrow\uparrow\ \uparrow\uparrow\right\rangle$	$\left\|\uparrow\uparrow\uparrow\downarrow\ \downarrow\downarrow\right\rangle$	$\left\|\uparrow\uparrow\downarrow\uparrow\ \uparrow\downarrow\right\rangle$	$\left\|\uparrow\uparrow\downarrow\downarrow\ \uparrow\uparrow\right\rangle$
$\{5,1\}$ E_u 2 A_{1u} n_I	1	$\sqrt{2}/2$	$\sqrt{2}/2$	$\sqrt{6}/6$	$\sqrt{6}/3$	$\sqrt{6}/6$
$\{4,2\}$ E_u 1 A_{1u} n_I		$-\sqrt{2}/2$	$\sqrt{2}/2$	$-\sqrt{2}/2$	0	$\sqrt{2}/2$
$\{3,3\}$ A_{1u} 0 A_{1u} 0				$-\sqrt{3}/3$	$\sqrt{3}/3$	$-\sqrt{3}/3$
	$\left\|\uparrow\uparrow\uparrow\uparrow\ \downarrow\downarrow\right\rangle$	$\left\|\uparrow\uparrow\uparrow\uparrow\ \downarrow\uparrow\right\rangle$		$\left\|\uparrow\uparrow\uparrow\downarrow\ \uparrow\downarrow\right\rangle$	$\left\|\uparrow\uparrow\downarrow\uparrow\ \uparrow\downarrow\right\rangle$	$\left\|\uparrow\uparrow\uparrow\uparrow\ \downarrow\downarrow\right\rangle$
$\{4,2\}$ T_{1g} 1 A_{2g} n_I	-1	0		-1	0	0
$\{4,2\}$ T_{1g} 1 A_{2g} n_I	0	1		0	1	0
$\{3,3\}$ A_{1g} 0 A_{1g} 0				0	0	-1

TABLE VII. *(Continued.)*

(b) B-type (A_2T_2E) clusters

	$n_I=3$	$n_I=2$		$n_I=1$				$n_I=0$			
{6, 0}	$\lvert\uparrow\uparrow\uparrow\uparrow\ \uparrow\uparrow\rangle$	$\lvert\uparrow\uparrow\uparrow\uparrow\ \downarrow\uparrow\rangle$	$\lvert\uparrow\uparrow\uparrow\uparrow\ \uparrow\downarrow\rangle$	$\lvert\uparrow\uparrow\uparrow\uparrow\ \downarrow\downarrow\rangle$	$\lvert\uparrow\uparrow\uparrow\downarrow\ \uparrow\downarrow\rangle$	$\lvert\uparrow\uparrow\downarrow\downarrow\ \uparrow\downarrow\rangle$	$\left\lvert\begin{smallmatrix}\uparrow\uparrow\\ \downarrow\downarrow\end{smallmatrix}\ \begin{smallmatrix}\uparrow\uparrow\\ \downarrow\downarrow\end{smallmatrix}\right\rangle_2$	$\lvert\uparrow\uparrow\uparrow\uparrow\downarrow\downarrow\rangle$	$\lvert\uparrow\uparrow\uparrow\uparrow\ \downarrow\downarrow\rangle$	$\lvert\uparrow\uparrow\uparrow\downarrow\ \uparrow\downarrow\rangle$	$\left\lvert\begin{smallmatrix}\uparrow\uparrow\\ \downarrow\downarrow\end{smallmatrix}\ \begin{smallmatrix}\uparrow\uparrow\\ \downarrow\downarrow\end{smallmatrix}\right\rangle_2$
$A_{2u}\ 3 = \left\lvert \begin{smallmatrix}1\\2\\3\\4\end{smallmatrix}\ \begin{smallmatrix}5\\6\end{smallmatrix}\right\rangle_{B_{1u}\ n_I}^{3}$	$\sqrt{3}/3$	$\sqrt{6}/3$		$\sqrt{15}/15$	$2\sqrt{30}/15$	$\sqrt{10}/5$	0	$\sqrt{5}/5$	$\sqrt{15}/5$	$\sqrt{5}/5$	0
{5, 1}											
$E_u\ 2 = -\left\lvert \begin{smallmatrix}1\\2\\3\\4\end{smallmatrix}\ \begin{smallmatrix}5\\6\end{smallmatrix}\right\rangle_{B_{1u}\ n_I}^{2}$	$\sqrt{6}/3$	$-\sqrt{3}/3$		$\sqrt{3}/3$	$\sqrt{6}/6$	$-\sqrt{2}/2$	0	$\sqrt{2}/2$	0	$-\sqrt{2}/2$	0
{4, 2}											
$A_{2u}\ 1 = \frac{2}{3}\left\lvert \begin{smallmatrix}1\\2\\3\\4\end{smallmatrix}\ \begin{smallmatrix}5\\6\end{smallmatrix}\right\rangle_{B_{1u}\ n_I}^{1} + \frac{\sqrt{5}}{3}\left\lvert \begin{smallmatrix}\beta\end{smallmatrix}\ \begin{smallmatrix}5\\6\end{smallmatrix}\right\rangle_{n_I}^{1}$				$2\sqrt{15}/15$	$-\sqrt{30}/15$	$\sqrt{10}/15$	$\sqrt{5}/3$	$\sqrt{30}/15$	$-2\sqrt{10}/15$	$\sqrt{30}/15$	$\sqrt{5}/3$
{4, 2}											
$E_u\ 1 = \frac{\sqrt{5}}{3}\left\lvert \begin{smallmatrix}1\\2\\3\\4\end{smallmatrix}\ \begin{smallmatrix}5\\6\end{smallmatrix}\right\rangle_{B_{1u}\ n_I}^{1} - \frac{2}{3}\left\lvert \begin{smallmatrix}\beta\end{smallmatrix}\ \begin{smallmatrix}5\\6\end{smallmatrix}\right\rangle_{n_I}^{1}$				$\sqrt{3}/3$	$-\sqrt{6}/6$	$\sqrt{2}/6$	$-2/3$	$\sqrt{6}/6$	$-\sqrt{2}/3$	$\sqrt{6}/6$	$-2/3$
		$\lvert\uparrow\uparrow\uparrow\uparrow\ \begin{smallmatrix}\uparrow\\ \downarrow\end{smallmatrix}\rangle$		$\lvert\uparrow\uparrow\uparrow\uparrow\ \begin{smallmatrix}\uparrow\\ \downarrow\end{smallmatrix}\rangle$				$\lvert\uparrow\uparrow\uparrow\uparrow\ \begin{smallmatrix}\uparrow\\ \downarrow\end{smallmatrix}\rangle$			
{5, 1}											
$T_{2g}\ 1 = \left\lvert \begin{smallmatrix}1\\2\\3\\4\end{smallmatrix}\ \begin{smallmatrix}5&6\end{smallmatrix}\right\rangle_{B_{2g}\ n_I}^{2}$		1		1				1			
								$\left\lvert\begin{smallmatrix}\uparrow\uparrow\\ \downarrow\downarrow\end{smallmatrix}\ \begin{smallmatrix}\uparrow\\ \downarrow\end{smallmatrix}\right\rangle$			
{3, 3}											
$T_{2g}\ 0 = -\left\lvert \begin{smallmatrix}\beta\end{smallmatrix}\ \begin{smallmatrix}5&6\end{smallmatrix}\right\rangle_{B_{2g}\ 0}^{0}$								−1			

TABLE VII. *(Continued.)*

(c) E-type (T_1T_2) clusters

	$n_I=2$	$n_I=1$		$n_I=0$		
$\{5,1\}$ T_{2g} E_g B_{1g}	1	$\sqrt{2}/2$	$\sqrt{2}/2$	$\sqrt{6}/6$	$\sqrt{6}/3$	$\sqrt{6}/6$
$\{4,2\}$ T_{1g} E_g		$-\sqrt{2}/2$	$\sqrt{2}/2$	$-\sqrt{2}/2$	0	$\sqrt{2}/2$
$\{3,3\}$ T_{2g} E_g B_{1g}				$-\sqrt{3}/3$	$\sqrt{3}/3$	$-\sqrt{3}/3$
$\{4,2\}$ T_{1u} E_u B_{1u}		1		1		

$$\left|\begin{matrix}\{\widetilde{4,2}\}\\ A_{2u}\\ B_{1u}\end{matrix}\right\rangle = (\sqrt{5}/3)\left((\sqrt{3}/2)\begin{array}{|c|c|}\hline 1&2\\\hline 3&4\\\hline\end{array}\ \begin{array}{|c|}\hline 5\\\hline 6\\\hline\end{array} + (1/2)\begin{array}{|c|c|}\hline 1&3\\\hline 2&4\\\hline\end{array}\ \begin{array}{|c|}\hline 5\\\hline 6\\\hline\end{array}\right) + (2/3)\begin{array}{|c|}\hline 1\\\hline 2\\\hline 3\\\hline 4\\\hline\end{array}\ \begin{array}{|c|}\hline 5\\\hline 6\\\hline\end{array}\ .$$

(Note change of sign in last term.) The A_{2u} factoring and the one for E_u are written as follows in Table VII:

$$\left|\begin{matrix}\{\widetilde{4,2}\}\\ A_{2u}\\ B_{1u}\end{matrix}\right\rangle = (\sqrt{5}/3)\begin{array}{|c|c|}\hline\beta&\\\hline&\\\hline\end{array}\ \begin{array}{|c|}\hline 5\\\hline 6\\\hline\end{array} + (2/3)\begin{array}{|c|}\hline 1\\\hline 2\\\hline 3\\\hline 4\\\hline\end{array}\ \begin{array}{|c|}\hline 5\\\hline 6\\\hline\end{array} \qquad (4.44a)$$

$$\left|\begin{matrix}\{\widetilde{4,2}\}\\ E_u\\ B_{1u}\end{matrix}\right\rangle = (-2/3)\begin{array}{|c|c|}\hline\beta&\\\hline&\\\hline\end{array}\ \begin{array}{|c|}\hline 5\\\hline 6\\\hline\end{array} + (\sqrt{5}/3)\begin{array}{|c|}\hline 1\\\hline 2\\\hline 3\\\hline 4\\\hline\end{array}\ \begin{array}{|c|}\hline 5\\\hline 6\\\hline\end{array}\ , \qquad (4.44b)$$

where the β tableau is defined by

$$\begin{array}{|c|c|}\hline\beta&\\\hline&\\\hline\end{array} \equiv (\sqrt{3}/2)\begin{array}{|c|c|}\hline 1&2\\\hline 3&4\\\hline\end{array} + (1/2)\begin{array}{|c|c|}\hline 1&3\\\hline 2&4\\\hline\end{array}\ . \qquad (4.44c)$$

This definition is discussed in Appendix B. Spin coupling for each of the four B_{1u} states $|\{6,0\}A_{2u}\rangle$, $|\{5,1\}E_u\rangle$, $|\{4,2\}A_{2u}\rangle$, and $|\{4,2\}E_u\rangle$ yields the factoring transformations on the upper right-hand side of Table VII(b) for $n_I=1$ and 0.

The pseudo-Hamiltonians for $n_I=1$ and 0 are represented by 4×4 matrices given in Appendix C. As usual, the tensor spin-rotation interaction has off-diagonal components in the $\{|A_{2u}\rangle|E_u\rangle|A_{2u}\rangle|E_u\rangle\}$ representation but is diagonal in the broken-tableau basis. In the original whole-tableau basis it is instructive to note some selection rules for the pure tensor (E_g, A_{1g}) component (4.2b) of the spin rotation operator. This occurs when $\alpha_a=0$ or for $\sigma=0$ and $a=-1$. Then all $\langle A_{2u}|H|A_{2u}\rangle$ components vanish identically since $E_g\otimes A_{2u}$ does not contain A_{2u}.

It is interesting to note that most of the spin tunneling amplitudes lead to off-diagonal contributions even in the broken-tableau basis. The ef-

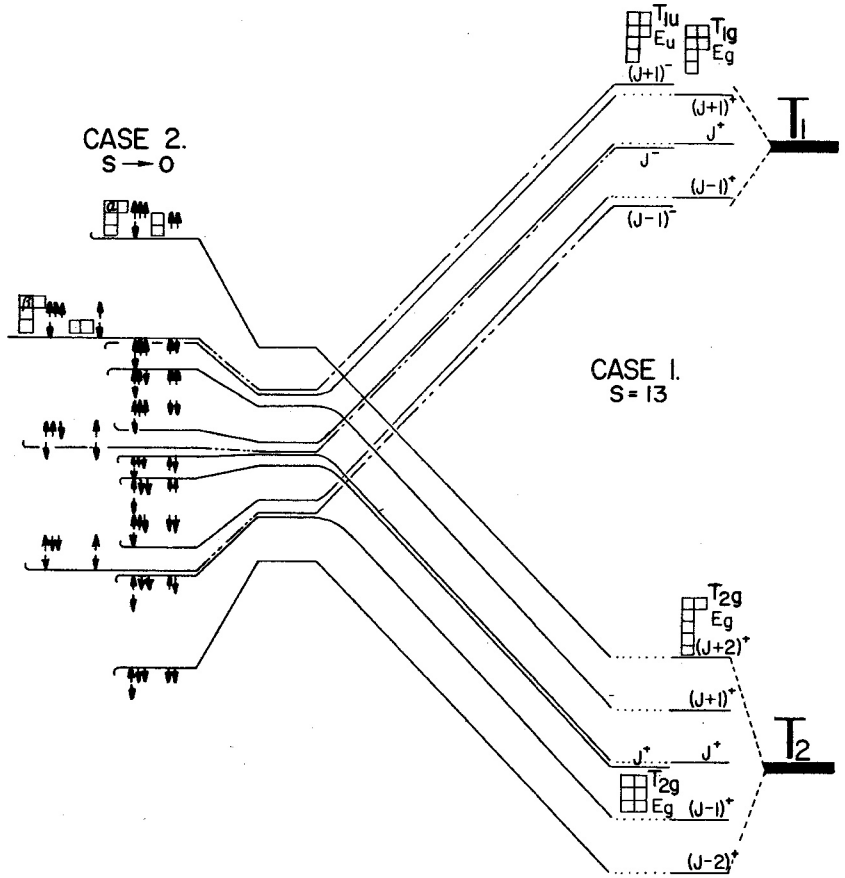

FIG. 17. Superhyperfine level correlations for the E-type tetragonal clusters ($\pm 1_4 \uparrow O = T_1 + T_2$).

fects of these amplitudes can derived by perturbation theory if they are small. In principle a 4×4 matrix can be diagonalized analytically (there are no larger matrices in the ECA for SF_6), but numerical treatment is probably preferable for intermediate coupling cases. This is especially true when the eigenvectors are needed to give spectral intensity ratios as shown in Sec. III C.

C. Type $\pm 1_4 \uparrow O = T_1 \oplus T_2$ clusters

The $(T_1 T_2)$ clusters belong to the most commonly found type in the fourfold spectra since any odd value of n_4 induces $(T_1 \oplus T_2)$. This type of cluster is correlated with those bases in Table V for which the D_{4h} label is E_g or E_u. Each E_g or E_u label comes with a pair of D_{2h} labels (B_{1g}, B_{2g}) or (B_{1u}, B_{2u}), respectively. For a D_{4h} symmetric pseudo-Hamiltonian it is only necessary to pick one of these components since the other must give the same matrix.

In Table VII(c) the E-type cluster bases belonging to the first B_{1g} or B_{1u} component are listed. The transformation of these bases into factored tableau states is given in the tables. The case-1 and -2 correlation diagram associated with this transformation is sketched in Fig. 17. Examples of pseudo-Hamiltonian matrices needed to derive such correlations quantitatively are given in Appendix C. There is a 2×2 matrix for $n_I = 1$ and a 3×3 matrix for $n_I = 0$.

However, it may be unnecessary to diagonalize these matrices if the states belong wholly in case 1 or case 2. As an example consider a transition between a strong case-2 ground cluster and an excited case-1 cluster. The rovibronic nomogram for this transition is sketched in Fig. 18. Some tensor and spin splittings may be exaggerated and may be in the wrong direction for many SF_6 clusters. The ground levels at the bottom of Fig. 18 come from the left-hand (case-1) side of Fig. 17. The excited levels along the left-hand side of Fig. 18 come from the right-hand (case-2) side of Fig. 17. The parameters for Fig. 17 were arbitrarily chosen.

Nevertheless, the squares of the transformation coefficients in Table VII(c) determine the intensity ratios if the case 1 and 2 clusters are true to form. The numbers next to transitions in Fig. 18 are the squared coefficients. The figure is drawn

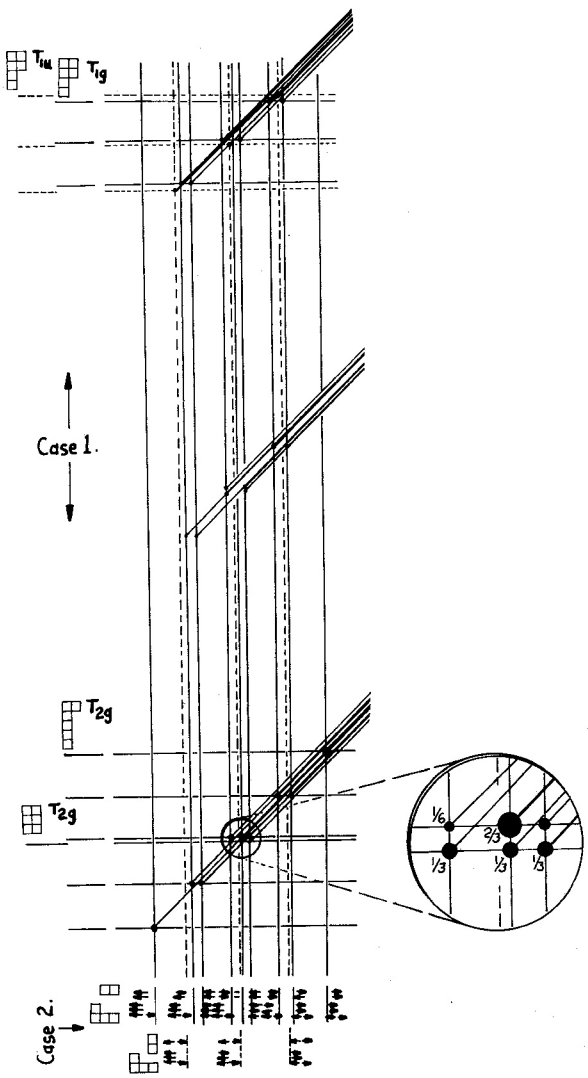

FIG. 18. Transition nomogram for transitions between a strong case-2 and a case-1 E-type (T_1,T_2) cluster. The relative transition rates are taken from Table VII(c) and indicated on the figure.

according to the procedures established in Fig. 9. An allowed spectral line leads upward at 45° from each allowed transitions point between an initial level and an excited level. Also, the crossover points are drawn halfway between a pair of transition points on a given line. (The crossovers between nearly adjacent points are not indicated in the figure, however.) Generally, the crossover intensities are proportional to the geometrical mean of the intensities of the two parent transitions.[5,6]

An example of a related transition involves the $Q(53)$ (T_2^6,T_1^6) cluster observed by Bordé *et al.*[4,6] This cluster has a fourfold component of momentum $n_4=45$. It has a (T_1-T_2) superfine splitting in the ground levels of 180 kHz and an uncertainty angle $\theta_{45}^{53}=33°$. The large angle indicates this is not a strong case-2 cluster. However, the hyperfine splitting is more than twice the superfine splitting, and so strong hyperfine mixing can occur.

The mixing results in transitions indicated by light dots in Fig. 19. The crossovers labeled C and D by Bordé *et al.*[6] are halfway between the light dots and heavy dots which indicate the main line allowed transitions. Even though the "forbidden" transitions associated with the light dots are hard to resolve directly, they manage to team up with allowed transitions to make easily observable crossovers. The splitting between the C and D groups allowed Bordé *et al.*[6] to measure t_{044}. A standard level diagram of the transitions and a comparison between laser spectra and computer synthesis is given in Ref. 6.

From the nomograms one may see that a significantly different scalar constant c_a of spin rotation for the excited vibration levels would cause more spectral structure to emerge. For example, the dots on the main A and F lines in Fig. 19 would each belong to separate lines. Apparently, the differences are not significant for the Q-branch spectra at their present level of resolution. However, Bordé *et al.*[4] have noted changes of c_a equal to 165 Hz for $R(28)$, $A_2^0(n_3=27)$ 125 Hz for $P(33)$, A_2^1 (borderline twofold case: $n_4\cong 26$ or $n_3\cong 30$), and 68 Hz for $P(59)$, A_2^3 (borderline case: $n_4\cong 47$ or $n_3\cong 54$), and they give a simple formula for these shifts by appealing to the scalar spin-vibration interaction. While these results involve weak clusters, they point the way toward possibilities for investigating the effects of rovibrational motion such as is sketched in Fig. 2. If strong case-2 clusters are involved in a transition this motion should effect the tensor as well as the scalar interactions.

Finally, one should remember that an accurate theory of weak clusters should include frame transformation effects.[1,14] The detailed consequences of the frame correlation effects will be discussed in later works.

V. TRIGONAL CLUSTER BASES

At any time about one third of the gas-phase SF_6 molecules will be rotating more or less uniformly on a threefold symmetry axis. Examples of the resulting threefold clusters (A_1,T_1,T_2,A_2) and (T_1,E,T_2) are shown on the right-hand side of Fig. 1(b) and 1(c). A complete cycle $((T_1,E,T_2),(A_2,T_2,T_1,A_1),(T_1,E,T_2))$ of threefold clusters contains exactly $2^6=64$ Pauli allowed states. In the preceeding section one counts the same number

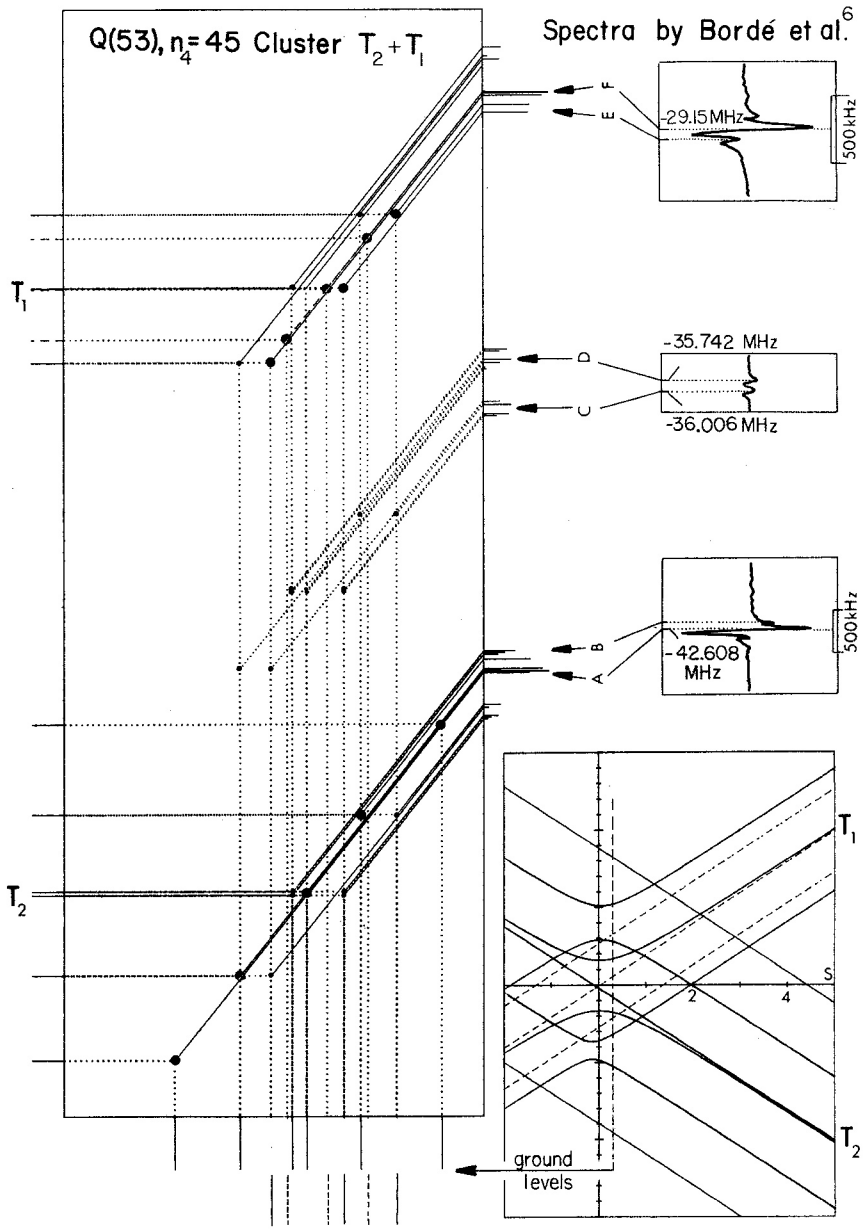

FIG. 19. Transition nomogram for transitions between a weak case-2 and a case-1 E-type (T_1, T_2) cluster. Frame transformation and diagonalization yield the level correlations shown in the lower right-hand inset. Spectra produced by Bordé *et al.*[4,6] are compared with the resulting spectral nomogram and intensities. The theoretical ground levels were obtained using constants $S = 0.3$, $\tau = 6.2$, and $a = -0.2$ in Table XI(c) with all other constants set equal to zero.

in a cycle $((A_1, T_1, E)(T_2, T_1)(E, T_2, A_2)(T_2, T_1))$ of fourfold clusters. Since there are about twice as many fourfold cycles in Fig. 1(b) and 1(c) as threefold cycles the threefold rotating molecules account for only one third of the total population.

The molecules involved in threefold clusters have an effective or spontaneously broken symmetry described by the subgroup D_{3d} of O_h. It is therefore convenient to use the trigonal subgroup chain $O_h \supset D_{3d} \supset C_{2i}$, instead of the tetragonal $O_h \supset D_{4h} \supset D_{2h}$ chain, for labeling the rotational states. Otherwise the mechanics for calculating states and operators is similar for threefold or fourfold clusters.

The desired transformations from S_6 tableau bases and trigonally defined bases are given in Table VIII. The transformations can be obtained directly by factored projection according to the $S_6 \supset O_h \supset D_{3d} \supset C_{2i}$ chain. The state geometry and coset operators are indicated in Fig. 20. Or else, given the D_{4h} transformations, one can simply rotate between fourfold and threefold axes. If the

TABLE VIII. Transformations between XY_6 tableau bases and octahedral-trigonally defined bases. The octahedral labeling is done using the subgroup chain $O_h \supset D_{3d} \supset C_{2i}$.

(a)

A_{2u}
A_{2u}
B_u
1

O_h D_{3d} C_{2i}

1
2
3
4
5
6

(b)

T_{2g} A_{1g} A_{1g}	E_g A_{1g}	A_{2g}	E_u E_u A_{1g}	A_{2g}
0	0	$\sqrt{2}/2$	$\sqrt{2}/2$	0
0	$\sqrt{2}/2$	0	0	$-\sqrt{2}/2$
$\sqrt{2}/2$	$-1/4$	$-\sqrt{3}/4$	$\sqrt{3}/4$	$-1/4$
$-\sqrt{30}/10$	$\sqrt{15}/20$	$-\sqrt{5}/4$	$\sqrt{5}/4$	$\sqrt{15}/20$
$\sqrt{5}/5$	$\sqrt{10}/5$	0	0	$\sqrt{10}/5$

O_h D_{3d} C_{2i}

1 2
3
4
5
6

1 3
2
4
5
6

1 4
2
3
5
6

1 5
2
3
4
6

1 6
2
3
4
5

(c)

T_{1u} E_u A_{1u}	A_{2u}	A_{2u} A_{2u}	T_{1g} E_g A_{1g}	A_{2g}	A_{2g} A_{2g}	E_u E_u A_{1u}	A_{2u}	A_{2u} A_{2u} A_{2u}
$-\sqrt{2}/4$	$-\sqrt{6}/12$	$\sqrt{3}/12$	0	$\sqrt{3}/3$	$\sqrt{6}/12$	1/2	$-\sqrt{3}/6$	$\sqrt{15}/12$
$\sqrt{6}/12$	$\frac{5\sqrt{2}}{12}$	1/12	$\sqrt{3}/3$	0	$-\sqrt{2}/4$	$\sqrt{3}/6$	$-1/6$	$\sqrt{5}/12$
$\sqrt{6}/12$	$-\sqrt{2}/4$	1/4	0	$-1/3$	$-\sqrt{2}/12$	$-\sqrt{3}/6$	$-1/2$	$\sqrt{5}/4$
$\sqrt{2}/4$	$\frac{-5\sqrt{6}}{36}$	$-\sqrt{3}/36$	$-1/3$	0	$-\sqrt{6}/4$	1/2	$\sqrt{3}/18$	$\frac{-\sqrt{15}}{36}$
0	$\frac{2\sqrt{3}}{9}$	$\frac{-5\sqrt{6}}{18}$	$-\sqrt{2}/3$	0	0	0	$\frac{-2\sqrt{6}}{18}$	$\frac{\sqrt{30}}{18}$
$-\sqrt{3}/3$	0	0	0	$\sqrt{2}/6$	$-2/3$	$-\sqrt{6}/6$	0	0
0	$-\sqrt{3}/9$	$\frac{-2\sqrt{6}}{18}$	$\sqrt{2}/6$	0	0	0	$\frac{-5\sqrt{6}}{18}$	$\frac{-\sqrt{30}}{9}$
$\sqrt{2}/4$	$\frac{5\sqrt{6}}{36}$	$\frac{5\sqrt{3}}{18}$	$-5/12$	$\sqrt{3}/4$	0	$-1/4$	$\frac{-5\sqrt{3}}{36}$	$\frac{-\sqrt{15}}{18}$
$\sqrt{30}/12$	$\frac{-\sqrt{10}}{12}$	$-\sqrt{5}/6$	$\sqrt{15}/12$	$\sqrt{5}/4$	0	$\frac{-\sqrt{15}}{12}$	$\frac{-\sqrt{5}}{12}$	1/6

O_h D_{3d} C_{2i}

1 2
3 4
5
6

1 3
2 4
5
6

1 2
3 5
4
6

1 3
2 5
4
6

1 4
2 5
3
6

1 2
3 6
4
5

1 3
2 6
4
5

1 4
2 6
3
5

1 5
2 6
3
4

(d)

T_{2g} A_{1g} A_{1g}	E_g A_{1g}	A_{2g}	A_{1u} A_{1u} A_{1u}	A_{1g} A_{1g} A_{1g}
1/4	$\sqrt{2}/4$	$-\sqrt{6}/4$	$\sqrt{6}/4$	1/4
$-\sqrt{3}/4$	$\sqrt{6}/4$	$\sqrt{2}/4$	$\sqrt{2}/4$	$-\sqrt{3}/4$
$\sqrt{3}/4$	$\sqrt{6}/4$	$\sqrt{2}/4$	$-\sqrt{2}/4$	$\sqrt{3}/4$
1/4	$-\sqrt{2}/4$	$\sqrt{6}/4$	$\sqrt{6}/4$	1/4
$\sqrt{2}/2$	0	0	0	$-\sqrt{2}/2$

O_h D_{3d} C_{2i}

1 2
3 4
5 6

1 3
2 4
5 6

1 2
3 5
4 6

1 3
2 5
4 6

1 4
2 5
3 6

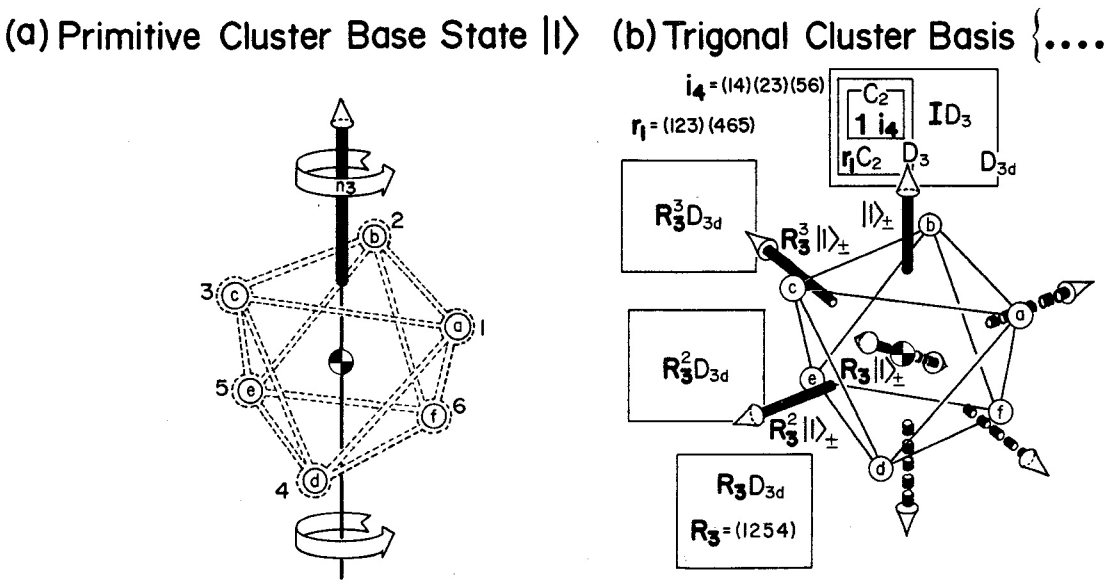

FIG. 20. XY_6 molecule rotating on threefold symmetry axes and coset structure appropriate for trigonal cluster bases. (a) Laboratory view of the first cluster base state $|1\rangle$. (b) Body view of the six positions of the rotor momentum N for the eight primitive cluster base states $g|1\rangle$.

latter is done it is convenient to interchange state numbers (3) and (5) so that top and bottom positions are numbered {123} and {456}, respectively, as in Fig. 20. This makes tableau factoring more convenient.

The transformation from $S_6 \supset O_h \supset D_{3d}$ symmetry defined states to Slater determinants is given in Table IX. We consider briefly the representations of some sample pseudo-Hamiltonians in the different bases.

The tensor spin-rotation operator plays no direct role for elementary threefold cluster states. If we ignore the spin-canting effects that couple states with different n_I then all six states in Fig. 20 are equivalent. Each nucleus rotates in the same way as all the others. The scalar spin-rotation operator is all that need be considered for the threefold ECA:

$$H_{sr} = \sigma N_z^- [I_z^-(1) + I_z^-(2) + \cdots + I_z^-(6)]. \qquad (5.1)$$

If there is no first-order tensor spin-rotation splitting then it is likely that the spin-spin interactions will play a more major role in determining superhyperfine structure. For example, spin-spin exchange tunneling operators analogous to (4.4) and (4.5) may be important:

$$H_{ss} = u[T(1 \rightleftharpoons 5) + T(2 \rightleftharpoons 4) + T(3 \rightleftharpoons 6)] + v[T(1 \rightleftharpoons 2) + T(1 \rightleftharpoons 3) + T(2 \rightleftharpoons 3) + T(4 \rightleftharpoons 5) + T(4 \rightleftharpoons 6) + T(5 \rightleftharpoons 6)]$$
$$+ w[T(1 \rightleftharpoons 4) + T(1 \rightleftharpoons 6) + T(2 \rightleftharpoons 5) + T(2 \rightleftharpoons 6) + T(3 \rightleftharpoons 4) + T(3 \rightleftharpoons 5)]. \qquad (5.2)$$

In addition the spin-spin energies, both scalar and tensor, should be important for states with $|n_I| < 2$. Some of these terms are included in Appendix D.

The Slater representations for sample pseudo-Hamiltonians are given now. For $n_I = 3$ and 2 the threefold analog of Eq. (4.6) is as follows:

$$\langle H_{sr} + H_{ss} \rangle_{n_I=3,2} = \begin{array}{c} 123456 \\ |||||| \\ |||||\downarrow \\ ||||\downarrow| \\ |||\downarrow|| \\ ||\downarrow||| \\ |\downarrow|||| \\ \downarrow||||| \end{array} \quad \begin{array}{c|cccccc} K & & & & & & \\ \hline & L & v & v & u & w & w \\ & v & L & v & w & w & u \\ & v & v & L & w & u & w \\ & u & w & w & L & v & v \\ & w & w & u & v & L & v \\ & w & u & w & v & v & L \end{array} \quad \begin{array}{l} \}n_I = 3 \\ \\ \\ \}n_I = 2 \\ \\ \\ \end{array} , \qquad (5.3a)$$

where

$$K = 3\sigma n_3\,,$$
$$L = 2\sigma n_3\,. \tag{5.3b}$$

The Slater representation for two-downon or $n_I = 1$ states is given by the following matrix:

TABLE IX. XY_6 octahedral trigonal cluster states expressed in terms of Slater determinants.

(a)

1 2 3 4 5 6	T_{2g} A_{1g} A_g	E_g A_g	B_g	E_u E_u A_u	B_u	A_{2u} A_{2u} B_u	: O_h : D_{3d} : C_{2i}
▮▮▮▮▮↓	1	2	0	0	2	1	
▮▮▮▮↓▮	1	−1	1	−1	−1	1	
▮▮▮↓▮▮	1	−1	−1	1	−1	1	
▮▮↓▮▮▮	−1	−2	0	0	2	1	
▮↓▮▮▮▮	−1	1	1	1	−1	1	
↓▮▮▮▮▮	−1	1	−1	−1	−1	1	
	$1/\sqrt{6}$	$1/2\sqrt{3}$	1/2	1/2	$1/2\sqrt{3}$	$1/\sqrt{6}$	

(b)

1 2 3 4 5 6	T_{1u} E_u A_u	B_u	A_{2u} B_u	T_{1g} E_g A_g	B_g	A_{2g} B_g	E_u E_u A_u	B_u	A_{2u} A_{2u} B_u	T_{2g} A_{1g} A_g	A_g	E_g B_g	E_u E_u A_u	B_u	A_{2u} A_{2u} B_u
▮▮▮↓↓↓	−1	1	1	−1	−3	0	1	−1	−1	1	1	1	−1	1	1
▮▮▮↓▮↓	1	1	1	−1	3	0	−1	−1	−1	1	1	−1	1	1	1
▮▮▮↓↓▮	0	−2	1	2	0	0	0	2	−1	1	−2	0	0	−2	1
▮▮↓▮▮↓	0	0	0	0	0	0	0	4	4	0	0	0	0	4	1
▮▮↓▮↓▮	1	−1	−1	−1	1	−1	1	−1	−1	0	−3	1	−1	1	1
▮▮↓↓▮▮	−1	−1	−1	−1	−1	1	−1	−1	−1	0	−3	−1	1	1	1
▮↓▮▮▮↓	−1	−1	−1	1	1	−1	−1	−1	−1	0	3	1	1	1	1
▮↓▮▮↓▮	0	2	−1	0	2	1	0	2	−1	0	0	2	0	−2	1
▮↓▮↓▮▮	0	0	0	0	0	0	2	−2	4	0	0	0	2	−2	1
▮↓↓▮▮▮	1	1	1	1	−3	0	−1	−1	−1	−1	−1	1	1	1	1
↓▮▮▮▮↓	1	−1	−1	1	−1	1	1	−1	−1	0	3	−1	−1	1	1
↓▮▮▮↓▮	0	0	0	0	0	0	−2	−2	4	0	0	0	−2	−2	1
↓▮▮↓▮▮	0	2	−1	0	−2	−1	0	2	−1	0	0	−2	0	−2	1
↓▮↓▮▮▮	−1	1	1	1	3	0	1	−1	−1	−1	−1	−1	−1	1	1
↓↓▮▮▮▮	0	−2	1	−2	0	0	0	2	−1	−1	2	0	0	−2	1
	$1/\sqrt{8}$	$1/2\sqrt{6}$	$1/2\sqrt{3}$	1/4	$1/4\sqrt{3}$	$1/\sqrt{6}$	1/4	$1/4\sqrt{3}$	$1/\sqrt{60}$	$1/\sqrt{6}$	$1/4\sqrt{3}$	1/4	1/4	$1/4\sqrt{3}$	$1/\sqrt{15}$

TABLE IX. *(Continued.)*

(c)

1 2 3 4 5 6	T_{2g} A_{1g} A_g	E_g A_g	B_g	A_{1u} A_{1u} A_u	A_{1g} A_{1g} A_g	T_{1u} E_u A_u	B_u	A_{2u} B_u	T_{1g} E_g A_g	B_g	A_{2g} B_g	E_u E_u A_u	B_u	A_{2u} A_{2u} B_u	T_{2g} A_{1g} A_g	E_g A_g	B_g	E_u E_u A_u	B_u	A_{2u} A_{2u} B_u
↑↑↑ ↓↓↓						↑↑↑↑ ↓↓									↑↑↑↑↓ ↓					↑↑↑↑↓↓
↓ ↓ ↓ ↑ ↑ ↑	−3	0	0	0	1	0	0	3	0	0	0	0	0	−3	3	0	0	0	0	1
↓ ↓ ↑ ↓ ↑ ↑	2	−1	1	1	0	0	0	0	−1	−1	−1	1	1	2	1	−1	1	−1	1	1
↓ ↓ ↑ ↑ ↓ ↑	2	−1	−1	−1	0	0	0	0	−1	1	1	−1	1	2	1	−1	−1	1	1	1
↓ ↓ ↑ ↑ ↑ ↓	−1	2	0	0	−1	0	−2	−1	0	0	0	0	0	−3	1	−4	0	0	0	1
↓ ↑ ↓ ↓ ↑ ↑	−1	−1	−1	0	−1	−1	1	−1	0	0	0	0	0	−3	1	2	2	0	0	1
↓ ↑ ↓ ↑ ↓ ↑	2	2	0	1	0	0	0	0	0	2	−1	0	−2	2	1	2	0	2	0	1
↓ ↑ ↓ ↑ ↑ ↓	2	−1	1	−1	0	0	0	0	1	1	1	1	1	2	1	−1	1	1	−1	1
↓ ↑ ↑ ↓ ↓ ↑	−2	1	1	−1	0	0	0	0	1	−1	−1	−1	1	2	−1	1	1	1	1	1
↓ ↑ ↑ ↓ ↑ ↓	1	1	−1	0	1	1	1	−1	0	0	0	0	0	−3	−1	−2	2	0	0	1
↓ ↑ ↑ ↑ ↓ ↓	−2	−2	0	1	0	0	0	0	0	−2	1	0	−2	2	−1	−2	0	2	0	1
↑ ↓ ↓ ↓ ↑ ↑	2	2	0	−1	0	0	0	0	0	−2	1	0	−2	2	1	2	0	−2	0	1
↑ ↓ ↓ ↑ ↓ ↑	−1	−1	1	0	−1	1	1	−1	0	0	0	0	0	−3	1	2	−2	0	0	1
↑ ↓ ↓ ↑ ↑ ↓	2	−1	−1	1	0	0	0	0	1	−1	−1	−1	1	2	1	−1	−1	−1	−1	1
↑ ↓ ↑ ↓ ↓ ↑	−2	1	−1	1	0	0	0	0	1	1	1	1	1	2	−1	1	−1	−1	1	1
↑ ↓ ↑ ↓ ↑ ↓	−2	−2	0	−1	0	0	0	0	0	2	−1	0	−2	2	−1	−2	0	−2	0	1
↑ ↓ ↑ ↑ ↓ ↓	1	1	1	0	1	−1	1	−1	0	0	0	0	0	−3	−1	−2	−2	0	0	1
↑ ↑ ↓ ↓ ↓ ↑	1	−2	0	0	1	0	−2	−1	0	0	0	0	0	−3	−1	4	0	0	0	1
↑ ↑ ↓ ↓ ↑ ↓	−2	1	1	1	0	0	0	0	−1	1	1	−1	1	2	−1	1	1	−1	−1	1
↑ ↑ ↓ ↑ ↓ ↓	−2	1	−1	−1	0	0	0	0	−1	−1	−1	1	1	2	−1	1	−1	1	−1	1
↑ ↑ ↑ ↓ ↓ ↓	3	0	0	0	−1	0	0	3	0	0	0	0	0	−3	−3	0	0	0	0	1
	$1/6\sqrt{2}$	1/6	$1/2\sqrt{3}$	$1/2\sqrt{3}$	$1/\sqrt{8}$	1/2	$1/2\sqrt{3}$	$1/2\sqrt{6}$	$1/\sqrt{8}$	$1/2\sqrt{6}$	$1/2\sqrt{3}$	$1/\sqrt{8}$	$1/2\sqrt{6}$	$1/2\sqrt{30}$	1/6	$1/6\sqrt{2}$	$1/2\sqrt{6}$	$1/2\sqrt{6}$	$1/\sqrt{8}$	$1/2\sqrt{5}$

$\langle H_{sr}+H_{ss}\rangle_{n_I=1}=$

	123456														
$\|\|\|\|\downarrow\downarrow$	M	v	v	w	u		w	w	·	·	u	w	·	·	·
$\|\|\|\downarrow\|\downarrow$	v	M	v	w		u	u	·	w	·	w	·	w	·	·
$\|\|\|\downarrow\downarrow\|$	v	v	M	·	w	u	·	u	w		·	w	u	·	·
$\|\|\downarrow\|\|\downarrow$	w	w	·	M	v	v	v	·	·	w	v	·	·	w	·
$\|\|\downarrow\|\downarrow\|$	u	·	w	v	M	v	·	v	·	w	·	v	·	u	·
$\|\|\downarrow\downarrow\|\|$	·	u	w	v	v	M	·	·	v	u	·	·	v	w	·
$\|\downarrow\|\|\downarrow$	w	u	·	v	·	·	M	v	v	u	v	·	·	·	w
$\|\downarrow\|\|\downarrow\|$	w	·	u	·	v	·	v	M	v	w	·	v	·	·	u
$\|\downarrow\|\downarrow\|\|$	·	w	w	·	·	v	v	v	M	w	·	·	v	·	w
$\|\downarrow\downarrow\|\|\|$	·	·	·	w	w	u	u	w	w	M	·	·	·	v	v
$\downarrow\|\|\|\downarrow$	u	w	·	v	·	·	v	·	·	·	M	v	v	u	w
$\downarrow\|\|\downarrow\|$	w	·	w	·	v	·	·	v	·	·	v	M	v	u	w
$\downarrow\|\|\downarrow\|\|$	·	w	u	·	·	v	·	·	v	·	v	v	M	w	u
$\downarrow\|\downarrow\|\|\|$	·	·	·	w	u	w	·	·	·	v	u	w	w	M	v
$\downarrow\downarrow\|\|\|\|$	·	·	·	·	·	·	w	u	w	v	w	w	u	v	M

, (5.4a)

where the diagonal components

$$M=\sigma n_3 \tag{5.4b}$$

are assumed to be equal here. Actually, there should be three slightly different values for M to reflect the spin-spin energies or downon interactions. This will be discussed in later articles. (See also Appendix D.)

Finally, the Slater representation for the top half of the $n_I=0$ manifold is given by the following matrix:

$\langle H_{sr}+H_{ss}\rangle_{n_I=0}=$

$\|\|\|\downarrow\downarrow\downarrow$	·	w	w	u	u	w	w	·	·	·	w	u	w	·	·	·	·	·	·	·
$\|\|\downarrow\|\downarrow\downarrow$	w	·	v	v	v	·	·	w	w	·	v	·	·	u	w	·	·	·	·	·
$\|\|\downarrow\downarrow\|\downarrow$	w	v	·	v	·	v	·	u	·	w	·	v	·	u	·	w	·	·	·	·
$\|\|\downarrow\downarrow\downarrow\|$	u	v	v	·	·	·	v	·	w	w	·	·	v	·	w	u	·	·	·	·
$\|\downarrow\|\|\downarrow\downarrow$	u	v	·	·	·	v	v	w	u	·	v	·	·	·	·	·	u	w	·	·
$\|\downarrow\|\downarrow\|\downarrow$	w	·	v	·	v	·	v	w	·	u	·	v	·	·	·	·	w	·	w	·
$\|\downarrow\|\downarrow\downarrow\|$	w	·	·	v	v	v	·	·	w	w	·	·	v	·	·	·	·	w	u	·
$\|\downarrow\downarrow\|\|\downarrow$	·	w	u	·	w	w	·	·	v	v	·	·	·	v	·	·	v	·	·	w
$\|\downarrow\downarrow\|\downarrow\|$	·	w	·	u	u	·	w	v	·	v	·	·	·	·	v	·	·	v	·	u
$\|\downarrow\downarrow\downarrow\|\|$	·	·	w	w	·	u	w	v	v	·	·	·	·	·	·	v	·	·	v	w

. (5.5)

The reflection symmetry discussed for Eq. (4.8) applies here as well. Again, small tensor spin-spin diagonal contributions may be important for accurate superhyperfine analysis. (See Appendix D.) We consider now the representations of the pseudo-Hamiltonians in tableau bases for specific types of clusters.

A. Type $O_3\uparrow O=A_1\oplus T_1\oplus T_2\oplus A_2$ clusters

The O_3 or A-type clusters have the richest superhyperfine structure of the threefold variety. They have more levels in the central ($n_I=0$) superhyperfine cluster than any other threefold or fourfold type. There are a total of twenty-four

Pauli-allowed O_h states with A-type (A_{1g}, A_{1u}, A_{2g}, or A_{2u}) D_{3d} labels, and eight of these are associated with $n_I = 0$. The central superhyperfine octet of A-type case-2 clusters might well be the most sensitive indicator of SF_6 structure and dynamics.

The representations of the tunneling pseudo-Hamiltonians in the $S_6 \supset O_h \supset D_{3d} \supset C_{2i}$ basis of Table IX are given in Appendix D [Table D(a)] for $n_I = 3, 2, 1$, and 0. (The energy matrices are given for whole and broken tableaus in the table.) It happens that no matrix for any of the threefold bases has a dimension larger than three.

Even though the tensor spin-rotation interaction is not so important for threefold clusters, it still may be useful to study the factored tableau states. Indeed, the threefold rotation effectively divorces the SF_6 molecule into two equivalent groups. One group consists of nuclei in states 1, 2, and 3 on top of the octahedron in Fig. 20, while the other group consists of nuclei in states 4, 5, and 6. However, since the O_h states have definite parity they will yield symmetrized (or antisymmetrized) combinations of the factored tableaus. Symmetrized outer products of tableaus are referred to as plethysms.[51,52] The theory of plethysms would be useful for studying molecules which divorce (or dissociate) into three or more separate groups, but it is not necessary here. Instead, it is easy to follow the procedures outlined in Sec. IV.

For example, using Table VIII(a) and VIII(b) and the factoring transformations in Table VI(b) one derives the following relations:

$$\underset{A_{2u},A_{2u}}{\{6,0\}} = \begin{array}{|c|c|}\hline 1 & 4 \\ \hline 2 & 5 \\ \hline 3 & 6 \\ \hline \end{array} \quad , \tag{5.6a}$$

$$\underset{T_{1u},A_{2u}}{\{4,2\}} = -(\sqrt{6}/6)\left(\begin{array}{|c|c|}\hline 1 & 2 \\ \hline 3 \\ \cline{1-1} \end{array}\ \begin{array}{|c|c|}\hline 4 & 5 \\ \hline 6 \\ \cline{1-1} \end{array} - \begin{array}{|c|c|}\hline 1 & 3 \\ \hline 2 \\ \cline{1-1} \end{array}\ \begin{array}{|c|c|}\hline 4 & 6 \\ \hline 5 \\ \cline{1-1} \end{array}\right)\Big/\sqrt{2} + (\sqrt{30}/6)\begin{array}{|c|c|}\hline 1 & 4 \\ \hline 2 & 5 \\ \hline 3 & 6 \\ \hline \end{array} \quad , \tag{5.6b}$$

$$\underset{A_{2u},A_{2u}}{\{4,2\}} = -(\sqrt{30}/6)\left(\begin{array}{|c|c|}\hline 1 & 2 \\ \hline 3 \\ \cline{1-1} \end{array}\ \begin{array}{|c|c|}\hline 4 & 5 \\ \hline 6 \\ \cline{1-1} \end{array} - \begin{array}{|c|c|}\hline 1 & 3 \\ \hline 2 \\ \cline{1-1} \end{array}\ \begin{array}{|c|c|}\hline 4 & 6 \\ \hline 5 \\ \cline{1-1} \end{array}\right)\Big/\sqrt{2} - (\sqrt{6}/6)\begin{array}{|c|c|}\hline 1 & 4 \\ \hline 2 & 5 \\ \hline 3 & 6 \\ \hline \end{array} \quad . \tag{5.6c}$$

One must use caution to preserve order and phase when coupling the spin states in the factored states above. The results for $n_I = 1$ are as follows:

$$\left|\begin{matrix}\{6,0\}\ 3 \\ A_{2u},A_{2u}\ 1\end{matrix}\right\rangle = (\sqrt{10}/5)[\uparrow\uparrow\uparrow\ \uparrow\downarrow\downarrow] + (\sqrt{15}/5)[\uparrow\uparrow\downarrow\ \uparrow\uparrow\downarrow] \quad ,$$

$$\left|\begin{matrix}\{4,2\}\ 1 \\ T_{1u},A_{2u}\ 1\end{matrix}\right\rangle = (\sqrt{2}/2)[\uparrow\uparrow\uparrow\ \uparrow\downarrow\downarrow] - (\sqrt{3}/3)[\uparrow\uparrow\downarrow\ \uparrow\uparrow\downarrow] - (\sqrt{6}/6)[\begin{smallmatrix}\uparrow\uparrow & \uparrow\uparrow \\ \downarrow & \downarrow\end{smallmatrix}] \quad , \tag{5.7a}$$

$$\left|\begin{matrix}\{4,2\}\ 1 \\ A_{2u},A_{2u}\ 1\end{matrix}\right\rangle = -(\sqrt{10}/10)[\uparrow\uparrow\uparrow\ \uparrow\downarrow\downarrow] + (\sqrt{15}/15)[\uparrow\uparrow\downarrow\ \uparrow\uparrow\downarrow] - (\sqrt{30}/6)[\begin{smallmatrix}\uparrow\uparrow & \uparrow\uparrow \\ \downarrow & \downarrow\end{smallmatrix}] \quad ,$$

where we define the following combinations:

$$[\uparrow\uparrow\uparrow\ \uparrow\downarrow\downarrow] \equiv \left(\left|\begin{array}{|c|}\hline 1 \\ \hline 2 \\ \hline 3 \\ \hline \end{array}\ \uparrow\uparrow\uparrow\ \begin{array}{|c|}\hline 4 \\ \hline 5 \\ \hline 6 \\ \hline \end{array}\ \uparrow\downarrow\downarrow\right\rangle + \left|\begin{array}{|c|}\hline 1 \\ \hline 2 \\ \hline 3 \\ \hline \end{array}\ \uparrow\downarrow\downarrow\ \begin{array}{|c|}\hline 4 \\ \hline 5 \\ \hline 6 \\ \hline \end{array}\ \uparrow\uparrow\uparrow\right\rangle\right)\Big/\sqrt{2} \quad ,$$

$$[\uparrow\uparrow\downarrow\ \uparrow\uparrow\downarrow] \equiv \left|\begin{array}{|c|}\hline 1 \\ \hline 2 \\ \hline 3 \\ \hline \end{array}\ \uparrow\uparrow\downarrow\ \begin{array}{|c|}\hline 4 \\ \hline 5 \\ \hline 6 \\ \hline \end{array}\ \uparrow\uparrow\downarrow\right\rangle \quad , \tag{5.7b}$$

$$[\begin{smallmatrix}\uparrow\uparrow & \uparrow\uparrow \\ \downarrow & \downarrow\end{smallmatrix}] \equiv \left(\left|\begin{array}{|c|c|}\hline 1 & 2 \\ \hline 3 \\ \cline{1-1} \end{array}\ \begin{matrix}\uparrow\uparrow \\ \downarrow\end{matrix}\ \begin{array}{|c|c|}\hline 4 & 5 \\ \hline 6 \\ \cline{1-1} \end{array}\ \begin{matrix}\uparrow\uparrow \\ \downarrow\end{matrix}\right\rangle - \left|\begin{array}{|c|c|}\hline 1 & 3 \\ \hline 2 \\ \cline{1-1} \end{array}\ \begin{matrix}\uparrow\uparrow \\ \downarrow\end{matrix}\ \begin{array}{|c|c|}\hline 4 & 6 \\ \hline 5 \\ \cline{1-1} \end{array}\ \begin{matrix}\uparrow\uparrow \\ \downarrow\end{matrix}\right\rangle\right)\Big/\sqrt{2} \quad .$$

This shows the difference between the trigonal and the tetragonal factoring. The trigonal factors are equivalent and so all results are symmetrized with respect to {123} and {456} factors. Mixing cannot occur between two states such as

$$\left|\begin{matrix}\{6,0\}\ 3\\ A_{2u},A_{2u}\ 2\end{matrix}\right\rangle \equiv [\uparrow\uparrow\uparrow\ \uparrow\uparrow\uparrow] = \left(\left|\begin{matrix}1\\2\\3\end{matrix}\ \uparrow\uparrow\uparrow\ \begin{matrix}4\\5\\6\end{matrix}\ \uparrow\uparrow\uparrow\right\rangle + \left|\begin{matrix}1\\2\\3\end{matrix}\ \uparrow\uparrow\downarrow\ \begin{matrix}4\\5\\6\end{matrix}\ \uparrow\uparrow\downarrow\right\rangle\right)\Big/\sqrt{2},$$

and

$$\left|\begin{matrix}\{5,1\}\ 2\\ T_{1g},A_{2g}\ 2\end{matrix}\right\rangle \equiv \{\uparrow\uparrow\uparrow\ \uparrow\uparrow\downarrow\} = \left(\left|\begin{matrix}1\\2\\3\end{matrix}\ \uparrow\uparrow\uparrow\ \begin{matrix}4\\5\\6\end{matrix}\ \uparrow\uparrow\downarrow\right\rangle - \left|\begin{matrix}1\\2\\3\end{matrix}\ \uparrow\uparrow\downarrow\ \begin{matrix}4\\5\\6\end{matrix}\ \uparrow\uparrow\uparrow\right\rangle\right)\Big/\sqrt{2},$$

unless parity is broken.

A complete listing of factored trigonal bases is given in Table X. The A-type states are given in Table X(a). Examples of pseudo-Hamiltonian representations are given in Appendix D. The factored representations are diagonal in the v-type tunneling amplitude. They are also diagonal for certain types of tensor spin-spin interactions.

The correlation between case-1 and case-2 A-type cluster levels is shown in Fig. 21. The zero down and one down ($n_I = 3$ and 2) have only one and two levels apiece. These three states are uncoupled in the ECA limit and they depend on pseudo-Hamiltonian parameters differently. A measurement of their energies would provide two linearly independent equations. However, most of the spectroscopic information will come from the rich $n_I = 1$ and $n_I = 0$ structures in the Case-2 limit. This will be helped by crossover observations, too. So far no Case-2 A-type clusters have been reported.

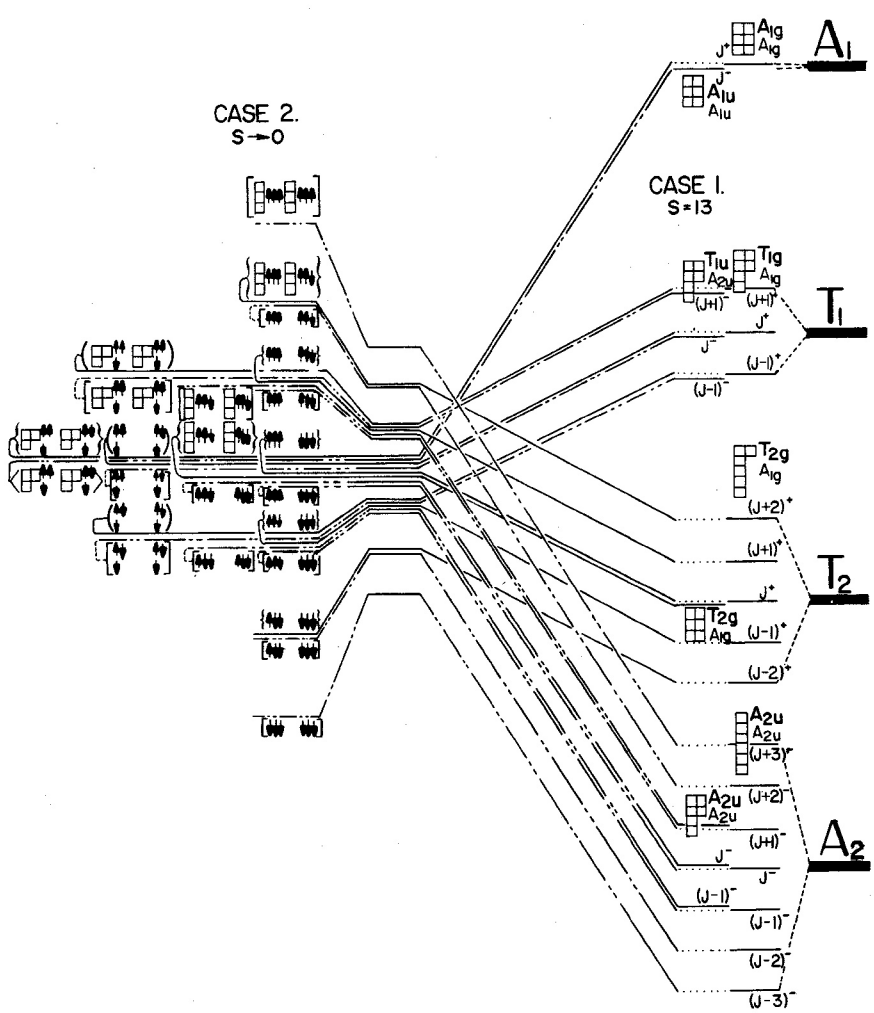

FIG. 21. Superhyperfine level correlations for the A-type trigonal clusters ($0_3 \uparrow O = A_1 + T_1 + T_2 + A_2$).

TABLE X. Factored eigenvectors for trigonal clusters.

(a) Type-A (A_1, T_1, T_2, A_2) trigonal cluster bases.

	$n_I=3$ [↑↑↑ ↑↑↑]	$n_I=2$ [↑↑↑ ↑↑↓]	$n_I=3$ [↑↑↑ ↑↓↓]	[↑↑↓ ↑↑↓]	[↑↑ ↑↓ / ↓ ↓]	$n_I=0$ [↑↑↑ ↓↓↓]	[↑↓↓ ↑↑↓]	[↑↑ ↑↓ / ↓ ↓]
{6,0} A_{2u} 3 $= \lvert$ 1 2 3 | 4 5 6 3 $n_I\rangle$	1	1	$\sqrt{10}/5$	$\sqrt{15}/5$	0	$\sqrt{10}/10$	$3\sqrt{10}/10$	0
A_{2u} n_I								
{4,2} T_{1u} 1 $= \frac{\sqrt{30}}{6}\lvert$ 1 2 3 | 4 5 6 1 $n_I\rangle - \frac{\sqrt{6}}{6}\left(\lvert$ 1 2 3 | 4 5 6 1 $n_I\rangle - \lvert$ 1 3 2 | 4 6 5 1 $n_I\rangle\right)/\sqrt{2}$			$\sqrt{2}/2$	$-\sqrt{3}/3$	$-\sqrt{6}/6$	$\sqrt{3}/2$	$-\sqrt{3}/6$	$-\sqrt{6}/6$
A_{2u} n_I								
{4,2} A_{2u} 1 $= \frac{-\sqrt{6}}{6}\lvert$ 1 2 3 | 4 5 6 1 $n_I\rangle - \frac{\sqrt{30}}{6}\left(\lvert$ 1 2 3 | 4 5 6 1 $n_I\rangle - \lvert$ 1 3 2 | 4 6 5 1 $n_I\rangle\right)/\sqrt{2}$			$-\sqrt{10}/10$	$\sqrt{15}/15$	$-\sqrt{30}/6$	$-\sqrt{15}/10$	$\sqrt{15}/30$	$-\sqrt{30}/6$
A_{2u} n_I								

	{↑↑↑ ↑↑↓}	{↑↑↑ ↑↓↓}	{↑↑↑ ↓↓↓}	{↑↑↓ ↑↑↓}	{↑↑ ↑↓ / ↓ ↓}
{5,1} T_{2g} 2 $= \lvert$ 1 2 3 | 4 5 6 2 $n_I\rangle$	1	1	$\sqrt{2}/2$	$\sqrt{2}/2$	0
A_{1g} n_I					
{3,3} T_{2g} 0 $= \frac{\sqrt{2}}{2}\lvert$ 1 2 3 | 4 5 6 0 0$\rangle - \frac{\sqrt{2}}{2}\left(\lvert$ 1 2 3 | 4 5 6 0 0$\rangle - \lvert$ 1 3 2 | 4 6 5 0 0$\rangle\right)/\sqrt{2}$			1/2	−1/2	$-\sqrt{2}/2$
A_{1g} 0					

TABLE X. *(Continued.)*

(a) *(Continued.)*

$\{3,3\}$  $A_{1g}\ 0$ $A_{1g}\ 0$ $= \frac{\sqrt{2}}{2}\left\vert \begin{smallmatrix}1&4\\2&5\\3&6\end{smallmatrix}\ 0\ 0\right\rangle - \frac{\sqrt{2}}{2}\left(\left\vert \begin{smallmatrix}1&2\\3\end{smallmatrix}\ \begin{smallmatrix}4&5\\6\end{smallmatrix}\ 0\ 0\right\rangle - \left\vert \begin{smallmatrix}1&3\\2\end{smallmatrix}\ \begin{smallmatrix}4&6\\5\end{smallmatrix}\ 0\ 0\right\rangle\right)\Big/\sqrt{2}$		$-1/2$	$1/2$ $-\sqrt{2}/2$
	$\left(\begin{smallmatrix}\uparrow\uparrow&\uparrow\uparrow\\\downarrow&\downarrow\end{smallmatrix}\right)$		$\left(\begin{smallmatrix}\uparrow\uparrow&\uparrow\uparrow\\\downarrow&\downarrow\end{smallmatrix}\right)$
$\{4,2\}$ 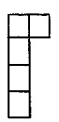 $T_{1g}\ 1$ $A_{2g}\ n_I$ $= \left(\left\vert \begin{smallmatrix}1&2\\3\end{smallmatrix}\ \begin{smallmatrix}4&6\\5\end{smallmatrix}\ 1\ n_I\right\rangle - \left\vert \begin{smallmatrix}1&3\\2\end{smallmatrix}\ \begin{smallmatrix}4&5\\6\end{smallmatrix}\ 1\ n_I\right\rangle\right)\Big/\sqrt{2}$	1		1
			$\left\langle\begin{smallmatrix}\uparrow\uparrow&\uparrow\uparrow\\\downarrow&\downarrow\end{smallmatrix}\right\rangle$
$\{3,3\}$  $A_{1u}\ 0$ $A_{1u}\ 0$ $= \left(\left\vert \begin{smallmatrix}1&2\\3\end{smallmatrix}\ \begin{smallmatrix}4&6\\5\end{smallmatrix}\ 0\ 0\right\rangle - \left\vert \begin{smallmatrix}1&3\\2\end{smallmatrix}\ \begin{smallmatrix}4&5\\6\end{smallmatrix}\ 0\ 0\right\rangle\right)\Big/\sqrt{2}$		1

TABLE X. *(Continued.)*

(b) Type-B (T_1, E, T_2) trigonal cluster bases.

	$n_I=2$	$n_I=1$			$n_I=0$		
	$\{\uparrow\uparrow \atop \downarrow \uparrow\uparrow\uparrow\}$	$\{\uparrow\uparrow \atop \downarrow \uparrow\uparrow\uparrow\}$	$\{\uparrow\uparrow \atop \downarrow \uparrow\uparrow\downarrow\}$	$\{\uparrow\uparrow \atop \downarrow \downarrow\}$	$\{\uparrow\uparrow \atop \downarrow \uparrow\uparrow\uparrow\}$	$\{\uparrow\uparrow \atop \downarrow \uparrow\uparrow\downarrow\}$	$\{\uparrow\uparrow \atop \downarrow \downarrow\}$
{51} E_u 2 $= \frac{\sqrt{2}}{2}\left\vert \begin{smallmatrix}1&2\\3\end{smallmatrix} \begin{smallmatrix}4\\5\\6\end{smallmatrix}\ 2\right\rangle - \frac{\sqrt{2}}{2}\left\vert \begin{smallmatrix}1\\2\\3\end{smallmatrix} \begin{smallmatrix}4&5\\6\end{smallmatrix}\ 2\right\rangle$ E_u, A_{1u} n_I	1	$\sqrt{1}/2$	$\sqrt{3}/2$	0	$\sqrt{2}/2$	$\sqrt{2}/2$	0
{4,2} E_u 1 $= \frac{\sqrt{6}}{6}\left\vert \begin{smallmatrix}1&2\\3\end{smallmatrix} \begin{smallmatrix}4\\5\\6\end{smallmatrix}\ 1\right\rangle + \frac{\sqrt{6}}{6}\left\vert \begin{smallmatrix}1\\2\\3\end{smallmatrix} \begin{smallmatrix}4&5\\6\end{smallmatrix}\ 1\right\rangle + \frac{\sqrt{3}}{3}\left\vert \begin{smallmatrix}1&2\\3\end{smallmatrix} \begin{smallmatrix}4&6\\5\end{smallmatrix}\ 1\right\rangle - \frac{\sqrt{3}}{3}\left\vert \begin{smallmatrix}1&3\\2\end{smallmatrix} \begin{smallmatrix}4&5\\6\end{smallmatrix}\ 1\right\rangle$ E_u, A_{1u} n_I		$\sqrt{1}/2$	$\sqrt{3}/6$	$\sqrt{6}/3$	$-\sqrt{6}/6$	$\sqrt{6}/6$	$\sqrt{6}/3$
{4,2} T_{1u} 1 $= \frac{-\sqrt{3}}{3}\left\vert \begin{smallmatrix}1&2\\3\end{smallmatrix} \begin{smallmatrix}4\\5\\6\end{smallmatrix}\ 1\right\rangle - \frac{\sqrt{3}}{3}\left\vert \begin{smallmatrix}1\\2\\3\end{smallmatrix} \begin{smallmatrix}4&5\\6\end{smallmatrix}\ 1\right\rangle + \frac{\sqrt{6}}{6}\left\vert \begin{smallmatrix}1&2\\3\end{smallmatrix} \begin{smallmatrix}4&6\\5\end{smallmatrix}\ 1\right\rangle - \frac{\sqrt{6}}{6}\left\vert \begin{smallmatrix}1&3\\2\end{smallmatrix} \begin{smallmatrix}4&5\\6\end{smallmatrix}\ 1\right\rangle$ E_u, A_{1u}		$\sqrt{2}/2$	$-\sqrt{6}/6$	$\sqrt{3}/3$	$\sqrt{3}/3$	$-\sqrt{3}/3$	$\sqrt{3}/3$
	$\left\langle \uparrow\uparrow \atop \downarrow \uparrow\uparrow\uparrow \right\rangle$	$\left\langle \uparrow\uparrow \atop \downarrow \uparrow\uparrow\uparrow \right\rangle$	$\left\langle \uparrow\uparrow \atop \downarrow \uparrow\uparrow\downarrow \right\rangle$		$\left\langle \uparrow\uparrow \atop \downarrow \uparrow\uparrow\uparrow \right\rangle$	$\left\langle \uparrow\uparrow \atop \downarrow \uparrow\uparrow\downarrow \right\rangle$	
{51} T_{2g} 2 $= \frac{\sqrt{2}}{2}\left\vert \begin{smallmatrix}1&3\\2\end{smallmatrix} \begin{smallmatrix}4\\5\\6\end{smallmatrix}\ 2\right\rangle - \frac{\sqrt{2}}{2}\left\vert \begin{smallmatrix}1\\2\\3\end{smallmatrix} \begin{smallmatrix}4&6\\5\end{smallmatrix}\ 2\right\rangle$ E_g, A_{1g} n_I	1	1/2	$\sqrt{3}/2$		$\sqrt{2}/2$	$\sqrt{2}/2$	

TABLE X. *(Continued.)*

(b) *(Continued.)*

$\{4,2\}$ T_{1g} E_g A_{1g} n_I $= \frac{\sqrt{2}}{2}\left\vert \begin{smallmatrix}1&3\\2\end{smallmatrix} \begin{smallmatrix}4&1\\5\\6&n_I\end{smallmatrix}\right\rangle + \frac{\sqrt{2}}{2}\left\vert \begin{smallmatrix}1\\2\\3\end{smallmatrix} \begin{smallmatrix}4&6&1\\5&&n_I\end{smallmatrix}\right\rangle$	$-\sqrt{3}/2$ $\quad$ $1/2$	$-\sqrt{2}/2$ $\quad$ $\sqrt{2}/2$
$\{3,3\}$		$\left\{\left\vert \begin{smallmatrix}\uparrow\uparrow&\uparrow\downarrow\\\downarrow&\downarrow\end{smallmatrix}\right\vert\right\}$
T_{2g} E_g A_{1g} $= \frac{-\sqrt{2}}{2}\left\vert \begin{smallmatrix}1&2\\3\end{smallmatrix} \begin{smallmatrix}4&6&0\\5&&0\end{smallmatrix}\right\rangle - \frac{\sqrt{2}}{2}\left\vert \begin{smallmatrix}1&3\\2\end{smallmatrix} \begin{smallmatrix}4&5&0\\6&&0\end{smallmatrix}\right\rangle$		1

Symbol key:

$$\left[\begin{smallmatrix}\uparrow\uparrow&\uparrow\downarrow\\\downarrow&\downarrow\end{smallmatrix}\right] = \left(\begin{smallmatrix}1&2\\3\end{smallmatrix} \begin{smallmatrix}4&5\\6\end{smallmatrix}\right)_{-}^{[+]}$$

$$\left\{\begin{smallmatrix}\uparrow\uparrow&\uparrow\downarrow\\\downarrow&\downarrow\end{smallmatrix}\right\} \equiv \left(\begin{smallmatrix}1&2\\3\end{smallmatrix} \begin{smallmatrix}4&5\\6\end{smallmatrix}\right)_{-}^{[-]}$$

$$\left(\begin{smallmatrix}\uparrow\uparrow&\uparrow\downarrow\\\downarrow&\downarrow\end{smallmatrix}\right) \equiv \left(\begin{smallmatrix}1&2\\3\end{smallmatrix} \begin{smallmatrix}4&6\\5\end{smallmatrix}\right)_{+}^{[+]}$$

$$\left\langle\begin{smallmatrix}\uparrow\uparrow&\uparrow\downarrow\\\downarrow&\downarrow\end{smallmatrix}\right\rangle \equiv \left(\begin{smallmatrix}1&2\\3\end{smallmatrix} \begin{smallmatrix}4&6\\5\end{smallmatrix}\right)_{+}^{[-]}$$

where

$$[\pm] = \left(\begin{smallmatrix}\uparrow\uparrow&\uparrow\uparrow\\\downarrow&\downarrow\end{smallmatrix} \pm \begin{smallmatrix}\uparrow\uparrow&\uparrow\uparrow\\\downarrow&\downarrow\end{smallmatrix}\right)/\sqrt{2}$$

$$\left(\begin{smallmatrix}1&2\\3\end{smallmatrix} \begin{smallmatrix}a&b\\c\end{smallmatrix}\right)_{\pm} = \left(\begin{smallmatrix}1&2\\3\end{smallmatrix} \begin{smallmatrix}a&b\\c\end{smallmatrix} \pm \begin{smallmatrix}1&3\\2\end{smallmatrix} \begin{smallmatrix}a&c\\b\end{smallmatrix}\right)/\sqrt{2}$$

B. Type $\pm 1_3 \uparrow O = T_1 + E + T_2$ clusters

The $(\pm 1_3)$- or E-type clusters occur twice as often as the A-type since they belong to any cluster momentum n_3 which is not evenly divisable by three. The octahedral states correlated with the D_{3d} labels E_g and E_u belong to the type-E cluster. There are two C_{2i} components A and B for each E label. It will only be necessary to use one of these components when representing D_{3d} symmetric pseudo-Hamiltonians. Also, the factoring transformation in Table X(b) is done only for the first component.

The representations of pseudo-Hamiltonians are given in Appendix D for the octahedral bases and for the factored bases. [See Table XII(b).] A sketch of the (T_1, E, T_2) energy level correlation diagram is shown in Fig. 22 for the two extremes of Case 1 and Case 2.

ACKNOWLEDGMENT

The author would like to thank Dr. Sanford Gordon of the NASA Lewis Research Center for support during the initial phases of this work. This work was supported in part by grants from the Research Corporation and the Theoretical Physics Division of the National Science Foundation.

APPENDIX A: APPROXIMATE FINE-STRUCTURE LEVEL AND FREQUENCY FORMULAS

In Eq. (2.8) the fine structure levels for the ground vibrational states were given approximately by

$$\langle H \rangle_0 = \langle H_{\text{scalar}} \rangle_0 + \langle H_{\text{tensor}} \rangle_0 = \langle H_{\text{scalar}} \rangle_0 + H_n^N , \tag{A1a}$$

where

$$H_n^N = \begin{cases} t(N, n_4) & \text{for fourfold clusters} \\ -(2/3)t(N, n_3) & \text{for threefold clusters} \end{cases} \tag{A1b}$$

and

$$t(N, n) = (t_{044}/2)[3(N+2)(N+1)N(N-1) - 5n^2(6N^2 + 6N - 5) + 35n^4] \equiv (t_{044}/2)[c_n^N] . \tag{A1c}$$

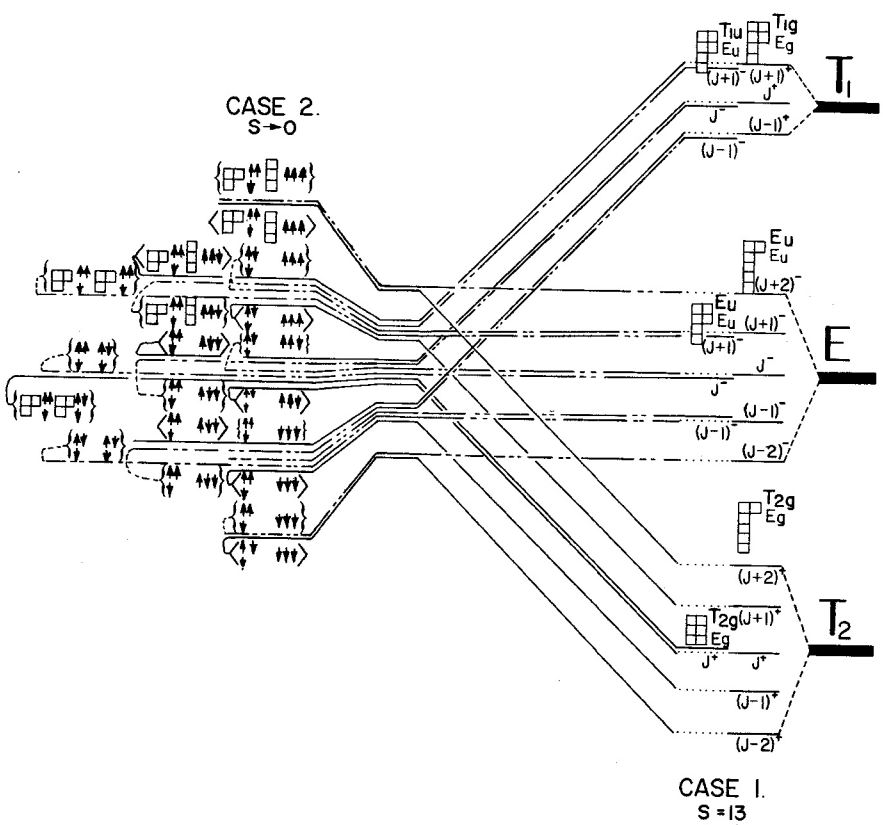

FIG. 22. Superhyperfine level correlations for the E-type trigonal clusters $(\pm 1_3 \uparrow O = T_1 + E + T_2)$.

Here similar formulas for the vibrationally excited ν_3 or ν_4 levels and related spectral frequencies will be given.

The excited levels with $J=N-1$ give the $P(N)$ lines that have energies given approximately by

$$P_n^N=\langle H_{\text{scalar}}\rangle_\nu+\langle H_{\text{tensor}}\rangle_\nu=\langle H_{\text{scalar}}\rangle_\nu^{P(N)}+\frac{[(2N-5)(N-2)t_{044}+2(N-2)t_{134}-2t_{224}]\,k_n^N}{2N(2N-1)}, \tag{A2a}$$

where

$$k_n^N=\begin{cases} c_{n_4}^N & \text{for fourfold clusters} \\ -\frac{2}{3}c_{n_3}^N & \text{for threefold clusters.}\end{cases} \tag{A2b}$$

The excited levels with $J=N$ give the $Q(N)$ lines that have energies given approximately by

$$Q_n^N=\langle H_{\text{scalar}}\rangle_\nu^{Q(N)}+\frac{[(N^2-N-10)t_{044}+4t_{134}+2t_{224}]\,k_n^N}{N(2N+2)}. \tag{A3}$$

Finally, the $R(N)$ levels with $J=N+1$ have approximate energies of

$$R_n^N=\langle H_{\text{scalar}}\rangle_\nu^{R(N)}+\frac{[(2N+7)(N+3)t_{044}-2(N+3)t_{134}-2t_{244}]\,k_n^N}{(2N+2)(2N+3)}. \tag{A4}$$

Each of these expressions involves various fourth rank molecular tensor constants t_{ijk} as defined by Hecht.[28]

By subtracting each of the expressions (A2)–(A4) for excited energies from the ground energy formula (A1) one obtains the line frequency formulas[34] for the P, Q, and R branches of ν lines in SF_6 we have

$$\begin{aligned} P(N)&=m-nN+pN^2-qN^3+[g+hN]k_n^N/[N(2N-1)(12/7)^{1/2}] \\ Q(N)&=m+vJ(J+1)-2gk_n^N/[N(2N+2)(12/7)^{1/2}] \\ R(N)&=m+n(N+1)+p(N+1)^2+q(N+1)^3+[g-h(N+1)]k_n^N/[(N+1)(2N+3)(12/7)^{1/2}]. \end{aligned} \tag{A5}$$

These involve spectroscopic coefficients g, h, m, n, p, q, and v. The first two are related to the molecular tensor constants:

$$\begin{aligned} g&=(12/7)^{1/2}(5t_{044}-2t_{134}-t_{224}), \\ h&=(12/7)^{1/2}(t_{134}-4t_{044}). \end{aligned} \tag{A6}$$

The remaining spectroscopic coefficients are related to scalar constants. The largest constants m and n are expressed as

$$m=\nu_{\text{vib}}-2B\zeta, \quad n=2B(1-\zeta) \tag{A7}$$

in terms of the SF_6 rotational constant $B=0.091\,11\pm0.000\,05\ \text{cm}^{-1}=2.731\times10^9$ Hz and the Coriolis constant ζ. [Recall Eqs. (2.1-4).] For the ν_3 or 948-cm^{-1} resonance of SF_6 the following numerical values are given by Loete *et al.*[30,34]

$$\begin{aligned} &\zeta=0.6937\pm0.0002 \text{ (dimensionless)} \\ &m=9.479\,765\,57\times10^2\ \text{cm}^{-1}=2.841\,962\,30\times10^{13}\ \text{Hz}, \\ &n=5.581\,767\times10^{-2}=1.673\,372\times10^9 \\ &p=1.618\,652\times10^{-4}=-4.852\,597\times10^6, \\ &q=1.0391\times10^{-8}=3.1151\times10^2, \end{aligned} \tag{A8}$$

$$\begin{aligned} &g=-2.458\,264\times10^{-5}=-7.369\,690\times10^5, \\ &h=-5.56\times10^{-10}=-16.67, \\ &v=-6.998\,65\times10^{-5}=-2.098\,14\times10^6. \end{aligned}$$

The constants which are known for the ν_4 or 615 cm^{-1} resonance of SF_6 [see Fig. 1(a)] are given by Kim *et al.*[3]

$$\begin{aligned} &\zeta=-(0.2156\pm0.0007), \\ &m=614.905\,2(11)\ \text{cm}^{-1}=1.843\,439\,4(59)\times10^{13}\ \text{Hz}, \\ &n=0.221\,143(13)=6.629\,70(43)\times10^9, \\ &p=2.37(4)\times10^{-5}=-7.11(7)\times10^5, \\ &g=(2.79\pm0.02)\times10^{-6}=(8.36\pm0.06)\times10^4, \\ &h=(6.3\pm0.3)\times10^{-9}=(1.88\pm0.09)\times10^2. \end{aligned} \tag{A9}$$

The spectroscopic coefficient g is about five hundred times larger than h for ν_4, and it is about fifty-thousand times larger for ν_3. In either case one has $g\simeq(12/7)t_{224}$ so that molecular constant t_{224} is the one that determines the scale of fine and superfine tensor splitting in infrared spectra.

APPENDIX B: TETRAGONALLY DEFINED TABLEAU COMBINATIONS

Various combinations of $S_4\times S_2$ broken tableaus are needed to construct states defined by tetragonal $D_{4h}\supset D_{2h}$ symmetry. According to Fig. 11 the tetragonal subgroup is generated by coset leaders $R_3=(1234)$ (90° $\bar{z}$ rotation) and $I=(13)(24)(56)$ (inversion) of the subgroup $D_2=\{1,R_1^2,R_2^2,R_3^2\}$.

For the $S_4\times S_2$ representations labeled by broken tableaus $\{\mu_+\}=\{\widetilde{3,1}\}\times\{\widetilde{1,1}\}=$ 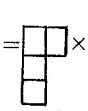 $\times$ and $\{\mu_-\}=\{\widetilde{3,1}\}\times\{\tilde{2}\}$ one needs to reduce the following representations:

$$\begin{array}{ccc} ab & ac & ad \\ c & b & b \\ d & d & c \end{array} \qquad \begin{array}{ccc} ab & ac & ad \\ c & b & b \\ d & d & c \end{array} \qquad \begin{array}{ccc} ab & ac & ad \\ c & b & b \\ d & d & c \end{array}$$

$$\mathfrak{D}^{\{\mu_\pm\}}(R_3)=\begin{pmatrix} 1\sqrt{2} & -\sqrt{3}/6 & \sqrt{6}/3 \\ \sqrt{3}/2 & 1/6 & -\sqrt{2}/3 \\ & \sqrt{8}/3 & 1/3 \end{pmatrix}, \quad \mathfrak{D}^{\{\mu_\pm\}}(I)=\pm\begin{pmatrix} 0 & \sqrt{3}/3 & \sqrt{6}/3 \\ \sqrt{2}/3 & -2/3 & \sqrt{2}/3 \\ \sqrt{6}/3 & \sqrt{2}/3 & -1/3 \end{pmatrix}, \quad \mathfrak{D}^{\{\mu_\pm\}}(R_2^2)=\pm\begin{pmatrix} -1/2 & -\sqrt{3}/2 & \cdot \\ -\sqrt{3}/2 & 1/2 & \cdot \\ \cdot & \cdot & -1 \end{pmatrix}. \tag{B1}$$

These are obtained using the tableau formulas discussed in Appendix A of article I. The reduction transformations are given by the following formulas:

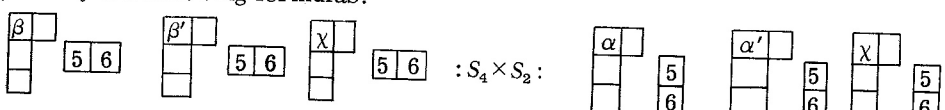

$$\begin{array}{ccc} E_u & E_u & A_{2g} \\ B_{1u} & B_{2u} & A_{2g} \end{array} \quad :D_{4h}: \quad :D_{2h}: \quad \begin{array}{ccc} E_g & E_g & A_{1u} \\ B_{1g} & B_{2g} & A_{1u} \end{array}$$

$$T=\begin{array}{c} ab \\ c \\ d \end{array}\begin{pmatrix} 1/2 & 1/2 & 1/\sqrt{2} \\ & & \\ \sqrt{3}/6 & \sqrt{3}/2 & 1/\sqrt{6} \\ & & \\ -\sqrt{6}/3 & 0 & 1/\sqrt{3} \end{pmatrix}\begin{array}{c} ac \\ \\ b \\ \\ d \end{array}, \qquad T=\begin{pmatrix} 1/2 & 1/2 & 1/\sqrt{2} \\ & & \\ -\sqrt{3}/2 & \sqrt{3}/6 & 1/\sqrt{6} \\ & & \\ 0 & -\sqrt{6}/3 & 1/\sqrt{3} \end{pmatrix}. \tag{B2b}$$

(B2a)

The α, β, and χ tableaus defined in Table VII are seen to conform with the above results.

A similar transformation of the broken tableaus $\{\mu_+\}=\{\widetilde{2,2}\}\times\{\widetilde{1,1}\}$ and $\{\mu_-\}=\{\widetilde{2,2}\}\times\{\tilde{2}\}$ is useful:

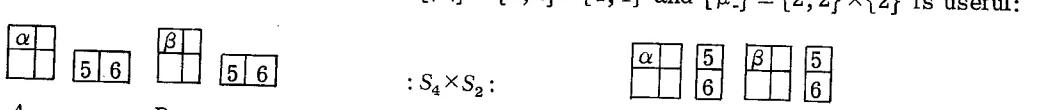

$$\begin{array}{ccc} A_{1g} & B_{2g} & D_{4h}: \\ A_{1g} & A_{2g} & D_{2h}: \end{array} \qquad \begin{array}{ccc} A_{2u} & B_{1u} \\ A_{2u} & A_{1u} \end{array}$$

$$T_+=\begin{array}{c} ab \\ cd \\ ac \\ bd \end{array}\begin{pmatrix} 1/2 & \sqrt{3}/2 \\ & \\ -\sqrt{3}/2 & 1/2 \end{pmatrix}, \tag{B3a}$$

$$T_-=\begin{pmatrix} 1/2 & \sqrt{3}/2 \\ & \\ -\sqrt{3}/2 & 1/2 \end{pmatrix}. \tag{B3b}$$

These α and β defined tableaus were also used in Table VII.

APPENDIX C: HAMILTONIAN REPRESENTATIONS IN TETRAGONAL CLUSTER BASES

Tables XI(a), XI(b), and XI(c) give the fourfold ECA representations of the molecular Hamiltonian ($H_{\text{scalar}}+H_{\text{tensor}}+H_{\text{sr}}+H_{\text{ss}}$). The parameters which are larger and which are likely to vary the most from cluster to cluster are given by capital letters. Parameters H and S depend on the scalar and tensor rovibrational Hamiltonian. The cluster center of gravity H depends on the scalar constants in Eqs. (2.1)–(2.4) and on the tensor constants t_{ijk} in Eqs. (A1), (A2), (A3), or (A4). The cluster splitting or tunneling parameter S in Eqs. (2.10) and (2.12) depends on t_{ijk}, too, but only very rough approximations to the S functions have been derived so far.[35] (Note also Ref. 11 of article I.) Parameters A, B, C, D, and E depend on the spin-rotation interaction according to Eqs. (4.6b), (4.7b), and (4.8b). These may be related to the conventional parameters through Eq. (4.3).

Finally, the spin-exchange or spin-spin tunneling parameters s, s', t, and t' belong to the phenom-

TABLE XI. Pseudo-Hamiltonian representations in tetragonal cluster bases.

(a) A-type tetragonal cluster bases.

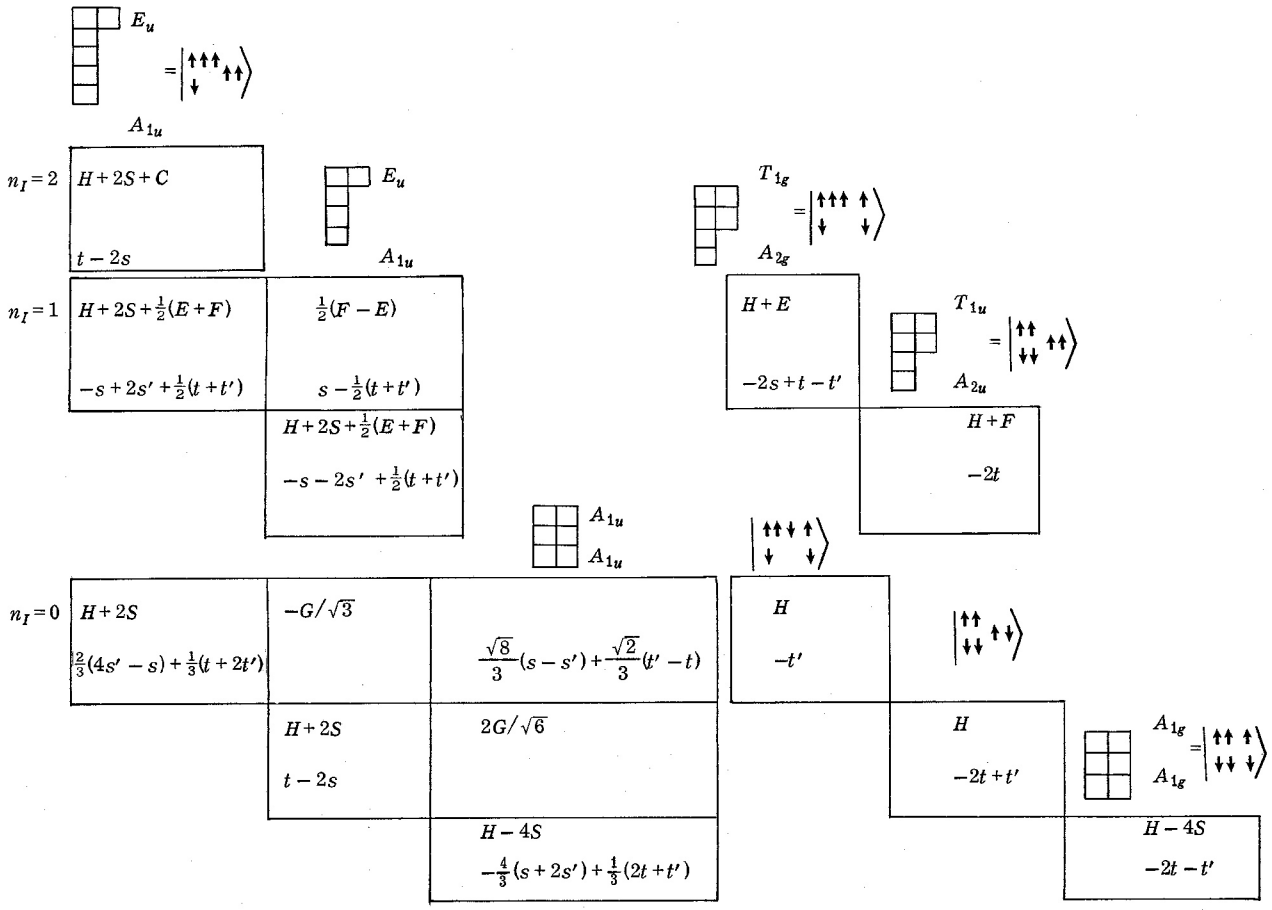

Broken tableau representations involving mixed species:

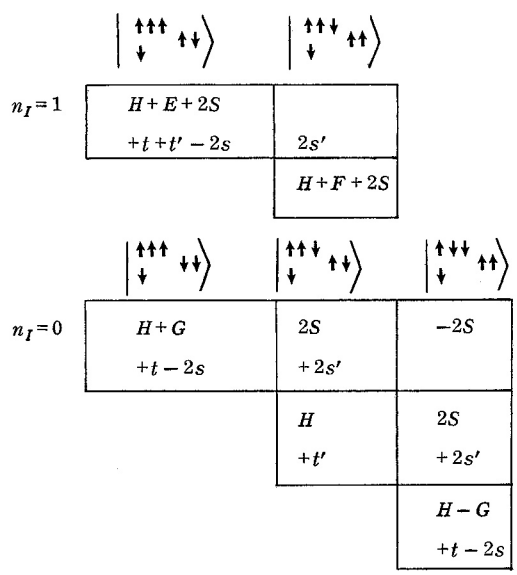

TABLE XI. *(Continued.)*

(b) B-type tetragonal (E, T_2, A_2) cluster bases.

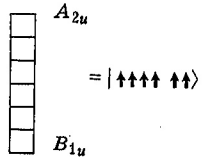

$= |\uparrow\uparrow\uparrow\uparrow\ \uparrow\uparrow\rangle$

$n_I = 3$

$H + 4S + A$

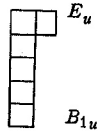

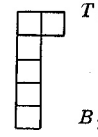

$= |\uparrow\uparrow\uparrow\uparrow\ \uparrow\downarrow\rangle$

$n_I = 2$

$H + 4S + \frac{1}{3}(B + 2C)$ $+ \frac{4}{3}(s + 2s') + \frac{1}{3}(2t + t')$	$\frac{\sqrt{8}}{6}(B - C)$ $- \frac{\sqrt{8}}{6}(s - s') - \frac{\sqrt{2}}{3}(t - t')$
$H - 2S + \frac{1}{3}(2B + C)$ $+ \frac{2}{3}(s - 4s') + \frac{1}{3}(t + 2t')$	

$H + B$ $- t'$

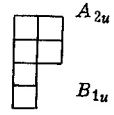

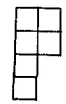

$|\uparrow\uparrow\uparrow\uparrow\ \uparrow\downarrow\rangle$

$n_I = 1$

$H + 4S + \frac{1}{15}(D + 8E + 6F)$ $+ \frac{32}{15}(s + 2s') + \frac{8}{15}(2t + t')$	$\frac{1}{\sqrt{45}}(D + 2E - 3F)$ $- \frac{2}{\sqrt{45}}(2s - 2s' + t - t')$	$\frac{2}{15}(D - 2E + F)$ $+ \frac{4}{15}(s + 2s' - 2t - t)$	$\frac{1}{\sqrt{45}}(D - 2E + F)$ $- \frac{2}{\sqrt{45}}(2s - 2s' - t + t')$
$H - 2S + \frac{1}{6}(2D + E + 3F)$ $+ \frac{1}{3}(5s - 2s') + \frac{1}{6}(5t + t')$	$\frac{1}{\sqrt{45}}(2D - E - F)$ $- \frac{1}{\sqrt{45}}(8s - 8s' - t + t')$	$\frac{1}{6}(2D - E - F)$ $- \frac{1}{6}(2s - 8s' + 5t + t')$	
$H + 4S + \frac{1}{15}(4D + 2E + 9F)$ $- \frac{4}{5}(s + 2s') + \frac{2}{15}(2t + t')$	$\frac{1}{\sqrt{45}}(2D + E - 3F)$ $+ \frac{1}{\sqrt{45}}(12s - 12s' - t + t')$		
$H - 2S + \frac{1}{6}(2D + E + 3F)$ $-(s + 2s') + \frac{1}{6}(5t + t')$			

$H + E$ $+ 2s + t - t'$

TABLE XI. *(Continued.)*

(b) *(Continued.)*

$n_I = 0$

$\left\vert \uparrow\uparrow\uparrow\uparrow \begin{smallmatrix}\uparrow\\ \downarrow\end{smallmatrix} \right\rangle$	T_{2g}	B_{2g}	$\left\vert \begin{smallmatrix}\uparrow\uparrow & \uparrow\\ \downarrow\downarrow & \downarrow\end{smallmatrix} \right\rangle$
H $+\frac{8}{3}s+\frac{4}{3}t-t'$	$2G/\sqrt{10}$	$-2\frac{\sqrt{2}}{3}(s-t)$	H $-\frac{8}{3}s+\frac{2}{3}t-t'$
$H+4S$ $+\frac{12}{5}(s+2s')+\frac{3}{5}(2t+t')$	$+\frac{\sqrt{24}}{15}(s+2s'-2t-t')$	$-\frac{\sqrt{30}}{15}(2s-2s'+t-t')$	
	$H-2S$ $+2s+t$	$G/\sqrt{3}$	
	$2G/\sqrt{15}$	$H+4S$ $-\frac{16}{15}(s+2s')+\frac{11}{15}(2t+t')$	$+\frac{2}{\sqrt{45}}(8s-8s'+t-t')$
			$H-2S$ $+\frac{1}{5}(2s-8s'+t+2t')$

Broken tableau representations involving mixed species:

$n_I = 2$

$\vert\uparrow\uparrow\uparrow\uparrow\ \downarrow\uparrow\rangle$	$\vert\uparrow\uparrow\uparrow\downarrow\ \uparrow\uparrow\rangle$
$H+B$ $+t'$	$H+\sqrt{8}S$ $+\sqrt{8}s'$
	$H+C+2S$ $+2s+t$

$n_I = 1$

$\vert\uparrow\uparrow\uparrow\uparrow\ \downarrow\uparrow\rangle$	$\vert\uparrow\uparrow\uparrow\downarrow\ \uparrow\uparrow\rangle$	$\vert\uparrow\uparrow\downarrow\uparrow\ \uparrow\uparrow\rangle$	$\left\vert \begin{smallmatrix}\uparrow\uparrow\\ \downarrow\uparrow\ \uparrow\end{smallmatrix} \right\rangle$
$H+D$	$2\sqrt{2}s'$	$\frac{2\sqrt{6}}{3}S$	$\frac{4}{\sqrt{3}}S$
	$H+E+2S$ $+2s+t+t'$	$\frac{4}{\sqrt{3}}S$ $+2\sqrt{3}s'$	$-\frac{2\sqrt{6}}{3}S$
		$H+F+\frac{2}{3}S$ $+\frac{8}{3}s+\frac{4}{3}t$	$\frac{2\sqrt{2}}{3}S$ $+\frac{2\sqrt{2}}{3}(s-t)$
			$H+F+\frac{4}{3}S$ $-\frac{8}{3}s+\frac{2}{3}t$

$n_I = 0$

$\vert\uparrow\uparrow\uparrow\uparrow\ \downarrow\downarrow\rangle$	$\left\vert \begin{smallmatrix}\uparrow\uparrow & \uparrow\\ \downarrow\downarrow & \downarrow\end{smallmatrix} \right\rangle$	$\vert\uparrow\uparrow\downarrow\downarrow\ \uparrow\uparrow\rangle$	$\left\vert \begin{smallmatrix}\uparrow\uparrow & \uparrow\\ \downarrow\downarrow & \uparrow\end{smallmatrix} \right\rangle$
$H+G$ $+2s+t$	$\frac{2}{\sqrt{3}}S$ $2\sqrt{3}s'$	$2S$	$\frac{2\sqrt{6}}{3}S$
	$H+\frac{8}{3}S$ $+\frac{8}{3}g+\frac{4}{3}t+t'$	$\frac{2}{\sqrt{3}}S$ $2\sqrt{3}s'$	$-\frac{4\sqrt{2}}{3}S$ $\frac{2\sqrt{2}}{3}(s-t)$
		$H-G$ $+2s+t$	$\frac{2\sqrt{6}}{3}S$
			$H+\frac{4}{3}S$ $-\frac{8}{3}s+\frac{2}{3}t+t'$

TABLE XI. *(Continued.)*

(c) E-type tetragonal (T_1, T_2) cluster bases.

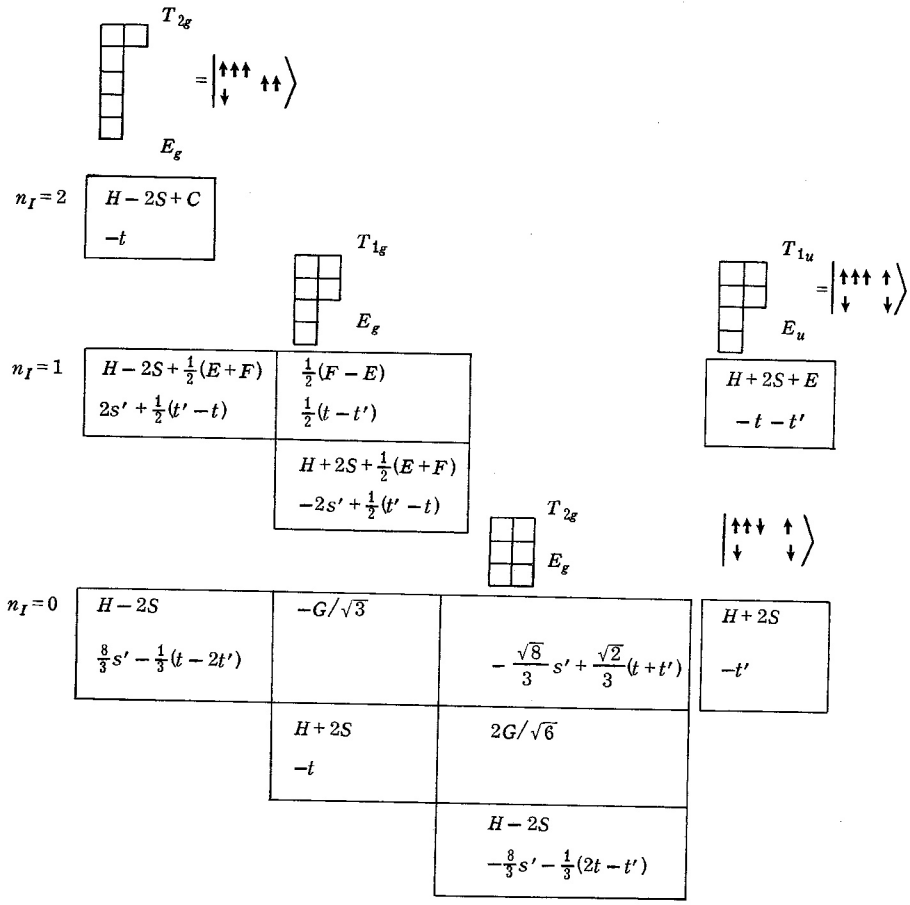

Broken tableau representations involving mixed species:

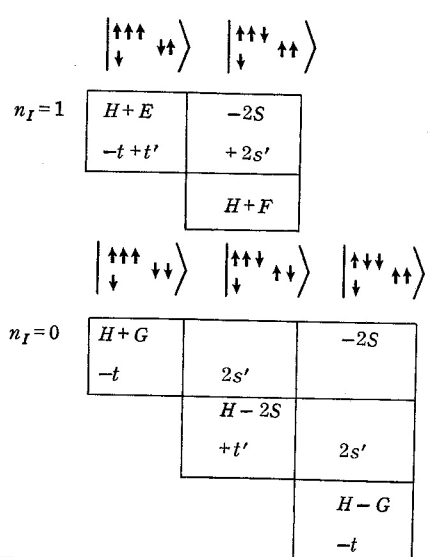

TABLE XII. Pseudo-Hamiltonian representations in trigonal cluster bases.

(a) A-type (A_1, T_1, T_2, A_2) trigonal cluster bases.

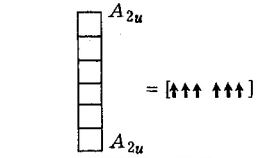

$= [\uparrow\uparrow\uparrow\ \uparrow\uparrow\uparrow]$

$n_I = 3$ | $H - 3S + K$

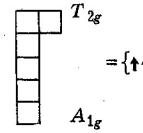

$= \{\uparrow\uparrow\uparrow\ \uparrow\uparrow\downarrow\}$

$H - S + L$
$-u + 2v - 2w$

$n_I = 2$ | $H - 3S + L$
$+u + 2v + 2w$

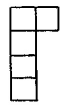

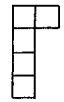

$n_I = 1$

$H - 3S + \frac{1}{5}(M_1 + 2M_2 + 2M_3)$ $+ \frac{8}{5}(u + 2v + w)$	$\frac{1}{5}(2M_1 - M_2 - M_3)$ $-\frac{2}{5}(2u - v - w)$	$\frac{1}{\sqrt{5}}(M_2 - M_3)$ $-\frac{2}{\sqrt{5}}(v - w)$
$H - 3S + \frac{1}{10}(8M_1 + M_2 + M_3)$ $+ \frac{2}{5}(u - 3v - 3w)$		$-\frac{1}{2\sqrt{5}}(M_2 - M_3)$ $-\frac{4}{\sqrt{5}}(v - w)$
		$H + S + \frac{1}{2}(M_2 + M_3)$ $-2(u - v + w)$

$\{\uparrow\uparrow\uparrow\ \uparrow\uparrow\downarrow\}$

$H - S + M_2$
$+2v$

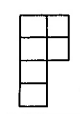

$= \begin{pmatrix} \uparrow\uparrow\ \uparrow\uparrow \\ \downarrow\ \downarrow \end{pmatrix}$

$H + S + M_3$
$-2v$

TABLE XII. *(Continued.)*

(a) *(Continued.)*

T_{2g} / A_{1g} ; A_{1g} / A_{1g} ; $\begin{pmatrix}\uparrow\uparrow & \uparrow\downarrow\\ \downarrow & \downarrow\end{pmatrix}$

$n_I=0$

$H-3S+\frac{3}{5}(N_1+2N_2+2N_3)$ $+\frac{9}{5}(u+2v+2w)$	$\frac{\sqrt{6}}{10}(2N_1-N_2-N_3)$ $-\frac{\sqrt{6}}{5}(2u-v-w)$	$\frac{\sqrt{30}}{10}(N_2-N_3)$ $-\frac{\sqrt{30}}{5}(v-w)$
	$H-3S+\frac{1}{10}(4N_1+13N_2+13N_3)$ $+\frac{11}{5}u-\frac{8}{5}(v+w)$	$-\frac{3\sqrt{5}}{10}(N_2-N_3)$ $-\frac{2}{\sqrt{5}}(v-w)$
		$H+S+\frac{1}{2}(5N_2+N_3)$ $-u$

$H-S+\frac{1}{3}(N_1+6N_2+2N_3)$ $+\frac{u}{3}+2v+\frac{2}{3}w$	$\frac{\sqrt{2}}{6}(2N_1-3N_2+N_3)$ $-\frac{\sqrt{2}}{3}(2u-3v+w)$	$\frac{\sqrt{2}}{2}(N_2-N_3)$ $-\sqrt{2}(v-w)$
	$H-S+\frac{1}{6}(4N_1+9N_2+5N_3)$ $-\frac{u}{3}-\frac{8w}{3}$	$-\frac{1}{2}(N_2-N_3)$ $-2(v-w)$
		$H+3S+\frac{3}{2}(N_2+N_3)$ $-3u$

$H+S+N_1+N_2+N_3$ $-u-2v+2w$	A_{1u} / A_{1u} $=\left\langle\begin{pmatrix}\uparrow\uparrow & \uparrow\downarrow\\ \downarrow & \downarrow\end{pmatrix}\right\rangle$
	$H-3S+N_1+N_2+N_3$ $+u-2v-2w$

Broken tableau representations involving mixed species:

$[\uparrow\uparrow\uparrow\ \uparrow\downarrow\downarrow]$ $[\uparrow\uparrow\downarrow\ \uparrow\uparrow\downarrow]$ $\begin{bmatrix}\uparrow\uparrow & \uparrow\uparrow\\ \downarrow & \downarrow\end{bmatrix}$

$n_I=1$

$H+M_2-S$ $+2v$	$-\frac{2\sqrt{6}}{3}S$ $+\frac{2\sqrt{6}}{3}(u+2w)$	$-\frac{2\sqrt{3}}{3}S$ $\frac{2}{\sqrt{3}}(u-w)$
	$H+\frac{1}{3}(M_1+2M_3)-\frac{5}{3}S$ $+4v$	$-\frac{\sqrt{2}}{3}(M_1-M_3)+\frac{2\sqrt{2}}{3}S$
		$H+\frac{1}{3}(2M_1+M_3)-\frac{7}{3}S$ $-2v$

TABLE XII. *(Continued.)*

(a) *(Continued.)*

$n_I = 0$

$[\uparrow\uparrow\uparrow\ \downarrow\downarrow\downarrow]$	$[\uparrow\downarrow\downarrow\ \uparrow\uparrow\downarrow]$	$\left[\begin{smallmatrix}\uparrow\uparrow & \uparrow\downarrow \\ \downarrow & \downarrow\end{smallmatrix}\right]$
$H+3N_2$	$-S$	$-\sqrt{2}\,S$
	$u+2w$	$\sqrt{2}\,(u-w)$
	$H+\frac{1}{3}(2N_1+3N_2+4N_3)$	$-\frac{\sqrt{2}}{3}(N_1-N_3)+\frac{\sqrt{2}}{3}S$
	$-\frac{8}{3}S$	
	$+\frac{4}{3}(u+3v+2w)$	$\frac{\sqrt{2}}{3}(u-w)$
		$H+\frac{1}{3}(N_1+3N_2+5N_3)$
		$-\frac{7}{3}S$
		$+\frac{1}{3}(5u-6v-2w)$

$\{\uparrow\uparrow\uparrow\ \downarrow\downarrow\downarrow\}$	$\{\uparrow\downarrow\downarrow\ \uparrow\uparrow\downarrow\}$	$\left\{\begin{smallmatrix}\uparrow\uparrow & \uparrow\downarrow \\ \downarrow & \downarrow\end{smallmatrix}\right\}$
$H+\frac{1}{3}(2N_1+3N_2+4N_3)$	$-S$	$-\frac{\sqrt{2}}{3}(N_1-N_3)+\sqrt{2}\,S$
$-\frac{4}{3}(u-3v+2w)$	$u+2w$	$-\frac{\sqrt{2}}{3}(u-w)$
	$H+3N_2$	$-\sqrt{2}\,S$
		$\sqrt{2}\,(u-w)$
		$H+\frac{1}{3}(N_1+3N_2+5N_3)$
		$+S$
		$-\frac{1}{3}(5u+6v-2w)$

(b) E-type (T_1,E,T_2) trigonal cluster bases.

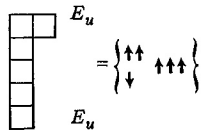

$= \left\{\begin{smallmatrix}\uparrow\uparrow & \uparrow\uparrow\uparrow \\ \downarrow\end{smallmatrix}\right\}$

$= \left\langle\begin{smallmatrix}\uparrow\uparrow & \uparrow\uparrow\uparrow \\ \downarrow\end{smallmatrix}\right\rangle$

$n_I = 2$

$H+L$	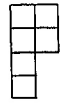	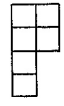	$H+2S+L$	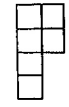
$+u-v-w$	E_u	T_{1u}	$-u-v+w$	T_{1g}
	E_u	E_u		E_g

$n_I = 1$

$H+\frac{1}{4}(2M_1+M_2+M_3)$	$\frac{1}{4}(2M_1-M_2-M_3)$	$\frac{1}{\sqrt{8}}(M_2-M_3)$	$H+2S+\frac{1}{4}(M_2+3M_3)$	$-\frac{\sqrt{3}}{4}(M_2-M_3)$
$+u+\frac{v}{2}+\frac{w}{2}$	$-u+\frac{v}{2}+\frac{w}{2}$	$-\frac{\sqrt{2}}{2}(v-w)$	$+\frac{v}{2}+\frac{3w}{2}$	$+\frac{\sqrt{3}}{2}(v-w)$
	$H+\frac{1}{4}(2M_1+M_2+M_3)$	$-\frac{1}{\sqrt{8}}(M_2-M_3)$		$H-2S+\frac{1}{4}(3M_2+M_3)$
	$+u-\frac{3v}{2}-\frac{3w}{2}$	$-\frac{\sqrt{2}}{2}(v-w)$		$-\frac{v}{2}-\frac{3}{2}w$
		$H-2S+\frac{1}{2}(M_2+M_3)$		
		$-2u-v+w$		

TABLE XII. *(Continued.)*

(b) *(Continued.)*

T_{2g}

E_g

$n_I=0$			
	$H+N_1+N_2+N_3$ $+u+v+w$		
		$H+N_1+N_2+N_3$ $+u-v-w$	$-\sqrt{2}(v-w)$
			$H-2S+N_2+2N_3$ $-u$

$H+2S+\frac{1}{3}(N_1+3N_2+5N_3)$ $+\frac{u}{3}+v+\frac{5w}{3}$		$\frac{\sqrt{2}}{3}(N_1-N_3)$ $-\frac{\sqrt{8}}{3}(u-w)$
	$H-2S+N_1+N_2+N_3$ $-u+v-w$	
		$H+2S+\frac{1}{3}(2N_1+3N_2+4N_3)$ $-\frac{u}{3}-2v-\frac{2}{3}w$

Broken tableau representations involving mixed species:

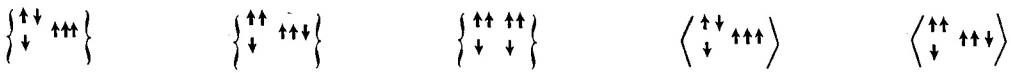

$n_I=1$			
	$H+M_2-S$ $-v$	$\frac{\sqrt{3}}{3}S$ $+\frac{1}{\sqrt{3}}(2u+w)$	$-\frac{\sqrt{6}}{3}S$ $-\frac{2\sqrt{6}}{3}(u-w)$
		$H+\frac{1}{3}(2M_1+M_3)-\frac{1}{3}S$ $+v$	$\frac{\sqrt{2}}{3}(M_1-M_3)+\frac{\sqrt{2}}{3}S$
			$H+\frac{1}{3}(M_1+2M_3)-\frac{2}{3}S$ $-2v$

$H+M_2-S$ $-v$	$\sqrt{3}S$ $+\sqrt{3}w$
	$H+M_3+S$ $+v$

TABLE XII. *(Continued.)*

$n_I = 0$

$H+\frac{1}{3}(2N_1+3N_2+4N_3)$	$\frac{1}{3}(N_1-N_3)$	$-\frac{1}{3}(N_1-N_3)$	$H+\frac{1}{3}(2N_1+3N_2+4N_3)$	$-\frac{1}{3}(N_1-N_3)+2S$	$\frac{1}{3}(N_1-N_3)$
$-\frac{2}{3}S$	$+\frac{2}{3}S$	$-\frac{2}{3}S$			
$+\frac{1}{3}(u+3v-w)$	$+\frac{2}{3}(u+2w)$	$-\frac{2}{3}(u-w)$	$-\frac{1}{3}(u-3v-w)$	$+\frac{2}{3}(u+2w)$	$-\frac{2}{3}(u-w)$
	$H+\frac{1}{3}(2N_1+3N_2+4N_3)$	$\frac{1}{3}(N_1-N_3)$	$H+\frac{1}{3}(2N_1+3N_2+4N_3)$	$\frac{1}{3}(N_1-N_3)$	$H+\frac{1}{3}(2N_1+3N_2+4N_3)$
	$-\frac{2}{3}S$	$+\frac{2}{3}S$			$+2S$
	$+\frac{1}{3}(u+3v-w)$	$+\frac{2}{3}(u-w)$	$-\frac{1}{3}(u-3v-w)$	$-\frac{2}{3}(u-w)$	$-\frac{1}{3}(u+6v+2w)$

enological Hamiltonian (4.5). These are expected to be small perturbations and are denoted accordingly by lower-case letters in the matrices of Table XI. Diagonal contributions from spin-spin energies have not been included in this calculation for tetragonal clusters, but they have been added to the trigonal representations in Table XII. Spin-spin effects probably play a lesser role in tetragonal clusters than in trigonal ones since the tetragonal tensor spin-rotation interactions tend to orient the spins more strongly.

The representations in Table XI which are not diagonal are given twice: once in the whole-tableau or species basis, and once in the broken tableau basis. For the A-type and E-type clusters [Tables XI(a) and XI(c)] the broken tableau representations are diagonalized with respect to the spin parameters $A, B, C, \ldots, F, s, t$ and t'. The rotational cluster tunneling parameter S and the polar-equatorial spin-tunneling parameter s' are off-diagonal perturbations near the case-2 limit.

It is interesting to note, however, that the spin exchange operators, in Eq. (4.5) associated with s and t do not commute. Hence, it is impossible to simultaneously diagonalize them in all representations. Indeed, three of the broken tableau representations in Table XI(b) have a 2×2 submatrix of the form

$$\langle E\rangle = \frac{2}{3}\begin{pmatrix} 4s+2t & \sqrt{2}(s-t) \\ \sqrt{2}(s-t) & -4s+t \end{pmatrix}, \tag{C1}$$

involving tunneling parameters s and t. This irreducible exchange matrix can be diagonalized for any single ratio of s and t, but its eigenvectors will change with that ratio.

APPENDIX D: HAMILTONIAN REPRESENTATIONS IN THE TRIGONAL CLUSTER BASIS

Tables XII(a) and XII(b) give the threefold ECA representations of the molecular Hamiltonian. They are given in a format similar to the fourfold matrices in Appendix C. The parameters H and S are used again.

The difference lies in the use of the spin-spin tunneling parameters u, v, and w defined in Eq. (5.2), and spin-spin interaction parameters M_1, M_2, and M_3 for $n_I=1$, and N_1, N_2, and N_3 for $n_I=0$. In the multidownon basis one supposes an interaction energy of N_1 for a pair of downons in positions numbered 1 and 5 or their equivalents in Fig. 20, N_2 for a pair in 1 and 2 positions, and N_3 for a pair in 1 and 4 positions. Then the energies for $(n_I=1)$ Slater states are given by the parameters

$$M_1 = M + N_1, \quad M_2 = M + N_2, \quad \text{or} \quad M_3 = M + N_3, \tag{D1}$$

where M was given in Eq. (5.4). Similarily, various combinations of N_j are meant to be included on the diagonal of Eq. (5.5) for $n_I = 0$.

For trigonal clusters the factored or broken tableau bases do not always provide the simplest representation of hyperfine interactions. For $(n_I = 0)$ the matrices in Table XII(b) for species $\{\widetilde{5,1}\}E_u$, $\{\widetilde{4,2}\}E_u$, and $\{\widetilde{4,2}\}T_{1u}$ are diagonal for all quantities except v and w. The broken tableau representations for the same set of states are only diagonal for N_2 and v.

[1]W. G. Harter, and C. W. Patterson, Phys. Rev. A 19, 2277 (1979).

[2]J. P. Aldridge, H. Filip, H. Flicker, R. F. Holland, R. S. McDowell, N. G. Nereson, and K. Fox, J. Mol. Spectrosc. 58, 165 (1975).

[3]K. C. Kim, W. B. Person, D. Seitz, and B. J. Krohn, J. Mol. Spectrosc. 76, 322 (1979).

[4]Ch. J. Bordé, M. Ouhayoun, A. Vanlerberghe, C. Salomon, S. Avrillier, C. D. Cantrell, and J. Bordé, *Laser Spectroscopy IV*, edited by H. Walther and K. W. Rothe (Springer-Verlag, Berlin, 1975).

[5]J. Bordé and Ch. J. Bordé, J. Mol. Spectrosc. 78, 353 (1979).

[6]J. Bordé, Ch. J. Bordé, C. Salomon, A. Van Lerberghe, M. Ouhayoun, and C. D. Cantrell, Phys. Rev. Lett. 45, 14 (1980).

[7]K. Fox, H. W. Galbraith, B. J. Krohn, and J. D. Louck, Phys. Rev. A 15, 1363 (1977).

[8]I. Ozier, L. Crapo, and S. Lee, Phys. Rev. 172, 63 (1968), N. F. Ramsey, I. Ozier, and P. N. Yi, J. Chem. Phys. 55, 5215 (1971), I. Ozier, P. N. Yi, and N. F. Ramsey, *ibid.* 66, 143 (1977).

[9]W. M. Itano, J. Mol. Spectrosc. 71, 193 (1978).

[10]F. Michelot, B. Bobin, and J. Moret-Bailly, J. Mol. Spectrosc. 76, 374 (1979).

[11]However, the meaning of "to analyze" in the current jargon of molecular spectroscopy is "to fit" or "to assign". It does not necessarily mean "to separate the whole into constituents ... with a view toward understanding ...."

[12]K. R. Lea, M. J. M. Leask, and W. P. Wolf, J. Phys. Chem. Solids 23, 1381 (1962).

[13]A. J. Dorney, and J. K. G. Watson, J. Mol. Spectrosc. 42, 135 (1972).

[14]W. G. Harter, C. W. Patterson, and F. J. Paixao, Rev. Mod. Phys. 50, 37 (1978).

[15]W. G. Harter, and C. W. Patterson, in *Advances in Laser Chemistry*, edited by A. H. Zewail (Springer-Verlag, Berlin, 1978).

[16]W. G. Harter, and C. W. Patterson, in *Group Theoretical Methods in Physics, Vol. 94, Lecture Notes in Physics*, edited by J. Ehlers *et al.* (Springer-Verlag, Berlin, 1979).

[17]J. D. Louck, Ph.D. thesis, Ohio State University, Columbus, Ohio, 1958 (unpublished).

[18]B. R. Judd, *Angular Momentum Theory for Diatomic Molecules* (Academic, New York 1975).

[19]W. G. Harter, Phys. Rev. A 3, 1891 (1971); 8, 2819 (1973).

[20]W. G. Harter and C. W. Patterson, Phys. Rev. A 13, 1067 (1976).

[21]W. G. Harter and C. W. Patterson, *A Unitary Calculus for Electronic Orbitals, Vol. 49, Lecture Notes in Physics*, edited by J. Ehlers *et al.* (Springer-Verlag, Berlin, 1976).

[22]G. W. F. Drake, and M. Schlesinger, Phys. Rev. A 15, 1990 (1977).

[23]B. R. Judd, in *The Permutation Group in Physics and Chemistry, Vol. 12, Lecture Notes in Chemistry*, edited by J. Hinze (Springer-Verlag, Berlin, 1979).

[24]W. G. Harter and C. W. Patterson, in *Unitary Group Methods for Electronic Orbitals, Vol. 22, Lecture Notes in Chemistry*, edited by J. Hinze (Springer-Verlag, Berlin, 1980).

[25]Ref. 14, Figs. 30–35.

[26]Ref. 14, Eq. (5.5).

[27]E. G. Brock, B. J. Krohn, R. S. McDowell, C. W. Patterson, and D. F. S. Smith, J. Mol. Spectrosc. 76, 301 (1973).

[28]K. T. Hecht, J. Mol. Spectrosc. 5, 355 (1960).

[29]J. Moret-Bailly, Cah. Phys. 15, 237 (1961); J. Mol. Spectrosc. 15, 344 (1965).

[30]Relations between several different conventions are given by A. G. Robiette, D. L. Gray, and F. W. Birss, Mol. Phys. 32, 1591 (1976).

[31]A discussion of fine-structure level patterns when N is not a good quantum number is given by W. G. Harter, C. W. Patterson, and H. W. Galbraith, J. Chem. Phys. 69, 4896 (1978).

[32]W. G. Harter and C. W. Patterson, J. Math. Phys. 20, 1453 (1979). A discussion of sixth-rank tensors is given.

[33]A. R. Edmonds, *Angular Momentum in Quantum Mechanics* (Princeton University Press, Princeton, 1957), p. 122.

[34]H. W. Galbraith, C. W. Patterson, B. J. Krohn, and W. G. Harter, J. Mol. Spectrosc. 73, 475 (1978).

[35]C. W. Patterson and W. G. Harter, J. Chem. Phys. 66, 4886 (1977).

[36]P. Rabinowitz, R. Keller, and J. La Tourette, Appl. Phys. Lett. 14, 376 (1969); AFOSR Report No. 70-2004 TR (unpublished).

[37]W. G. Harter, H. P. Layer, F. R. Peterson, Opt. Lett. 4, 90 (1979).

[38]M. Loete, A. Claron, A. Fricket, R. S. McDowell, H. W. Galbraith, J. C. Hillico, J. Moret-Bailly, and L. Henry, C. R. Acad. Sci. B 158, 1301 (1977).

[39]B. J. Krohn, Report LA-6554-MS, Los Alamos Scientific Laboratory, Los Alamos, NM (unpublished).

[40]W. G. Harter and C. W. Patterson, Phys. Rev. Lett. 38, 224 (1977).

[41]W. G. Harter and C. W. Patterson, J. Chem. Phys. 66, 4872 (1977).

[42]J. Bordé, J. de Physique Letters 12, L-175 (1978).

[43]C. D. Cantrell and H. W. Galbraith, J. Mol. Spectrosc. 58, 158 (1975).
[44]A. Szoke, A. Javan, Phys. Rev. Lett. 10, 521 (1963); R. A. McFarlane, W. R. Bennett, W. E. Lamb, Jr., Appl. Phys. Lett. 2, 189 (1963), T. W. Hansch, M. D. Levenson, A. L. Schawlow, Phys. Rev. Lett. 26, 946 (1971).
[45]J. L. Hall, C. Bordé, Phys. Rev. Lett. 30, 1101 (1973).
[46]C. J. Bordé, G. Camy, and B. Decomps, Phys. Rev. A 20, 254 (1979).
[47]A. P. Kol'chenko, S. G. Rantian, and R. I. Sokolovskii, Zh. Eksp. Teor. Fiz. 17, 1313 (1968) [Sov. Phys.—JETP 28, 986 (1969)].
[48]See, for example, Ref. 14 pp. 53–55.
[49]C. W. Patterson and W. G. Harter, Phys. Rev. A 15, 2372 (1977).
[50]S. Blaha, J. Math. Phys. 10, 2156 (1969).
[51]G. de. B. Robinson, *Representation Theory of the Symmetric Group* (University of Toronto Press, Toronto, 1961), p. 52.
[52]B. G. Wybourne, *Symmetry Principles and Atomic Spectroscopy* (Wiley-Interscience, New York, 1969), p. 49.